Sequestering Carbon Dioxide in Coalbeds

Technical Progress Report

Reporting Period
from September 28, 1999 to October 28, 2000

K. A. M. Gasem
R. L. Robinson, Jr.

Oklahoma State University
School of Chemical Engineering
Stillwater, Oklahoma 74078-0537

L. R. Radovic

Pennsylvania State University
Department of Energy and
Geo-Environmental Engineering
University Park, PA 16802

PREPARED FOR THE UNITED STATES
DEPARTMENT OF ENERGY
DE-FC26-98FT40426

DISCLAIMER

ABSTRACT

The authors' long term goal is to develop accurate prediction methods for describing the adsorption behavior of gas mixtures on solid adsorbents over complete ranges of temperature, pressure and adsorbent types. The major objectives of the project are to

- measure the adsorption behavior of pure CO_2, methane, nitrogen and their binary and ternary mixtures *on several selected coals having different properties* at temperatures and pressures applicable to the particular coal being studied,
- generalize the adsorption results in terms of appropriate properties of the coals, to facilitate estimation of adsorption behavior for coals other than those studied experimentally,
- delineate the sensitivity of the *competitive* adsorption of CO_2, methane and nitrogen to the specific characteristics of the coal on which they are adsorbed; establish the major differences (if any) in the nature of this competitive adsorption on different coals, and
- test and/or develop theoretically-based mathematical models to represent accurately the adsorption behavior of mixtures of the type for which measurements are made.

The specific accomplishments of this project during this reporting period are summarized below in three broad categories outlining experimentation, model development, and coal characterization.

Experimental Work: A second adsorption apparatus, utilizing equipment donated by BP Amoco, was assembled. Having confirmed the reliability of this additional experimental apparatus and procedures, adsorption isotherms for *pure* CO_2, methane, ethane, and nitrogen on wet Fruitland coal and on dry activated carbon were measured at 319.3 K (115 °F) and pressures to 12.4 MPa (1800 psia). The addition of this new facility has allowed us to essentially double our rate of data production. In addition, adsorption isotherms for pure CO_2, methane, and nitrogen on wet Illinois-6 coal and on activated carbon were measured at 319.3 K (115 °F) and pressures to 12.4 MPa (1800 psia) on our first apparatus. The activated carbon measurements showed good agreement with literature data and with measurements obtained on our second apparatus The Illinois-6 adsorption measurements are a new addition to the existing database. All the pure-fluid adsorption data show an expected uncertainty of about 3%.

Adsorption from *binary mixtures* of methane, nitrogen and carbon dioxide at a series of compositions was also measured on the wet Fruitland coal at 319.3 K (115 °F), using our first apparatus. The nominal feed compositions of these mixtures are 20%/80%, 40%/60%, 60%/40%, and 80%/20%. The experiments were conducted at pressures from 0.69 MPa (100 psia) to 12.4 MPa (1800 psia). The expected uncertainty for these binary mixture data varies from 2 to 9%.

A study addressing the previously-reported rise in the CO_2 absolute adsorption on wet Fruitland coal at 319.3 K (115 °F) was completed. Our additional adsorption

measurements on Fruitland coal and on activated carbon show that: (a) the Gibbs adsorption isotherm for CO_2 under study exhibits typical adsorption behavior for supercritical gas adsorption, and (b) a slight variation from Type I absolute adsorption may be observed for CO_2, but the variation is sensitive to the estimates used for adsorbed phase density.

Model Development: The experimental data were used to evaluate the predictive capabilities of various adsorption models, including the Langmuir/loading ratio correlation, a two-dimensional cubic equation of state (EOS), a new two-dimensional (2-D) segment-segment interactions equation of state, and the simplified local density model (SLD).

Our model development efforts have focused on developing the 2-D analog to the Park-Gasem-Robinson (PGR) EOS and an improved form of the SLD model. The new PGR EOS offers two advantages: (a) it has a more accurate repulsive term, which is important for reliable adsorption predictions, and (b) it is a segment-segment interactions model, which should more closely describe the gas-coal interactions during the adsorption process. In addition, a slit form of the SLD model was refined to account more precisely for heterogeneity of the coal surface and matrix swelling.

In general, all models performed well for the Type I adsorption exhibited by methane, nitrogen, and carbon dioxide up to 8.3 MPa (average deviations within 2%). In comparison, the SLD model represented the adsorption behavior of all fluids considered within 5% average deviations, including the near-critical behavior of carbon dioxide beyond 8.3 MPa (1200 psia). Work is in progress to (a) derive and implement the micropore form of the SLD model, which would expand the number of structural geometries used to represent the heterogeneity of coal surface; and (b) extend the SLD model to mixture predictions.

Accurate gas-phase compressibility (Z) factors are required for methane, ethane, nitrogen and carbon dioxide and their mixtures to properly analyze our experimental adsorption data. A careful evaluation of the current literature, led us to conclude that an adequate predictive capability for the mixture Z factors does not exist. Therefore, we have elected to develop such a capability using the Benedict-Webb-Rubin (BWR) equation of state. Specifically, we have used the available pure-fluid and binary mixture data to refit the BWR equation and improve its accuracy significantly; in general, the new BWR EOS parameters yield deviations in the Z factor within 0.2%.

Coal Characterization: At Pennsylvania State University, we have completed determining CO_2 and methane adsorption properties for six coals of different rank. The coals used in this study are from the Argonne Premium sample bank, covering the rank range from lignite to low-volatile bituminous, including Beulah (lignite), Smith Roland (subbituminous), Illinois-6 (high-volatile bituminous), Pittsburg-8 (high-volatile bituminous), Stockton-Lewiston (medium-volatile bituminous), and Pocahontas (low-volatile bituminous). Significant differences in CO_2 sequestration ability have been observed for different coals. Furthermore, when these differences are compared to the relative affinities of coals for CO_2 vs. methane, it is concluded that they are mostly due to differences in CO_2 uptakes on different coals.

TABLE OF CONTENTS

A. Executive Summary

During the present reporting period, six complementary tasks involving experimentation, model development, and coal characterization were undertaken to meet our project objectives:

1. A second adsorption apparatus, utilizing equipment donated by BP Amoco, was assembled. Having confirmed the reliability of this additional experimental apparatus and procedures, adsorption isotherms for CO_2, methane, ethane, and nitrogen on wet Fruitland coal and on activated carbon were measured at 319.3 K (115 °F) and pressures to 12.4 MPa (1800 psia). These measurements showed good agreement with our previous data and yielded an expected uncertainty of about 3%. The addition of this new facility has allowed us to essentially double our rate of data production.

2. Adsorption isotherms for pure CO_2, methane, and nitrogen on wet Illinois-6 coal and on activated carbon were measured at 319.3 K (115 °F) and pressures to 12.4 MPa (1800 psia) on our first apparatus. The activated carbon measurements showed good agreement with literature data and with measurements obtained on our second apparatus. The expected uncertainty of the data is about 3%. The Illinois-6 adsorption measurements are a new addition to the existing database. Preparations are underway to measure adsorption isotherms for pure methane, carbon dioxide and nitrogen on DESC-8 coal.

3. Adsorption from binary mixtures of methane, nitrogen and CO_2 at a series of compositions was also measured on the wet Fruitland coal at 319.3 K (115 °F), using our first apparatus. The nominal compositions of these mixtures are 20%/80%, 40%/60%, 60%/40%, and 80%/20%. The experiments were conducted at pressures from 100 psia to 1800 psia. The expected uncertainty for these binary mixture data varies from 2 to 9%.

4. A study was completed to address the previously-reported rise in the CO_2 absolute adsorption on wet Fruitland coal at 115 °F and pressures exceeding 1200 psia. Our additional adsorption measurements on Fruitland coal and on activated carbon show that: (a) the Gibbs adsorption isotherm for CO_2 under study exhibits typical adsorption behavior for supercritical gas adsorption, and (b) a slight variation from Type I absolute adsorption may be observed for CO_2, but the variation is sensitive to the estimates used for adsorbed phase density.

5. The experimental data were used to evaluate the predictive capabilities of various adsorption models, including the Langmuir/loading ratio correlation, a two-dimensional cubic equation of state (EOS), a new two-dimensional (2-D) segment-segment interactions equation of state, and the simplified local density model (SLD).

Our model development efforts have focused on developing the 2-D analog to the Park-Gasem-Robinson (PGR) EOS and an improved form of the SLD model. The new PGR EOS offers two advantages: (a) it has a more accurate repulsive term, which is important for reliable adsorption predictions, and (b) it is a segment-segment interactions model, which should more closely describe the gas-coal interactions during the adsorption process. In addition, a slit form of the SLD model was refined to account more precisely for heterogeneity of the coal surface and matrix swelling.

In general, all models performed well for the Type I adsorption exhibited by methane, nitrogen, and carbon dioxide up to 8.3 MPa (average deviations within 2%). In comparison, the SLD model represented the adsorption behavior of all fluids considered within 5% average deviations, including the near-critical behavior of carbon dioxide beyond 8.3 MPa (1200 psia). Work is in progress to (a) derive and implement the biporous form of the SLD model, which would expand the number of structural geometries used to represent the heterogeneity of coal surface; and (b) extend the SLD model to mixture predictions.

6. Proper reduction of our adsorption data requires accurate gas-phase compressibility (Z) factors for methane, ethane, nitrogen and carbon dioxide and their mixtures to properly analyze our experimental adsorption data. A careful evaluation of the current literature, leads us to concluded that an adequate predictive capability for the mixture Z factors dose not exist. Therefore, we have elected to develop such a capability using the Benedict-Webb-Rubin (BWR) equation of state. Specifically, we have used the available pure-fluid and binary mixture data to refit the BWR equation and improve its accuracy significantly; in general, the new BWR EOS parameters yield deviations in the Z factor within 0.2%.

At Pennsylvania State University, we have completed determining CO_2 and methane adsorption properties for six coals of different rank. The coals used in this study are from the Argonne Premium sample bank, covering the rank range from lignite to low-volatile bituminous, including, Beulah (lignite), Smith Roland (subbituminous), Illinois #6 (high-volatile bituminous), Pittsburgh-8 (high-volatile bituminous), Stockton-Lewiston (medium-volatile bituminous), and Pocahontas (low-volatile bituminous).

Significant differences in CO_2 sequestration ability have been observed for different coals. Furthermore, when these differences are compared to the relative affinities of coals for CO_2 vs. methane, it is concluded that they are mostly due to differences in CO_2 uptakes on different coals.

Future studies will be focused, therefore, on rationalizing these differences. Results to date suggest that they are due primarily to the different surface chemistries of the coals. To what extent the coal's surface area, pore size distribution and molecular sieving ability also contribute to these differences remains an important fundamental question. The results of the Penn State studies, when combined with the studies at OSU, are expected to reveal which coalbeds are best suited for sequestering CO_2 in them and for simultaneously releasing the largest quantity of methane.

B. Experimental Work

1. Experimental Facility

Currently, we have two experimental facilities dedicated to gas adsorption measurements. The first apparatus was developed in a prior project sponsored by Amoco Corporation and the Oklahoma Center for the Advancement of Science and Technology. As a precursor to the data acquisition, the apparatus was thoroughly re-tested and revised as necessary for operations in the present project. Details of the equipment design have been described previously [1,2]. A brief description of experimental methods and procedures is given in the following section.

The second apparatus was assembled from an equipment donation from BP Amoco. The donation consisted of essentially the complete coalbed methane research equipment housed at BP Amoco's Tulsa Technology Center. In August 1999, the second apparatus was reassembled in OSU's new Advanced Technology Research Center, a $35 million state-of-the-art complex dedicated to research and technology development. Mr. Don Morgan, who formerly operated the equipment at BP Amoco, served as a consultant in reassembling and validating this apparatus.

The new facility has allowed us to essentially double our rate of data production. Although the efforts in reassembling, testing, and validating the new apparatus may have caused temporary delays in data acquisition on the existing apparatus, the overall result should be to significantly increase the total amount of data produced by the end of the project.

2. Experimental Methods and Procedures

Our experimental technique in both facilities employs an identical mass balance method, utilizing volumetric accounting principles. The experimental apparatus, shown schematically in Figure 1, has been used successfully in previous measurements [1, 2]. A brief description of the experimental apparatus and procedures follows.

The entire apparatus is maintained in a constant temperature air bath. The equilibrium cell (EC, Figure 1) is filled with the adsorbent to be studied, and the cell is placed under vacuum prior to gas injection. The void (gas) volume, V_{void}, in the equilibrium cell is then determined by injecting a known quantity of helium from a calibrated injection pump (P_2). Since helium is not adsorbed, the void volume can be determined from measured values of the temperature, pressure and amount of helium injected into the cell. The equations are

$$V_{void} = n_{He}(Z_{He}RT/p)_{cell} \quad (1)$$

$$n_{He} = (pV/Z_{He}RT)_{pump} \quad (2)$$

In these equations, n_{He} is the number of moles of helium injected into the cell, V is the volume of gas injected from the pump, Z_{He} is the compressibility factor of helium, R is the universal gas constant, T is the temperature, p is the pressure, and the subscripts "cell" and "pump" refer to conditions in the cell and pump sections of the apparatus, respectively.

The amount of gas (methane, for example) adsorbed at a given pressure can be calculated based on the preliminary calibrations done above. First, a given quantity of methane, n_{inj}, is injected into the cell. This amount is determined by an equation analogous to Equation 2, above. A recirculating pump is used to circulate methane over the adsorbent until equilibrium is reached, where no further methane is adsorbed. The amount of unadsorbed methane, n_{unads}, is then determined based on the fact that any unadsorbed methane will remain in the void volume (determined from the helium calibration). The expression for this quantity is

$$n_{unads} = (pV_{void}/Z_{methane}RT)_{cell} \quad (3)$$

where the pressure p is measured after equilibrium is reached in the cell. The amount of adsorbed methane, n_{ads}, is then calculated by difference as

$$n_{ads} = n_{inj} - n_{unads} \quad (4)$$

These steps are repeated at sequentially higher pressures to yield a complete adsorption isotherm.

In mixture studies, the procedure is only slightly more complicated. The individual gases can be injected separately (or a gas mixture of known composition can be injected), so the total amount of each gas in the cell is known. The amount of unadsorbed gas at each pressure is calculated by Equation 3 with $Z_{methane}$ replaced by Z_{mix}, the gas mixture compressibility factor. The composition of the gas mixture in the void volume is determined by chromatographic analysis of a microliter-size sample of the gas mixture captured in a sampling valve (SV_1). This permits the total amount of unadsorbed gas to be apportioned among the various components according to their mole fractions in the gas. Then, Equation 4 can be applied to each component in the gas mixture. For methane, nitrogen, and CO_2 mixtures, the mixture Z factor is determined accurately from available experimental data and accurate equations of state.

Relationship between Gibbs and Absolute Adsorption

The Gibbs adsorption definition considers the gas phase volume as the sum of the gas (V_{gas}) and adsorbed phase (V_{ads}) volumes (ignoring the reduction in gas phase volume due to presence of the adsorbed phase volume.) Rewriting the above equation in terms of vapor volume (V_{gas}) and adsorbed phase volume (V_{ads}), using the specific molar volume (of each phase), v_{gas}, and v_{ads},

$$n_{ads}^{Gibbs} = n_{inj} - \left[\frac{V_{gas} + V_{ads}}{v_{gas}} \right] \quad (5)$$

For absolute adsorption, the amount adsorbed within the equilibrium cell is given correctly as

$$n_{ads}^{Abs} = n_{inj} - \left[\frac{V_{gas}}{v_{gas}} \right] \quad (6)$$

By combining Equations 5 and 6, the Gibbs adsorption expression can be rewritten as:

$$n_{ads}^{Gibbs} = n_{ads}^{Abs} - \left[\frac{V_{ads}}{v_{gas}} \right] \quad (7)$$

Since

$$n_{ads} = \left[\frac{V_{ads}}{v_{ads}} \right] \quad (8)$$

then

$$\left[\frac{V_{ads}}{V_{gas}} \right] = n_{ads}^{Abs} \left[1 - \left(\frac{v_{ads}}{v_{gas}} \right) \right]. \quad (9)$$

At low pressures, this correction is negligible, but at higher pressures it becomes significant. Rewriting Equation 9 in terms of gas (ρ_{gas}) and adsorbed (ρ_{ads}) phase densities:

$$n_{ads}^{Gibbs} = n_{ads}^{Abs} \left[1 - \left(\frac{\rho_{gas}}{\rho_{ads}} \right) \right]. \quad (10)$$

A common approximation for the density of the adsorbed phase is to use the liquid density at the atmospheric pressure boiling point, as done by Yee [5]. Carbon dioxide, however, is a solid at its atmospheric boiling point. As a result, the density for a saturated liquid at the triple point was used instead. This work, unless otherwise noted, uses the adsorbed phase density approximation suggested by Yee. For nitrogen, methane, and carbon dioxide, the densities 0.808 g/cc, 0.421 g/cc, and 1.18 g/cc, respectively, are used to estimate the absolute adsorption from the Gibbs adsorption data.

C. Results and Discussion

1. Experimental Data

A summary of the progress of our experimental program is presented in Table 1. Thus far, we have completed pure-gas (methane, nitrogen, ethane, and carbon dioxide) adsorption measurements on four solid matrices comprised of two samples of wet Fruitland coal (OSU#2 and OSU#3), wet Illinois-6 coal, and dry activated carbon. Tables 2-3 present the compositional analyses for the various matrices considered in this study to date.

Binary mixture adsorption measurements were also completed for three binary systems (methane/carbon dioxide, methane/nitrogen, and nitrogen/carbon dioxide) on wet OSU#2 Fruitland coal. Similar binary mixture measurements on Illinois-6 are underway and should be completed shortly.

The present measurements are conducted mostly at 115 °F and cover the pressure range from 100 to 1800 psia. Our error analysis indicates that the uncertainty estimates for the pure-gas adsorption measurements are approximately 2%. The expected uncertainty for the individual component adsorption from binary mixtures varies from 2 to 9%. These estimates, which are depicted as error bars in some of the figures presented below, were generated by error propagation of uncertainties in all measured quantities. The estimated uncertainties in each of the experimentally measured quantities are as follows: temperature 0.2°F; pressure 0.2 psia; injected gas volumes 0.02 cc. The newly acquired data confirm the estimated precision of our measurements and agree well with our previous data [2].

Following is a brief description of our new measurements and the associated analyses.

(a) Pure-Gas Adsorption on Fruitland Coal

To confirm the reliability of our second adsorption apparatus (equipment donation from BP Amoco), adsorption isotherms for pure nitrogen, and carbon dioxide on wet Fruitland coal were measured at 115 °F and pressures to 1800 psia. Tables 4-5 present replicate runs for nitrogen and carbon dioxide, respectively. These measurements show good agreement, on a mineral matter-free basis, with our previous data and yield an expected uncertainty of about 3%.

Figures 2-3 present the Gibbs adsorption behavior for the nitrogen and carbon dioxide data, respectively. The figures indicate that while the nitrogen adsorption measurements show variations within the experimental uncertainty among the various coal samples characterized in Table 2, carbon dioxide adsorption data show greater variations among the Fruitland coal samples considered.

(b) Pure-Gas Adsorption on Activated Carbon

To provide "base-line" data on well-characterized substrate and to further confirm the reliability of our experimental measurements, two sets of replicate carbon dioxide adsorption measurements on dry activated carbon were conducted and compared to recent data by Tomasko [16]. As indicated in Table 6, our measurements were acquired on two separate facilities at 113°F, covering the pressure range from 100 to 1800 psia. Following Tomasko and coworkers, the activated carbon used (Filtrasorb-400, 12X40 mesh, Calgon Carbon) was washed in demineralized water and dried under vacuum at 110°C for three days before the adsorption experiments. An analysis of the activated carbon employed in this study is given in Table 3.

Figures 4 and 5 present comparisons of our data with those of Tomasko, which were acquired using a different experimental technique (a high-pressure flow gravimetric apparatus). The figures differ in that the adsorption isotherm is shown as function of density and pressure, respectively. Although the experimental techniques differ, the data show excellent agreement. Specifically, variations within 5% are observed, which are within the combined uncertainty of the two data sets.

The results in Figures 4 and 5 were considered to have verified the viability of our procedures. Gas adsorption measurements for pure ethane, methane and nitrogen on dry activated carbon at 113 °F were also completed, as presented in Tables 7, 8 and 9. Replicate runs were conducted for both fluids to confirm the precision of our measurements.

Figure 6 and 7 present comparisons for Gibbs and absolute adsorption behavior of methane, ethane, nitrogen and CO_2 on activated carbon. Figure 6 indicates that (a) all fluids exhibit a similar trend of maximum Gibbs adsorption at bulk density of 0.05-0.15 g/cc, and (b) greater amount of CO_2 adsorbs on activated carbon (about 40% more than ethane and 60% more than methane.) Figure 7 depicts the variation of absolute adsorption with pressure. The observed "humps' in the adsorption behavior of both CO_2 and ethane suggests that we have used a high estimate for the adsorbed phase density.

(c) Pure-Gas Adsorption on Illinois-6 Coal

Gas adsorption measurements for pure nitrogen, methane and CO_2 on wet Illinois-6 coal at 115 °F are presented in Tables 10 through 12. Replicate runs were conducted for each gas to confirm the precision of our measurements and to investigate the effect of variations in moisture content and coal sample preparation on the adsorption behavior. These new measurements indicate that both methane and nitrogen adsorption on wet Illinois-6 are about half that adsorbed on wet Fruitland coal at the same conditions.

The pure-gas adsorption behavior is illustrated in Figure 8, which indicates that the relative amounts of nitrogen, methane and CO_2 adsorbed are in the approximate ratio of 1: 2.5: 6. The figure also shows that both methane and nitrogen produce Type I

adsorption. In all the figures, the smooth curves were generated from a Langmuir fit to the data.

The present adsorption data were acquired using two coal samples of different moisture content. Both measurement sets indicate that water content values beyond the equilibrium water content do not significantly affect the adsorption behavior. This finding supports similar conclusions reached in previous studies [2, 3].

(d) Binary Mixture Adsorption on Fruitland Coal

Binary adsorption of methane, nitrogen and carbon dioxide at a series of compositions has been measured on the wet Fruitland coal at 115 °F. Tables 13-18 presented the experimental data for four different mixtures. The nominal compositions of these injection-gas mixtures are 20%/80%, 40%/60%, 60%/40%, and 80%/20%. The uncertainties for binary mixtures vary for different compositions and different mixtures. In general, the expected uncertainty in the methane/carbon dioxide, methane/nitrogen, nitrogen/carbon dioxide mixtures are 2-7%, 2-9%, and 2-7%, respectively, for the individual component adsorption from the mixtures.

As shown in Figures 9-17, the component absolute adsorption for all the binary mixtures is well represented by Type I adsorption. Specifically, methane/carbon dioxide binary mixture adsorption results are shown on Figures 9-11. For the pure gas adsorption, carbon dioxide has higher adsorption than methane. In the binary mixture, carbon dioxide is more strongly adsorbed than methane. At the composition of methane/carbon dioxide of 80%/20%, methane has more absolute adsorption than carbon dioxide. At methane/carbon dioxide feed gas compositions of 60%/40%, 40%/60%, and 20%/80%, the absolute carbon dioxide adsorption is higher than methane adsorption. As the composition of carbon dioxide increases, the absolute carbon dioxide adsorption increases, while the absolute methane adsorption decreases. In comparison, the total absolute adsorption, depicted in Figure 11, increases when more carbon dioxide is in the mixtures. The total adsorption is above the absolute adsorption amount of pure methane, but less than the absolute adsorption of pure carbon dioxide, as expected.

Methane/nitrogen binary mixture adsorption results are shown in Figures 12-14. Pure methane has higher adsorption than pure nitrogen. In the methane/nitrogen binary mixture adsorption, methane is also more strongly adsorbed. At compositions of 80%, 60%, 40% methane/nitrogen mixture, methane has higher absolute adsorption than nitrogen. But at composition methane/nitrogen 20%/80%, nitrogen has higher adsorption than methane. As shown in Figure 14, the total adsorption of methane/nitrogen binary mixture is higher than the pure nitrogen adsorption and lower than pure methane adsorption.

Nitrogen/carbon dioxide binary mixture adsorption results are shown in Figures 15-17. For pure gas adsorption, carbon dioxide has much higher adsorption than nitrogen. With the composition from nitrogen/carbon dioxide 20%/80% to 80%/20%, carbon dioxide has higher adsorption than nitrogen. The total adsorption of this binary mixture,

shown in Figure 17, is higher than the pure nitrogen adsorption and lower than the pure carbon dioxide adsorption.

Previously, Amoco [5] has collected data for pure nitrogen, methane and carbon dioxide adsorption on wet Fruitland coal at 115 °F at pressures from 100 psia to 1400 psia. Hall at Oklahoma State University [3] has also performed similar experiments extending to 1800 psia. Comparison of these data indicates that the current data for methane and carbon dioxide pure gases are about 3% lower than Amoco's data and nitrogen is about 10% lower. Similarly, the binary adsorption data show comparable disagreement with our previous data. These variations in the adsorption data are attributable to variation in the coal samples, which have originated from different wells and have different content of mineral matter. A data comparison based on carbon content produces closer agreement among the various data. Although more detailed a comparison would be useful in establishing the consistency of the various data sets, such comparisons will be more meaningful when reliable a characterization method is established. Efforts are currently underway to develop such procedures.

(e) Comments on Near-Critical Adsorption Isotherms

Previous studies [2] have indicated a sharp rise in the CO_2 absolute adsorption on wet Fruitland coal at 115 °F, as exemplified by Figure 18. Several interpretations have been given for the observed behavior, including the possibility of (a) CO_2 condensation in lines connecting the injection pump to the equilibrium cell (see Figure 1), (b) CO_2 capillary condensation within the coal matrix, and (c) the critical phenomenon influencing the adsorption behavior at the experimental conditions considered.

During this reporting period, efforts were extended to ascertain the accurate adsorption behavior for this isotherm. Repeated measurements conducted carefully to avoid condensation, and a thorough evaluation of the data reduction procedure associated with experimental method used, revealed the following:

- The calculated amount of adsorbed CO_2 is highly sensitive to the value of the compressibility factor employed; thus, accurate compressibility factor predictions are required in this near-critical portion of the CO_2 phase diagram. Specifically, the large increase in CO_2 adsorption on Fruitland coal reported by Hall, et al. [2] was traced to use of the Redlich-Kwong (RK) equation of state for representing the CO_2 compressibility factors. The RK predictions are inadequate in this region. Use of a highly-precise equation of state [19] eliminated the anomalous jump in the calculated adsorption.
- As shown in Figure 19, estimates of the adsorbed phase density, required to determine absolute CO_2 adsorption, affect the shape of the adsorption isotherm at pressures exceeding 1200 psia. Specifically, although a plot of the Gibbs adsorption isotherm for CO_2 at the conditions under study shows a typical supercritical behavior, as shown in Figure 20, significant variations are observed in the absolute adsorption depending on the estimates used for the adsorbed phase density.

- Our new data for the CO_2 adsorption on activated carbon and similar studies in the literature suggest that a closer proximity to the critical point is required for significant manifestation of the effects of critical phenomenon on the adsorption behavior.

4. Model Development

We are currently investigating five avenues for representing adsorption equilibrium. These include (a) enhanced forms of the Langmuir-type isotherms (see, e.g., [4]), (b) two-dimensional equations of state, (c) the simplified local density models, (d) introduction of two-dimensional analogs of the activity coefficients used in vapor-liquid equilibrium calculations, and (e) treating adsorption as a constrained form of vapor-liquid equilibrium [5]. In so doing, our objective is to develop reliable, simple analytic models capable of describing multilayer adsorption of near-critical and supercritical components on heterogeneous surfaces.

In this report, we briefly outline the first three methods and discuss the quality of their representation of the methane, nitrogen, ethane and CO_2 pure-fluid adsorption.

(a) Langmuir Models

In general, simple models have been used to represent the behavior of pure and mixed gas adsorption on coal. The extended Langmuir model is used almost exclusively in literature studies [e.g., 5], although the Ideal Adsorbed Solution (IAS) model [6] has also been employed [7]. Both these models work well for essentially ideal adsorbed solutions, but neither is capable of handling nonidealities in the adsorbed phase with any accuracy. The extended Langmuir model is shown below as an illustration of the simple modeling approach used in most previous studies. For mixtures it takes the form

$$\theta = \frac{\omega_i}{L_i} = \frac{B_i P y_i}{1 + \sum_j B_j P y_j} \tag{11}$$

where ω_i is the amount of component "i" adsorbed (moles "i" adsorbed per unit mass of coal), L_i and B_i are Langmuir constants for "i", p is pressure, and y_i is the mole fraction of "i" in the gas phase. This relation allows mixture adsorption to be calculated from pure-component data, since values of L_i and B_i may be determined from the pure-component form of Equation 11.

The combined Langmuir-Freundlick adsorption isotherm, expressed in terms of ω_i, yields the loading ratio correlation (LCR) for mixtures

$$\theta = \frac{\omega_i}{L_i} = \frac{B_i (P y_i)^{\eta_i}}{1 + \sum_j B_j (P y_j)^{\eta_i}} \tag{12}$$

The additional parameter in the LRC (η_i) lends the Langmuir model more flexibility. Although the simplicity of Langmuir models is attractive, our data show that they are not adequate to represent the behavior of mixtures of the gases CO_2, methane, and nitrogen. In fact, previously we found errors greater than 100% when the extended Langmuir model was applied to our data on the adsorption of nitrogen from nitrogen + CO_2 mixtures [3].

(b) Equation-of-State Models

Simulations of coalbed gas recovery and CO_2 sequestering require reliable, yet simple analytic models beyond Langmuir-type correlations. Equation-of-state (EOS) frameworks offer an attractive potential for meeting such requirements.

In our previous annual report, we have presented the generalized form of the 2-D EOS. Our recent EOS studies focused on developing 2-D analog to the Park-Gasem-Robinson (PGR) EOS. This new EOS offers two advantages: (a) The PGR EOS has a more accurate repulsive term, which is essential for reliable adsorption predictions, and (b) it is a segment-segment interactions model, which more closely depicts the realities of gas-coal interactions during the adsorption process. Following is a brief description of both equations.

2D ZGR EOS

A general form of the popular three-dimensional equations of state can be expressed by [11]:

$$\left[p+\frac{a\rho^2}{1+Ub\rho+W(b\rho)^2}\right][1-b\rho]=\rho RT \tag{13}$$

where a and b are the traditional EOS parameters, and numerical values of U and W may be specified to give various forms of three-dimensional equations of state. An even more general two-dimensional analog can be written as follows (by introducing an additional coefficient, m):

$$\left[A\pi+\frac{\alpha\omega^2}{1+U\beta\omega+W(\beta\omega)^2}\right][1-(\beta\omega)^m]=\omega RT \tag{14}$$

where A is the specific surface area, π is the spreading pressure, ω is the specific amount adsorbed, and α and β are model parameters. The model coefficients, U, W, and m must be specified to obtain a specific form of the 2-D EOS for application. For example, an analog of the van der Waals (VDW) EOS is obtained by setting m = 1 and U = W = 0, similarly for the Soave-Redlich-Kwong (SRK) (m = U = 1 and W = 0), the Peng-Robinson (PR) (m = 1, U = 2, and W = -1), and the Eyring (m = 1/2 and U = W = 0) EOS.

This general 2-D EOS can be used to investigate EOS behaviors by specifying various combinations of model coefficients. Selection of the model coefficient m is the most important among the EOS model coefficients, because it has a significant effect on the shape of the pure adsorption isotherm. If U and W are equal to zero, then by setting m to values of ∞, 1, and 1/2, we obtain the 2-D ideal gas law, the VDW EOS, and the Eyring EOS, respectively. Actually, the pure gas isotherms vary considerably in shape and we have found that it is sometimes desirable to select an m value even smaller than 1/2 to describe pure isotherms. Based on preliminary calculations, we have found that an equation with m = 1/3 and U = W = 0 (the ZGR EOS) is promising [12]. The 2-D EOS can be applied to adsorbed phases containing mixtures by utilizing the traditional mixing rules (where x is the mole fraction in the adsorbed phase):

$$\alpha = \sum_i \sum_j x_i x_j \alpha_{ij} \tag{15}$$

$$\beta = \sum_i \sum_j x_i x_j \beta_{ij} \tag{16}$$

where

$$\begin{aligned} \alpha_{ij} &= (1 - C_{ij})(\alpha_i + \alpha_j)/2 \\ \beta_{ij} &= \sqrt{\beta_i \beta_j} \end{aligned} \tag{17}$$

2D PGR EOS

The new 2-D EOS is expressed as follows:

$$A\pi = \omega RT + cRT\omega\left(\frac{\beta_1 \tau v l \omega}{1 - \beta_2 \tau l \omega} - \frac{Z_M Y l \omega}{1 + U l \omega + W(l\omega)^2} - \frac{Q_1 Z_M Y L \omega}{1 + Q_2 L \omega}\right) \tag{18}$$

where

$$Y = \exp(F_t) - 1$$

$$F_t = \omega_1\left(\frac{1}{2\tilde{T}}\right)^{1/2} + \omega_2\left(\frac{1}{2\tilde{T}}\right) + \omega_3\left(\frac{1}{2\tilde{T}}\right)^{3/2} + \omega_4\left(\frac{1}{2\tilde{T}}\right)^2$$

$$\tilde{T} = \frac{T}{T^*}$$

where ω is the absolute adsorption and L=V*/A. The other universal EOS constants and the component parameters are listed in Tables 19 and 20. Further details are given elsewhere [15].

(c) The Simplified Local Density Model

Our experience to date indicates that the 2-D EOS approach is, in general, superior to the more widely-used theories such as the Ideal Adsorbed Solution (IAS) and extended Langmuir isotherm. However, present applications of this approach are inherently deficient in representing multilayer adsorption; especially, when it is applied to heterogeneous surfaces as in the case of coal.

Therefore, we are currently attempting to augment the EOS framework and render it useful for adsorption behavior beyond Type I isotherms by (a) using solid-fluid site characterization based on characteristic curves similar to those generated by the Polanyi potential theory (see, e. g., [13]), and (b) superimposing the fluid-solid potential on an improved EOS phase description to predict the near-critical adsorption behavior. The latter is well exemplified by the simplified local density (SLD) model (see, e.g., Lira and coworkers [14]). We believe such developments will facilitate the use of highly efficient EOS computational frameworks for representing adsorption behavior, as well as improving our understanding of the phenomenon.

The SLD model is developed from statistical mechanical theory. The SLD model is a compromise between the traditional empirical and semi-empirical methods, which are computationally less demanding but are unable to account for the various adsorption isotherms seen near the critical region, and the computationally intensive molecular simulation methods. In applying the SLD adsorption model, the fluid-solid potential is superimposed on an equation of state (EOS) and the configurational energy integral in the inhomogeneous fluid phase is simplified with a local density approximation [14].

In this study, we evaluate the predictive capability of the SLD model for the supercritical adsorption systems encountered in CO_2 sequestering and coalbed methane recovery. Specifically, we correlate the experimental data on the adsorption of methane, nitrogen and carbon dioxide on wet coals and dry activated carbon using the *flat-surface* and *slit* forms of the SLD. The SLD model predictions are then compared to the predictions obtained from the Langmuir, LRC, and the 2-D EOS models.

Flat-Surface SLD Model

The SLD model is formulated in terms of the surface excess adsorption (Γ^{ex}), defined as the excess number of moles per unit area of adsorbent, or

$$\Gamma^{ex} = \int_{Z_\circ}^{\infty} (\rho(z) - \rho_{bulk}) dz \qquad (19)$$

For a flat *surface geometry*, the lower limit of integration is the surface of the solid and is taken as the plane at $z_\circ = \sigma_{ff}/2$, where σ_{ff} is the molecular distance between two solid molecules.

As indicated by Equation 19, the SLD theory predicts the Gibbs excess, not the absolute adsorption. To calculate the absolute adsorption, one must assume a value for the adsorbed phase density or volume.

In flat-surface adsorption, the SLD model asserts that the equilibrium chemical potential at any point z above the adsorbent surface is equal to the bulk phase chemical potential. Accordingly, the equilibrium chemical potential is calculated by contributions from fluid-fluid and fluid-solid interaction as

$$\mu = \mu_{bulk} = \mu_{ff}(z) + \mu_{fs}(z) \tag{20}$$

where the subscript bulk refers to the bulk fluid, ff refers to fluid-fluid interactions, and fs refers to the fluid-solid interactions.

The fluid-solid potential at a given point z is independent of temperature and the number of molecules at and around that point. The fluid-solid potential is given in terms of the molecular interactions potential $\psi(z)$ and N_A is Avogadro's Number as

$$\mu_{fs} = N_A \Psi(z) \tag{21}$$

Lee's partially integrated 10-4 Lennard-Jones potential [8] is used to describe the adsorbate-adsorbent interactions

$$\Psi(z) = 4\pi\rho_{atom}\varepsilon_{fs}\sigma_{fs}^6\left(\frac{\sigma_{fs}^6}{5x_1^{10}} - \frac{1}{2}\sum_{i=1}^{4}\frac{1}{x_i^4}\right) \tag{22}$$

where ε_{fs} is the fluid-solid interaction energy parameter, $\rho_{atom} = 0.382\,\text{Å}^{-2}$, x_i is the intermolecular distance between fluid-molecule centers and the ith plane of solid molecules, σ_{fs} is taken as the arithmetic mean of the fluid and solid diameters. As indicated by Equation 22, the interactions are truncated at the fourth plane of solid atoms with an interplanar spacing of 3.35 Å.

The fluid-fluid potential is then calculated as

$$\mu_{ff} = \mu_{bulk} - N_A \Psi(z) \tag{23}$$

where

$$\mu_{bulk} = \mu_\circ + RT\ln(f_{bulk}/f_\circ)$$
$$\mu_{ff} = \mu_\circ + RT\ln(f_{ff}(z)/f_\circ)$$

After rearrangement this leads to

$$f_{ff}(z) = f_{bulk} \exp[-\Psi(z)/(kT)] \tag{24}$$

In this study, we have used the PR and PGR equations of state to determine the fluid and the bulk fugacities. The fugacity expressions for the PR EOS are (similar expressions for the PGR EOS are given elsewhere [15])

$$\ln f_b = \frac{b\rho_b}{1-b\rho_b} - \frac{a_b\rho_b}{RT\left(1+2b\rho_b-b^2\rho_b^2\right)} - \ln\left(\frac{1-b\rho_b}{RT\rho_b}\right) - \frac{a_b}{2\sqrt{2}RT}\ln\left(\frac{1+b\left(1+\sqrt{2}\right)\rho_b}{1+b\left(1+\sqrt{2}\right)\rho_b}\right) \tag{25}$$

$$\ln f_{ff}(z) = \frac{b\rho(z)}{1-b\rho(z)} - \frac{a(z)\rho(z)}{RT\left(1+2b\rho(z)-b^2\rho^2(z)\right)} - \ln\left(\frac{1-b\rho(z)}{RT\rho(z)}\right) - \frac{a(z)}{2\sqrt{2}RT}\ln\left(\frac{1+b\left(1+\sqrt{2}\right)\rho(z)}{1+b\left(1+\sqrt{2}\right)\rho(z)}\right) \tag{26}$$

where a_b is the PR EOS constant, and $a(z)$ is evaluated as follows

$$a(z) = a_b\left(\frac{5}{16} + \frac{6}{16}\frac{z}{\sigma_{ff}}\right) \quad \text{for} \quad 0.5 \le \frac{z}{\sigma_{ff}} \le 1.5 \tag{27}$$

$$a(z) = a_b\left[1 - \frac{1}{8\left(\frac{z}{\sigma_{ff}} - \frac{1}{2}\right)^3}\right] \quad \text{for} \quad 1.5 \le \frac{z}{\sigma_{ff}} < \infty \tag{28}$$

Once the fugacity at the local point is determined, the EOS is used to calculate the corresponding local density $\rho(z)$. To apply the PR-SLD model, we have assumed that (a) the pure fluids are adsorbed on flat, homogenous coal surface, and (b) the coal has pseudo-crystalline structure. Details of our calculation procedure are given elsewhere [15].

Slit SLD Model

We also have evaluated a slit *form* of the SLD model, where the adsorbed fluid resides within a slit instead of residing near a flat surface. That is, in contrast to Equation 19, a slit width L is used to determine excess adsorption:

$$\Gamma^{ex} = \int_{\sigma_{ff}/2}^{L-\sigma_{ff}/2} \left[\rho(z) - \rho_b\right] \cdot dz \tag{29}$$

The value of slit width L is regressed from experimental data. Details for applying the slit theory are given elsewhere [17].

In this case, the adsorbed molecule has fluid-solid interactions with two surfaces, or

$$\mu_{fs}(z) = \mu_{fs1}(z) + \mu_{fs2}(L - z) \tag{30}$$

The fluid-solid potential, represented by $\Psi(z)$, is defined on a molecular basis by

$$\Psi(z) = 4\pi\rho_{atoms}\,\varepsilon_{fs}\sigma_{fs}^2\left(\frac{\sigma_{fs}^{10}}{5(z')^{10}} - \frac{1}{2}\sum_{i=1}^{4}\frac{\sigma_{fs}^4}{(z' + (i-1)\cdot\sigma_{ss})}\right) \tag{31}$$

where ε_{fs} is the fluid-solid interaction energy parameter and ρ_{atom} = 0.382 A. The molecular diameter of the adsorbate and the carbon interplanar distance are σ_{ff} and σ_{ss}, respectively. Molecular diameters were obtained from Reid [18] and are presented in Table 23. Following Chen [17], the interplanar spacing is 0.335 nm.

Two other definitions are needed for convenience:

$$\sigma_{fs} = \frac{\sigma_{ff} + \sigma_{ss}}{2} \tag{32}$$

$$z' = z + \sigma_{ss}/2 \tag{33}$$

The potential energy is related to the fugacity, as

$$f_{ff}(z) = f_b\,\exp\left(-\frac{\Psi(z) + \Psi(L - z)}{kT}\right) \tag{34}$$

The fugacity expressions for the PR EOS are given by Equations 25 and 26. The formulas for a(z) given below depend on the ratio of the slit width L and the molecular diameter σ_{ff}. To obtain these formulas, one integrates the sum of all the two body interactions between an arbitrarily selected central molecule and all the other molecules around it. After the density profile along the slit is computed, the Gibbs adsorption Γ is numerically integrated, as expressed by Equation 29.

To calculate the Gibbs adsorption, the area SA and the slit width L must be regressed from experimental data. These parameters are not necessarily constant because matrix swelling makes them vary with pressure (and density.) A simple empirical model was chosen to represent the change in slit width L with density,

$$L(\rho_b) = L_s\rho_b + L_A \tag{35}$$

The empirical parameter L_s is the rate of change of slit width with bulk density, which was used only to improve carbon dioxide and ethane predictions.

A key feature of SLD theory is that it predicts the Gibbs excess, not absolute adsorption. To calculate the absolute adsorption, one must assume the adsorbed phase density or volume. Past researchers have assumed that the phase density is close to the van der

Waals co-volume. This assumption creates uncertainty in the absolute adsorption. In comparison, SLD uses only the Gibbs excess, which does not rely on phase density assumptions, to obtain model parameters. Furthermore, SLD may be used to predict an average adsorbed phase density as a function of pressure:

Equations for the Local Attractive Parameter a(z)

Region	**Case 1:** $\frac{L}{\sigma_{ff}} \geq 3$
$0.5 \leq \frac{z}{\sigma_{ff}} \leq 1.5$	$\frac{a(z)}{a_b} = \frac{3}{8}\left(\frac{z}{\sigma_{ff}} + \frac{5}{6} - \frac{1}{3\left(\frac{L-z}{\sigma_{ff}} - 0.5\right)^3}\right)$
$1.5 \leq \frac{z}{\sigma_{ff}} \leq \frac{L}{\sigma_{ff}} - 1.5$	$\frac{a(z)}{a_b} = \frac{3}{8}\left(\frac{8}{3} - \frac{1}{3\left(\frac{z}{\sigma_{ff}} - 0.5\right)^3} - \frac{1}{3\left(\frac{L-z}{\sigma_{ff}} - 0.5\right)^3}\right)$
$\frac{L}{\sigma_{ff}} - 1.5 \leq \frac{z}{\sigma_{ff}} \leq \frac{L}{\sigma_{ff}} - 0.5$	$\frac{a(z)}{a_b} = \frac{3}{8}\left(\frac{L-z}{\sigma_{ff}} + \frac{5}{6} - \frac{1}{3\left(\frac{z}{\sigma_{ff}} - 0.5\right)^3}\right)$
	Case 2: $2 \leq \frac{L}{\sigma_{ff}} \leq 3$
$0.5 \leq \frac{z}{\sigma_{ff}} \leq \frac{L}{\sigma_{ff}} - 1.5$	$\frac{a(z)}{a_b} = \frac{3}{8}\left(\frac{z}{\sigma_{ff}} + \frac{5}{6} - \frac{1}{3\left(\frac{L-z}{\sigma_{ff}} - 0.5\right)^3}\right)$
$\frac{L}{\sigma_{ff}} - 1.5 \leq \frac{z}{\sigma_{ff}} \leq 1.5$	$\frac{a(z)}{a_b} = \frac{3}{8}\left(\frac{L}{\sigma_{ff}} - 1\right)$
$1.5 \leq \frac{z}{\sigma_{ff}} \leq \frac{L}{\sigma_{ff}} - 0.5$	$\frac{a(z)}{a_b} = \frac{3}{8}\left(\frac{L-z}{\sigma_{ff}} + \frac{5}{6} - \frac{1}{3\left(\frac{z}{\sigma_{ff}} - 0.5\right)^3}\right)$
	Case 3: $1.5 \leq \frac{L}{\sigma_{ff}} \leq 2$
Anywhere within slit	$\frac{a(z)}{a_b} = \frac{3}{8}\left(\frac{L}{\sigma_{ff}} - 1\right)$

$$\bar{\rho}_{ads} = \frac{\Gamma^{ex}}{L} + \rho_b \tag{36}$$

This average adsorbed phase density can be applied then to calculate the absolute adsorption:

$$n_{abs} = \frac{\Gamma^{ex}}{\left(1 - \frac{\rho_{bulk}}{\bar{\rho}_{ads}}\right)} \tag{37}$$

(d) Model Evaluation Results

Pure Gas Adsorption

Tables 21-22 present a summary of our model evaluation results for five models we have used to correlate the present adsorption data for methane, nitrogen, and CO_2 on Fruitland and Illinois-6 coals, respectively. The models include the Langmuir and LCR correlations, the ZGR and PGR 2-D EOS, and two forms of the PR-SLD model. The model parameters, shown in Tables 22-23, were determined by minimizing the sum of squares of percentage absolute errors in the calculated adsorption, ω, for the pure gas of interest. The quality of the fit, expressed in terms of the absolute average deviation (%AAD), is given in Table 21. Figures 21-24 illustrate the abilities of the LRC, the PGR EOS, and SLD model to describe the present pure-fluid adsorption data.

Our results indicate that the LRC produces better quality fit than the Langmuir correlation for the three gases studied (within 2% AAD), reflecting in part the use of one additional parameter (η_i) in the regressions. Detailed LRC correlation results for Fruitland coal are presented in Table 24. Similarly, Table 25 presents the results for Illinois-6 coal.

The summary results also reveal the ability of the ZGR EOS to represent the present systems well within their expected experimental uncertainty. As shown in Tables 26and 27, the ZGR EOS represent the adsorption on wet Fruitland coal within 2.0% AAD and yields slightly worse fit (3% AAD) for wet Illinois-6. Comparable results are obtained using the PGR EOS, as given in Table 28.

The flat-surface PR-SLD model exhibits good representation for methane adsorption comparable to the LRC, but it exhibits larger deviations for the nitrogen and CO_2 (2.9% and 5.1%, respectively). The regression results for the flat-surface SLD model are given in Table 29-30 for the Fruitland coal and Illinois-6 coal, respectively.

The summary results and model parameters for the slit PR-SLD model are presented in Table 23. Average deviations within 9% are observed for the all fluids considered. In contrast to other models, including the flat-surface PR-SLD, the slit PR-SLD correlates

the adsorption data over the full range pressure, including CO_2 and ethane. However, Figures 22-24 and %AAD in Table 23 indicate that the quality of representation for methane and nitrogen is better than that obtained for the near-critical CO_2 and ethane. The PR-SLD model results are not surprising in light of the assumptions made regarding the structure of the coal surface and the accuracy of the density predictions from of the PR EOS. Work is in progress to improve the SLD predictions for highly non-ideal adsorption systems, such as CO_2. Specifically, we anticipate significant gains by (a) modifying the local attractive parameter a(z); and (c) incorporating an equation of state capable of producing accurate phase densities predictions.

Our results to date indicate that the SLD model may be a suitable choice for modeling the coalbed gas adsorption and CO_2 sequestering. However, model improvements are required to (a) account for coal heterogeneity and structure complexity, and (b) provide for more accurate equations of state, which are capable of modeling coalbed gas environments. In addition, future work will also address the competitive adsorption of mixed gases on coal.

Binary Mixture Data Correlation

The results of the binary adsorption data correlation are shown in Tables 31-32 and a sample illustration in Figure 25. Our results for different binary mixtures show that the LRC model can describe component adsorption data at some compositions within 5%; however, deviations of up to 30% are observed for the component adsorption in methane/nitrogen mixture. In comparison, the LRC model can correlate the total mixture adsorption of all the mixtures considered within 5%.

The regression results for the ZGR EOS are shown in the Table 32. Similar to the LRC model, the total adsorption are represented within 5%, but the individual component adsorption produce up to 30% deviations. Nevertheless, for the data considered here, the ZGR EOS yielded better correlation results than the LRC correlation.

(e) BWR EOS Development

As outlined earlier in the experimental procedure, accurate compressibility (Z) factors are required for analyzing our adsorption data for methane, ethane, nitrogen and CO_2 and their mixtures. A careful evaluation of the current literature led us to conclude that an adequate predictive capability for the mixture Z factors does not exist. This is in clear contrast to the availability of highly accurate equations of state for pure-fluid compressibility factors [20-22]. Therefore, we have elected to develop such a capability using the Benedict-Webb-Rubin (BWR) equation of state. Specifically, we have used the available pure-fluid and binary mixture data to refit the BWR equation and improve its accuracy significantly.

The original BWR equation of state is given as:

$$Z = 1 + \left(B_0 - \frac{A_0}{RT} - \frac{C_0}{RT^3} \right)\rho + \left(b - \frac{a}{RT} \right)\rho^2 + \frac{a\alpha}{RT}\rho^5 + \frac{c\rho^2}{RT^3}\left(1 + \gamma\rho^2\right)e^{-\gamma\rho^2} \qquad (38)$$

where T is temperature; ρ is density; R is the gas constant; a-c, A-C, α-γ are EOS parameters. To extend the BWR to mixtures, the flowing mixing rules suggested by Bishnoi et al. [23] are employed:

$$B_0 = \sum_{i=1}^{n}\sum_{j=1}^{n} x_i x_j B_{0ij} \qquad \text{where } B_{0ij} = \sqrt{B_{0i}B_{0j}}$$

$$A_0 = \sum_{i=1}^{n}\sum_{j=1}^{n} x_i x_j A_{0ij} \qquad A_{0ij} = \sqrt{A_{0i}A_{0j}}(1-k_{ij})$$

$$C_0 = \sum_{i=1}^{n}\sum_{j=1}^{n} x_i x_j C_{0ij} \qquad C_{0ij} = \sqrt{C_{0i}C_{0j}}(1-k_{ij})^3$$

$$b = \sum_{i=1}^{n}\sum_{j=1}^{n}\sum_{k=1}^{n} x_i x_j x_k (b_{ij}b_{jk}b_{ik})^{1/3} \qquad b_{ij} = \sqrt{b_i b_j}$$

$$a = \sum_{i=1}^{n}\sum_{j=1}^{n}\sum_{k=1}^{n} x_i x_j x_k (a_{ij}a_{jk}a_{ik})^{1/3} \qquad a_{ij} = \sqrt{a_i a_j}(1-k_{ij})$$

$$c = \sum_{i=1}^{n}\sum_{j=1}^{n}\sum_{k=1}^{n} x_i x_j x_k (c_{ij}c_{jk}c_{ik})^{1/3} \qquad c_{ij} = \sqrt{c_i c_j}(1-k_{ij})^3$$

$$\alpha = \sum_{i=1}^{n}\sum_{j=1}^{n}\sum_{k=1}^{n} x_i x_j x_k (\alpha_{ij}\alpha_{jk}\alpha_{ik})^{1/3} \qquad \alpha_{ij} = \sqrt{\alpha_i \alpha_j}$$

$$\gamma = \sum_{i=1}^{n}\sum_{j=1}^{n} x_i x_j \gamma_{ij} \qquad \gamma_{ij} = \sqrt{\gamma_i \gamma_j} \qquad (39)$$

In the above equations, n is the number of components, x is the mole fraction, and k_{ij} is the binary interaction parameter. Following customary notation [1], for a given parameter β, $\beta_{ii} = \beta_i$, and the pure-fluid interaction parameters are equal zero (or $k_{ii} = k_{jj} = 0$).

Table 33 details the sources of pure-fluid and binary experimental data used in our BWR regressions, along with the temperature, pressure and composition range for each system. To meet the specific needs of our experiments, the data selected for this task range in temperature from 300 to 350 K and extend in pressure to 2000 psia.

Table 34 presents the new BWR EOS parameters. These parameters were generated by a simultaneous regression of the pure-fluid parameters and the binary interaction parameters. Figures 26-28 illustrate the quality of the fits obtained for the various binaries. As indicated by the figures, the deviations in the Z factor are within 0.1% and 0.15% for the methane/nitrogen and methane/carbon dioxide binaries, respectively. However, for nitrogen/carbon dioxide, while most of the deviations are within 0.2%, some are within 0.6%.

It should be noted that a sequential regression of the pure parameters followed by a regression of the binary parameters did not yield the required level of accuracy for the binary mixtures.

D. Penn State Collaboration

The progress report for the Penn State portion of this project is attached on Page 85 in a form of an independent manuscript.

E. Conclusions

Following is a summary of our accomplishments and conclusions:

- A second adsorption apparatus was assembled, which has essentially doubled our rate of data acquisition.
- We have measured the adsorption behavior of pure CO_2, methane, ethane, nitrogen and some of their binary mixtures on wet Fruitland coal, wet Illinois-6 and dry activated carbon at temperatures at 319.3 K (115 °F) and pressures to 12.4 MPa (1800 psia). The pure-fluid adsorption isotherms show an expected uncertainty of about 3%, and the binary measurements yield an expected uncertainty that varies from 2 to 9%. The current measurements showed good agreement with literature data and with measurements obtained previously.

  The newly-acquired data constitute a valuable addition to the literature, especially the Illinois-6 adsorption isotherms and measurements involving ethane, which are a new addition to the existing database.

- Our additional adsorption measurements on Fruitland coal and on activated carbon show that: (a) the Gibbs adsorption isotherm for CO_2 under study exhibits typical adsorption behavior for supercritical gas adsorption, and (b) a slight variation from Type I absolute adsorption may be observed for CO_2, but the variation is sensitive to the estimates used for adsorbed phase density.

- We have evaluated the predictive capabilities of various adsorption models, including the Langmuir/loading ratio correlation, a two-dimensional cubic equation of state (EOS), a new two-dimensional (2-D) segment-segment interactions equation of state, and the simplified local density model (SLD). Our model development efforts have focused on developing the 2-D analog to the Park-Gasem-Robinson (PGR) EOS and an improved form of the SLD model. The new PGR EOS offers two advantages: (a) it has a more accurate repulsive term, which is important for reliable adsorption predictions, and (b) it is a segment-segment interactions model, which should more closely describe the gas-coal interactions during the adsorption process. Similarly, a slit form of the SLD model was refined to account more precisely for heterogeneity of the coal surface and matrix swelling.

  In general, all models performed well for the Type I adsorption exhibited by methane, nitrogen, and carbon dioxide up to 8.3 MPa (average deviations within 2%). In comparison, the SLD model represented the adsorption behavior of all fluids considered within 5% average deviations, including the near-critical behavior of carbon dioxide beyond 8.3 MPa (1200 psia). Work is in progress to (a) derive and implement the micropore form of the SLD model, which would expand the number of structural geometries used to represent the heterogeneity of coal surface; and (b) extend the SLD model to mixture predictions.

- Accurate gas-phase compressibility (Z) factors are required for methane, ethane, nitrogen and carbon dioxide and their mixtures to properly analyze our experimental

adsorption data. A careful evaluation of the current literature, led us to conclude that an adequate predictive capability for the mixture Z factors does not exist. Therefore, we elected to develop such a capability using the Benedict-Webb-Rubin (BWR) equation of state. Specifically, we have used the available pure-fluid and binary mixture data to refit the BWR equation and improve its accuracy significantly; in general, the new BWR EOS parameters yield deviations in the Z factor within 0.2% for the mixtures of interest in the present work.

- At Pennsylvania State University, we completed determining CO_2 and methane adsorption properties for six coals of different rank. The coals used in this study are from the Argonne Premium sample bank, covering the rank range from lignite to low-volatile bituminous, including Beulah (lignite), Smith Roland (subbituminous), Illinois-6 (high-volatile bituminous), Pittsburgh-8 (high-volatile bituminous), Stockton-Lewiston (medium-volatile bituminous), and Pocahontas (low-volatile bituminous).

  Significant differences in CO_2 sequestration ability have been observed for different coals. Furthermore, when these differences are compared to the relative affinities of coals for CO_2 vs. methane, it is concluded that they are mostly due to differences in CO_2 uptakes on different coals.

F. References

1. Seidle, J. P., Jeansonne, M. W., and Erickson, D. J., *Application of Matchstick Geometry to Stress Dependent Permeability in Coals*, SPE Paper 24361, presented at the Rocky Mountains Regional Meeting, Casper, WY, May 18-21, 1992.

2. Hall, F. E., Zhou, Chunhe, Gasem, K. A. M., and Robinson, Jr., R. L., *Adsorption of Pure Methane, Nitrogen, and Carbon Dioxide and their Binary Mixtures on Wet Fruitland Coal*, SPE Paper 29194, presented at the 1994 Eastern Regional Conference & Exhibition, Charleston, West Virginia, November 8-10, 1994.

3. Hall, F. E., *Adsorption of Pure and Multicomponent Gases on Wet Fruitland Coal*, M. S. Thesis, Oklahoma State University, December 1993.

4. Kapoor, A., Ritter, J. A., and Yang, R. T., *An Extended Langmuir Model for Adsorption of Gas Mixtures on Heterogeneous Surfaces*, Langmuir 6 660-664 (1990).

5. Arri, L. E., and Yee, D., *Modeling Coalbed Methane Production With Binary Gas Sorption*, SPE Paper 24363, presented at the SPE Rocky Mountain Regional Meeting, Casper, Wyoming, May 18-21, 1992.

6. Myers, A. L., and Prausnitz, J. M., *Thermodynamics of Mixed-Gas Adsorption*, AIChE J. 11 121-129 (1965).

7. Stevenson, M. D., Pinczewski, W. V., Somers, M. L., and Bagio, S. E., *Adsorption/Desorption of Multicomponent Gas Mixtures on Coal at In-Seam Conditions*, SPE Paper 23026, presented at the SPE Asia-Pacific Conference, Perth, Western Australia, November 4-7, 1991.

8. Danner, R. P., and Choi, E. C. F., *Mixture Adsorption Equilibria of Ethane and Ethylene on 13X Molecular Sieves,* Ind. Eng. Chem. Fundam. 17 248-253 (1978).

9. Suwanayuen, S., and Danner, R. P., *Vacancy Solution Theory of Adsorption From Gas Mixtures,* AIChE J 26 76-83 (1980).

10. DeGance, A. E., *Multicomponent High-Pressure Adsorption Equilibria on Carbon Substrates: Theory and Data*, Fluid Phase Equilibria, 78 99-137 (1992).

11. Chaback, J. J., Yee, D., Volz, R. R., Seidle, J. P., and Puri, R., *Method for Treating a Mixture of Gaseous Fluids within a Solid Carbonaceous Subterranean Formation*, U. S. Patent 5,439,054.

12. Zhou, C., Gasem, K. A. M., and Robinson, Jr., R. L., *Predicting Gas Adsorption Using Two-Dimensional Equations of State*, I&EC Research 33 1280-1289 (1994).

13. Ross, S., and Oliver, J. P., On Physical Adsorption, Interscience Publ., New York, 1964.

14. Rangarajan, B., Lira, T. C., and Subramanian, R., *Simplified Local Model for Adsorption over Large Pressure Ranges,* AIChE J., 41 838-845 (1995).

15. Liang, E., *Adsorption of Pure and Multicomponent Gases on Wet Fruitland Coal*, M. S. Thesis, Oklahoma State University, July 1999.

16. Tomasko, D., Personal Communication, December 1999.

17. Chen, J. H., et al., *Adsorption and Desorption of Carbon Dioxide onto and from Activated Carbon at High Pressures*, Ind. Eng. Chem. Res., 36, 2808-2815 (1997).

18. Reid, R. C.; Prausnitz, J. M.; Poling, B. E. *The Properties of Gases and Liquids*, 4th ed.; McGraw-Hill: New York, 1987.

19. Span, R. and Wagner; W., *A New Equation of State for Carbon Dioxide Covering the Fluid Region from the Triple Point Temperature to 1100 K at Pressures up to 800 MPa*, J. Phys. Chem. Ref. Data, 25, 1509-1590 (1996).

20. International Thermodynamic Tables of the Fluid State: Carbon Dioxide, International Union of Pure and Applied Chemistry (1976).

21. International Thermodynamic Tables of the Fluid State: Methane, International Union of Pure and Applied Chemistry (1978).

22. Younglove, B. A., *Thermophysical Properties of Fluids. I. Argon, Ethylene, Parahydrogen, Nitrogen, Nitrogen Trifluoride, and Oxygen*, J. Phys. Chem. Ref. Data. Vol. 11, Suppl. 1, (1982).

23. Bishnoi, P. R. and Robinson, D. B., *Mixing Rules improve BWR Use,* Hydrocarbon Processing, November, 152-156 (1972).

24. Keyes, F. G. and Burks, H. G., *The Equation of State for Binary Mixtures of Methane and Nitrogen,* J. Am. Chem. Soc., 50, 1100-1106 (1928).

25. Brugge, H. B, Holste, J. C., and Hall, K. R., Gammon, B. E. and Marsh, K. N., *Densities of Carbon Dioxide + Nitrogen from 225 K to 450 K at Pressures up to 70 MPa,* J. Chem. Eng. Data, 42, 903-907 (1997).

26. Hwang, C. A., Iglesias-Silva, G. A., Holste, J. C., and Hall, K. R., Gammon, B. E. and Marsh, K. N., *Densities of Carbon Dioxide + Methane Mixtures from 225 K to 350 K at pressures up to 35 MPa,* J. Chem. Eng. Data, 42, 897-899 (1997).

Table 1. Status of Experimental Program

Solid Matrix / Gas	Carbon Dioxide	Methane	Ethane	Nitrogen	Binary Mixtures
Fruitland Coal-OSU#2	Done	Done	Done	Done	Done
Illinois-6 Coal	Done	Done	----	Done	Underway
DESC-8 Coal	Year 3	Year 3	Year 3	Year 3	Year 3
Activated Carbon	Done	Done	Done	Done	

Table 2. Compositional Analyses of Coals Used in This Study*

Analysis	Fruitland Amoco	Fruitland OSU #1	Fruitland OSU #2	Illinois-6
Ultimate				
Carbon %	68.56	68.63	66.34	71.47
Hydrogen %	5.74	4.27	4.25	5.13
Oxygen %	7.19	0.89	5.38*	9.85
Nitrogen %	1.40	1.57	1.46	1.46
Sulfur %	0.65	4.19	0.72	1.27
Ash %	16.45	20.45	21.92	10.81
Proximate				
Vol. Matter %	19.12	20.2	20.26	30.61
Fixed Carbon %	64.42	59.35	57.54	55.90

*** Characterization of OSU#3 Fruitland coal is underway**

Table 3. Analysis of BPL Activated Carbon Used in This Study

Analysis	Unit	Value	Lower Limit	Upper Limit
Abrasion Number		87	75	-
Apparent Density	g/cc	0.53	0.44	-
Ash	%	7	-	9
Effective Size	mm	0.64	0.55	0.75
Iodine Number	mg/g	1046	1000	-
US Sieve Series on 12	%	1	-	5
US Sieve Series –40 Mesh	%	1	-	4
Fixed Carbon		1.7	-	1.9

Table 4. Pure Nitrogen Gibbs Adsorption on Fruitland Coal-OSU#2 at 115°F Using Second Apparatus

Run 1 (14.0% Moisture)		Run 2 (10.2% Moisture)	
Pressure (psia)	Adsorption (mmole/g coal)	Pressure (psia)	Adsorption (mmole/g coal)
215.7	0.0934	205.8	0.09791
397.8	0.1491	420.5	0.1680
598.9	0.2055	605.7	0.2151
800.4	0.2483	813.1	0.2613
1000.3	0.2903	1000.2	0.2958
1203.6	0.3251	1206.0	0.3296
1400.2	0.3602	1413.5	0.3646
1599.8	0.3900	1590.2	0.3896
1799.4	0.4180		

Table 5. Pure Carbon Dioxide Adsorption on Fruitland Coal-OSU#2 at 115°F Using Second Apparatus

Run 1 (7.7% Moisture)		Run 2 (7.5% Moisture)	
Pressure (psia)	Adsorption (mmole/g coal)	Pressure (psia)	Adsorption (mmole/g coal)
189.4	0.5975	221.0	0.6437
443.3	0.8260	426.0	0.8147
610.4	0.8877	632.9	0.9086
825.7	0.9185	821.6	0.9459
1007.9	0.9157	1027.7	0.9412
1195.8	0.8838	1206.9	0.9256
1335.0	0.8480	1412.2	0.8220
1515.9	0.7194	1603.4	0.5982
1792.3	0.4222	1790.4	0.4087

Table 6. Pure Carbon Dioxide Gibbs Adsorption on Dry Activated Carbon at 113 °F

Apparatus 1 Run 1		Apparatus 1 Run 2		Apparatus 2 Run 1		Apparatus 2 Run 2	
Pressure (psia)	Gibbs Adsorption (mmol/g)	Pressure (psia)	Gibbs Adsorption (mmol/g)	Pressure (psia)	Gibbs Adsorption (mmol/g)	Pressure (psia)	Gibbs Adsorption (mmol/g)
56.1	3.161	52.2	2.962	72.9	3.570	86.1	3.831
106.9	4.344	105.9	4.170	160.4	5.053	167.4	5.051
174.1	5.242	172.6	5.064	279.5	6.036	274.6	5.878
254.1	5.908	259.6	5.783	394.1	6.510	381.1	6.343
363.2	6.466	365.1	6.300	579.3	6.908	503.7	6.682
474.3	6.799	478.2	6.650	793.7	7.037	716.2	6.892
620.5	7.024	622.8	6.962	993.8	6.867	861.6	6.873
799.6	7.076	806.3	7.078	1203.6	6.328	992.1	6.748
1013.8	6.857	1017.4	6.882	1321.9	5.425	1153.9	6.395
1199.2	6.267	1203.1	6.348	1493.2	3.864	1253.8	5.993
1413.2	4.395	1398.2	4.810	1678.9	3.051	1330.2	5.434
1600.6	3.236	1603.4	3.449	1886.7	2.604	1452.7	4.188
1969.5	2.485	1937.9	2.638			1611.1	3.335
						1870.8	2.706

Table 7. Pure Ethane Adsorption on Activated Carbon at 113 °F

Run 1			Run 2		
Pressure (psia)	**Gibbs Adsorption (mmol/g)**	**Absolute Adsorption (mmol/g)**	**Pressure (psia)**	**Gibbs Adsorption (mmol/g)**	**Absolute Adsorption (mmol/g)**
22.1	2.807	2.817			
76.6	3.839	3.892	73.0	3.806	3.855
158.7	4.421	4.552	181.0	4.449	4.603
259.5	4.663	4.908	330.1	4.694	5.026
432.0	4.769	5.257	513.8	4.721	5.351
640.2	4.613	5.538	702.5	4.466	5.580
805.2	4.131	5.747	906.0	2.975	5.457
959.5	2.583	5.607	1097.3	1.741	4.728
1190.3	1.788	5.344	1311.4	1.381	4.543
1513.9	1.408	5.280	1556.6	1.149	4.405
1937.3	1.169	5.415	1922.6	1.027	4.715

Table 8. Pure Methane Adsorption on Activated Carbon at 113°F

Run 1			Run 2		
Pressure (psia)	Gibbs Adsorption (mmol/g)	Absolute Adsorption (mmol/g)	Pressure (psia)	Gibbs Adsorption (mmol/g)	Absolute Adsorption (mmol/g)
85.0	1.975	1.991	80.1	1.870	1.885
192.9	2.861	2.917	179.0	2.762	2.812
361.4	3.547	3.683	370.1	3.586	3.728
514.7	3.889	4.108	505.2	3.891	4.106
689.7	4.113	4.436	696.3	4.145	4.474
906.2	4.256	4.715	896.0	4.283	4.739
1111.1	4.292	4.885	1107.5	4.339	4.936
1303.6	4.286	5.008	1309.7	4.337	5.072
1503.3	4.247	5.107	1504.3	4.286	5.154
1718.6	4.163	5.168	1705.7	4.209	5.216
1916.0	4.077	5.216	1921.7	4.106	5.259

Table 9. Pure Nitrogen Adsorption on Activated Carbon at 113 °F

Run 1			Run 2		
Pressure (psia)	Gibbs Adsorption (mmol/g)	Absolute Adsorption (mmol/g)	Pressure (psia)	Gibbs Adsorption (mmol/g)	Absolute Adsorption (mmol/g)
100.7	0.996	1.005	129.7	1.190	1.204
250.9	1.741	1.782	262.5	1.795	1.839
415.4	2.224	2.311	405.8	2.217	2.301
594.9	2.566	2.711	607.3	2.600	2.751
801.9	2.823	3.042	806.7	2.841	3.063
1011.0	2.990	3.288	1009.5	3.005	3.304
1204.6	3.086	3.459	1202.4	3.105	3.480
1401.0	3.155	3.604	1407.5	3.173	3.628
1609.6	3.199	3.731	1623.4	3.214	3.754
1807.8	3.199	3.805	1806.3	3.229	3.840
1981.2	3.197	3.869	1979.7	3.235	3.914

Table 10. Pure Nitrogen Adsorption on Wet Illinois-6 Coal at 115°F

Run 1 (15.6% Moisture)			Run 2 (14.6% Moisture)		
Pressure (psia)	Gibbs Adsorption (mmol/g)	Absolute Adsorption (mmol/g)	Pressure (psia)	Gibbs Adsorption (mmol/g)	Absolute Adsorption (mmol/g)
114.5	0.0207	0.0209	99.9	0.0217	0.0219
203.8	0.0344	0.0351	202.9	0.0386	0.0395
401.5	0.0656	0.0681	403.6	0.0689	0.0720
603.9	0.0892	0.0943	625.5	0.0944	0.1012
810.8	0.1083	0.1168	803.6	0.1102	0.1206
1003.7	0.1240	0.1362	996.3	0.1259	0.1410
1204.4	0.1355	0.1518	1199.7	0.1353	0.1552
1405.5	0.1476	0.1687	1405.7	0.1505	0.1769
1600.5	0.1577	0.1837	1600.1	0.1593	0.1918
1801.1	0.1692	0.2010	1799.0	0.1672	0.2062

Table 11. Pure Methane Adsorption on Wet Illinois-6 Coal at 115°F

Run 1 (13.6% Moisture)			Run 2 (12.6% Moisture)		
Pressure (psia)	Gibbs Adsorption (mmol/g)	Absolute Adsorption (mmol/g)	Pressure (psia)	Gibbs Adsorption (mmol/g)	Absolute Adsorption (mmol/g)
99.8	0.0843	0.0852	98.3	0.1000	0.1010
204.4	0.1425	0.1455	202.6	0.1415	0.1445
395.8	0.2136	0.2226	398.8	0.2145	0.2237
604.5	0.2656	0.2836	604.2	0.2739	0.2923
801.8	0.3007	0.3287	806.5	0.2959	0.3237
1001.8	0.3220	0.3611	1004.0	0.3186	0.3574
1206.0	0.3328	0.3836	1207.2	0.3377	0.3893
1371.5	0.3480	0.4104	1401.9	0.3473	0.4114
1600.9	0.3591	0.4378	1601.7	0.3538	0.4314
1807.9	0.3707	0.4662	1798.7	0.3590	0.4508

Table 12. Pure Carbon Dioxide Adsorption on Illinois #6 Coal at 115 °F

Run 1 (5.7% Moisture)			Run 2 (5.5% Moisture)		
Pressure (psia)	Gibbs Adsorption (mmol/g)	Absolute Adsorption (mmol/g)	Pressure (psia)	Gibbs Adsorption (mmol/g)	Absolute Adsorption (mmol/g)
105.9	0.2992	0.3023	88.7	0.2581	0.2604
209.7	0.4245	0.4339	200.4	0.4147	0.4235
400.0	0.5826	0.6094	396.4	0.5720	0.5980
606.5	0.6800	0.7329	604.0	0.6935	0.7472
805.2	0.7412	0.8289	795.4	0.7513	0.8384
999.2	0.7788	0.9148	1000.9	0.8057	0.9469
1194.5	0.7946	1.0102	1202.6	0.7956	1.0161
1366.3	0.7680	1.1283	1345.9	0.7522	1.0783
1516.9	0.6840	1.2409	1500.6	0.6742	1.1981
1738.6	0.6043	1.3251	1746.5	0.5863	1.2920

Table 13. Methane/Carbon Dioxide Mixture Adsorption on Wet Fruitland Coal-OSU#2 at 115 °F

Pressure (psia)	Methane Gas Mole Fraction	Methane Adsorption (mmole/g coal)	Carbon Dioxide Adsorption (mmole/g coal)
Methane Feed Composition: 80% (9.7% moisture)			
105.0	0.8921	0.1648	0.0792
207.8	0.8810	0.2464	0.1282
401.0	0.8774	0.3354	0.2102
605.4	0.8702	0.3970	0.2751
810.2	0.8612	0.4411	0.3135
1008.5	0.8536	0.4756	0.3461
1204.8	0.8461	0.5163	0.3601
1404.3	0.8377	0.5571	0.3590
1603.2	0.8302	0.6042	0.3612
1805.8	0.8261	0.6347	0.3709
Methane Feed Composition: 60% (9.6% moisture)			
107.6	0.7787	0.1283	0.1526
209.4	0.7625	0.1860	0.2502
403.5	0.7521	0.2340	0.3927
602.2	0.7323	0.2636	0.4896
807.9	0.7165	0.2901	0.5620
1005.5	0.7048	0.3121	0.6117
1206.8	0.6921	0.3435	0.6231
1404.9	0.6831	0.3685	0.6427
1605.3	0.6731	0.4040	0.6535
1801.0	0.6662	0.4210	0.6617

Table 14. Methane/Carbon Dioxide Mixture Adsorption on Wet Fruitland Coal-OSU#2 at 115°F (Continued)

Pressure (psia)	Methane Gas Mole Fraction	Methane Adsorption (mmole/g coal)	Carbon Dioxide Adsorption (mmole/g coal)
Methane Feed Composition: 40% (9.2% moisture)			
111.4	0.5916	0.0774	0.2204
208.2	0.5850	0.0957	0.3466
410.2	0.5826	0.1065	0.5935
602.7	0.5512	0.1313	0.7152
802.1	0.5288	0.1508	0.8039
1002.8	0.5148	0.1623	0.8851
1203.8	0.5009	0.1833	0.9351
1402.2	0.4865	0.2224	0.9439
1601.5	0.4768	0.2555	0.9572
1801.6	0.4700	0.2822	0.9721
Methane Feed Composition: 20% (7.6 % moisture)			
112.0	0.3318	0.0445	0.3744
207.7	0.3089	0.0586	0.5422
398.2	0.2950	0.0651	0.8094
608.6	0.2764	0.0619	0.9535
804.8	0.2607	0.0688	1.0383
1006.1	0.2486	0.0764	1.1001
1203.8	0.2386	0.0854	1.1250
1400.0	0.2308	0.1020	1.1566
1600.3	0.2253	0.1143	1.1911
1790.0	0.2202	0.1477	1.2403

Table 15. Methane/Nitrogen Mixture Adsorption on Wet Fruitland Coal-OSU#2 at 115 °F

Pressure (psia)	Methane Gas Mole Fraction	Methane Adsorption (mmole/g coal)	Nitrogen Adsorption (mmole/g coal)
Methane Feed Composition: 80% (8.5% moisture)			
105.1	0.7424	0.1411	0.0164
208.8	0.7483	0.2363	0.0249
405.3	0.7525	0.3664	0.0287
606.2	0.7577	0.4633	0.0311
808.2	0.7640	0.5331	0.0379
1005.2	0.7697	0.5836	0.0480
1205.8	0.7720	0.6358	0.0499
1402.0	0.7742	0.6792	0.0534
1605.2	0.7762	0.7135	0.0564
1803.2	0.7802	0.7336	0.0768
Methane Feed Composition: 60% (8.7% moisture)			
108.8	0.5442	0.1010	0.0333
208.1	0.5535	0.1654	0.0525
402.2	0.5639	0.2547	0.0820
601.5	0.5678	0.3298	0.0973
808.1	0.5699	0.3943	0.1036
1004.5	0.5728	0.4423	0.1136
1209.3	0.5780	0.4752	0.1299
1408.0	0.5810	0.5092	0.1377
1605.1	0.5835	0.5311	0.1487
1801.8	0.5848	0.5705	0.1594

Table 16. Methane/Nitrogen Mixture Adsorption on Wet Fruitland Coal-OSU#2 at 115 °F (Continued)

Pressure (psia)	Methane Gas Mole Fraction	Methane Adsorption (mmole/g coal)	Nitrogen Adsorption (mmole/g coal)
Methane Feed Composition: 40% (9.4% moisture)			
109.7	0.3326	0.0672	0.0368
202.6	0.3435	0.1166	0.0697
409.4	0.3539	0.1820	0.0987
612.2	0.3606	0.2366	0.1227
808.7	0.3662	0.2757	0.1487
1011.1	0.3719	0.3082	0.1764
1213.9	0.3769	0.3254	0.1984
1404.6	0.3792	0.3551	0.2141
1605.7	0.3825	0.3670	0.2373
1805.0	0.3841	0.4000	0.2526
Methane Feed Composition: 20% (8.1% moisture)			
115.2	0.1481	0.0388	0.0478
207.8	0.1526	0.0645	0.0769
404.1	0.1581	0.1106	0.1223
603.7	0.1634	0.1473	0.1592
800.2	0.1683	0.1741	0.1870
1002.4	0.1731	0.1948	0.2160
1205.0	0.1753	0.2177	0.2354
1402.4	0.1792	0.2289	0.2621
1600.2	0.1828	0.2345	0.2839
1803.5	0.1854	0.2448	0.3264

Table 17. Nitrogen/Carbon Dioxide Mixture Adsorption on Wet Fruitland Coal-OSU#1 at 115 °F

Pressure (psia)	Nitrogen Gas Mole Fraction	Nitrogen Adsorption (mmole/g coal)	Carbon Dioxide Adsorption (mmole/g coal)
Nitrogen Feed Composition: 80% (10.5% moisture)			
117.4	0.9605	0.0380	0.0754
211.2	0.9491	0.0602	0.1252
402.8	0.9328	0.0989	0.2080
605.9	0.9176	0.1286	0.2695
802.5	0.9094	0.1531	0.3255
1004.2	0.9050	0.1745	0.3847
1193.3	0.9014	0.2129	0.4402
1395.0	0.8972	0.2495	0.4900
1602.0	0.8912	0.2620	0.5144
1803.0	0.8662	0.2770	0.5544
Nitrogen Feed Composition: 60% (10.0% moisture)			
116.2	0.8193	0.0271	0.1537
205.0	0.8128	0.0380	0.2542
398.7	0.8011	0.0581	0.4034
604.9	0.7753	0.0725	0.5222
806.0	0.7549	0.0837	0.6024
1006.1	0.7427	0.0882	0.6803
1208.0	0.7304	0.0990	0.7359
1405.8	0.7190	0.1176	0.7725
1606.3	0.7106	0.1322	0.8098
1805.3	0.7046	0.1433	0.8519

Table 18. Nitrogen/Carbon Dioxide Mixture Adsorption on Wet Fruitland Coal-OSU#2 at 115°F (Continued)

Pressure (psia)	Nitrogen Gas Mole Fraction	Nitrogen Adsorption (mmole/g coal)	Carbon Dioxide Adsorption (mmole/g coal)
Nitrogen Feed Composition: 40% (7.7% moisture)			
102.5	0.6664	0.0287	0.2186
202.9	0.6343	0.0375	0.3666
394.8	0.5904	0.0429	0.5582
604.5	0.5553	0.0487	0.6891
805.8	0.5293	0.0606	0.7697
1002.0	0.5132	0.0657	0.8383
1202.6	0.5004	0.0713	0.8956
1400.0	0.4898	0.0833	0.9456
1602.0	0.4791	0.1069	0.9756
1802.0	0.4744	0.1122	1.0397
Nitrogen Feed Composition: 20% (10.5% moisture)			
110.6	0.3983	0.0170	0.3363
206.5	0.3703	0.0152	0.5021
406.7	0.3240	0.0190	0.7111
605.7	0.2967	0.0249	0.8369
807.5	0.2795	0.0257	0.9222
1003.7	0.2682	0.0300	1.0065
1202.5	0.2566	0.0449	1.0596
1354.7	0.2505	0.0541	1.1069
1500.1	0.2454	0.0664	1.157
1752.0	0.2392	0.0750	1.208

Table 19. Universal Constants of PGR Equation of State

Constants	Value
τ	0.74048
U	-2.8969
W	2.6944
Q_1	10.5121
Q_2	1.0226
Z_M	0.4
ω_1	0.076354
ω_2	2.0124
ω_3	-0.22322
ω_4	-0.70301

Table 20. Pure Fluid Parameters for PGR Equation of State [6]

Component	T^*(K)	C
Methane	81.287	1.0
Nitrogen	95.0	1.0
Carbon Dioxide	111.31	1.6565

Table 21. Summary of the Model Results for Gas Adsorption on Wet Fruitland Coal at 115 °F

Model	No. Parameters	% Average Absolute Deviation				
		Methane (0-1800 psia)		Nitrogen (0-1800 psia)		Carbon Dioxide (0-1000 psia)
		Fruitland	Illnois-6	Fruitland	Illnois-6	Fruitland
Langmuir	2	2.9	3.0	2.1	2.4	2.3
LRC	2	2.0	1.6	1.7	3.2	1.6
ZGR EOS	3	1.6	1.7	1.6	3.1	1.3
PGR	3	1.8	2.0	1.8	3.5	1.8
Flat Surface PR-SLD	2	1.9	8.5	2.9	3.5	5.1
Slit PR-SLD	3	2.2	8.5	2.6	3.5	8.5 (0-1800 psia)

Table 22. Regression Results for Adsorption of Methane, Nitrogen, and Carbon Dioxide on Wet Fruitland Coal at 115 °F

Model	Model Parameters	Pure Gas Adsorbed		
		Methane (0-1800 psia)	Nitrogen (0-1800 psia)	Carbon Dioxide (0-1000 psia)
Langmuir	B_i (1/psia)	0.001953	0.000626	0.004487
	L_i (mmole/g coal)	1.099	0.7428	1.445
LCR	η_i	0.87	0.87	0.87
	B_i (1/psia)	0.003448	0.000954	0.007518
	L_i (mmole/g coal)	1.234	1.011	1.580
ZGR EOS	$\alpha_i \times 10^{-4}$	5.080	-2.261	0.8265
	β_I (g coal/mmole)	0.4298	0.001	0.1661
	$-\ln k_i$	1.779	4.736	0.4587
PGR EOS	Z_M	0.40	0.40	0.40
	V^* / A (m)	0.2675	0.4205	0.1649
	$-\ln k_i$	3.289	4.922	2.171
Flat surface PR-SLD	ε_{fs} / k (K)	44.9	24.04	49.16
	SA (m^2)	125.90	128.40	92.01

Table 23. Regression Results for the Slit Form of the SLD Adsorption Model

Model Parameters	Pure Gas Adsorbed			
	Nitrogen	**Methane**	**Carbon Dioxide**	**Ethane**
Activated Carbon				
ε_{fs}/k (K)		107.5	96.3	103.4
SA (m^2)		362	610	608
L (nm)		1.23	1.23	1.23
L_S (cc·nm/mol)		0	-25.2	-34.3
σ_{ff} (nm)		0.3758	0.3941	0.4443
RMSE (mmol/g)		0.120	0.233	0.234
AAD (%)		3.3	3.2	6.6
Wet Fruitland Coal				
ε_{fs}/k (K)	37.9	61.0	59.8	
SA (m^2)	56.1	86.2	110.0	
L (nm)	1.13	1.13	1.13	
L_S (cc·nm/mol)	0	0	-17.5	
σ_{ff} (nm)	0.3798	0.3758	0.3941	
RMSE (mmol/g)	0.0063	0.0102	0.0739	
AAD (%)	2.4	2.2	8.5	
Wet Illinois-6 Coal				
ε_{fs}/k (K)	23.7	53.2		
SA (m^2)	47.1	51.2		
L (nm)	1.38	1.38		
L_S (cc·nm/mol)	0	0		
σ_{ff} (nm)	0.3798	0.3758		
RMSE (mmol/g)	0.0036	0.013		
AAD (%)	2.6	3.5		

Table 24. LRC Model Representation of Adsorption on Fruitland Coal (h =0.87)

Component	L (mmole/g coal)	B (psia^{-1})	RMSE (mmole/g coal)	%AAD
CH_4 (Run1)	1.203	0.00367	0.0124	1.9
CH_4 (Run2)	1.249	0.00324	0.004	0.43
CH_4 (Run3)	1.258	0.00317	0.0057	0.9
CH_4 (Overall)	1.234	0.00344	0.0166	2.01
N_2 (Run1)	0.959	0.00101	0.0029	1.72
N_2 (Run2)	1.028	0.000930	0.0012	0.31
N_2 (Run3)	1.053	0.000916	0.0029	1.86
N_2 (Overall)	1.011	0.000953	0.0037	1.68
CO_2 (Run1)	1.513	0.00839	0.0088	0.92
CO_2 (Run2)	1.595	0.00738	0.0148	1.64
CO_2 Run3)	1.640	0.00684	0.0136	1.05
CO_2 (Overall)	1.580	0.00751	0.0166	1.55

Table 25. LRC Model Representation of Adsorption on Illinois-6 Coal (h =0.87)

Component	L (mmole/g coal)	B (psia^{-1})	RMSE (mmole/g coal)	%AAD
CH_4 (Run1)	0.747	0.00231	0.0042	0.93
CH_4 (Run2)	0.693	0.00267	0.0053	2.15
CH_4 (Overall)	0.719	0.00248	0.0056	1.58
N_2 (Run1)	0.744	0.000539	0.0019	3.12
N_2 (Run2)	0.698	0.000616	0.0014	1.36
N_2 (Overall)	0.719	0.000578	0.0031	3.20

Table 26. ZGR Equation of State Representation of Adsorption on Fruitland Coal

Component	a	b	– ln k	RMSE (mmole/g coal)	%AAD
CH_4 (Run1)	34992	0.3612	1.56	0.0087	0.69
CH_4 (Run2)	55500	0.4479	1.84	0.0052	0.61
CH_4 (Run3)	47546	0.4122	1.79	0.0051	0.69
CH_4 (Overall)	50800	0.4298	1.77	0.0105	1.61
N_2 (Run1)	-24030	0.0010	4.72	0.0032	1.55
N_2 (Run2)	-17878	0.0069	4.56	0.0013	0.27
N_2 (Run3)	-19101	0.0010	4.79	0.0048	1.18
N_2 (Overall)	-22611	0.0010	4.73	0.0041	1.55
CO_2 (Run1)	7333	0.1692	0.37	0.0079	0.43
CO_2 (Run2)	6208	0.1509	0.48	0.0092	0.70
CO_2 (Run3)	33100	0.2973	0.60	0.0172	0.97
CO_2 (Overall)	8265	0.1661	0.45	0.0145	1.33

Table 27. ZGR Equation of State Representation of Adsorption on Illinois-6 Coal

Component	a	b	– ln k	RMSE (mmole/g coal)	%AAD
CH_4 (Run1)	113270	0.853	2.77	0.0069	1.25
CH_4 (Run2)	40935	0.486	2.56	0.0053	1.53
CH_4 (Overall)	100760	0.802	2.69	0.0060	1.65
N_2 (Run1)	-25915	0.001	5.78	0.0028	2.02
N_2 (Run2)	-31879	0.003	5.53	0.0013	0.74
N_2 (Overall)	-19545	0.014	5.46	0.0031	3.09

Table 28. PGR Equation of State Representation of Adsorption on Wet Fruitland Coal

Component	L	$-\ln k$	RMSE (mmole/g coal)	%AAD
CH_4 (Run1)	0.284	3.16	0.0141	1.84
CH_4 (Run2)	0.259	3.34	0.0046	0.72
CH_4 (Run3)	0.262	3.33	0.0074	0.96
CH_4 (Overall)	0.267	3.28	0.0111	1.78
N_2 (Run1)	0.441	4.91	0.0045	1.61
N_2 (Run2)	0.440	4.88	0.0055	1.89
N_2 (Run3)	0.391	4.95	0.0015	0.64
N_2 (Overall)	0.420	4.92	0.0046	1.77
CO_2 (Run1)	0.174	2.08	0.0102	1.04
CO_2 (Run2)	0.165	2.15	0.0189	1.98
CO_2 (Run3)	0.155	2.25	0.0166	1.05
CO_2 (Overall)	0.164	2.17	0.0184	1.78

Table 29. SLD Model Representation of Adsorption on Fruitland Coal

Component	e_{ff} / k(K)	SA(m^2)	RMSE (mmole/g coal)	%AAD
CH_4 (Run1)	47.46	119.9	0.0134	1.21
CH_4 (Run2)	43.58	129.5	0.0076	0.86
CH_4 (Run3)	43.54	129.3	0.0084	0.83
CH_4 (Overall)	44.9	125.9	0.0122	1.94
N_2 (Run1)	24.67	122.6	0.0047	2.45
N_2 (Run2)	23.61	131.3	0.0057	3.74
N_2 (Run3)	23.2	136.4	0.0028	1.95
N_2 (Overall)	24.04	128.4	0.0055	2.86
CO_2 (Run1)	45.12	105.7	0.0479	4.99
CO_2 (Run2)	51.90	84.36	0.0422	4.27
CO_2 (Run3)	53.47	80.79	0.0490	5.75
CO_2 (Overall)	49.16	92.01	0.0474	5.13

Table 30. SLD Model Representation of Adsorption on Illinois-6 Coal

Component	e_{ff} / k(K)	SA(m^2)	RMSE (mmole/g coal)	%AAD
CH_4 (Run1)	29.51	102.6	0.0163	7.73
CH_4 (Run2)	28.61	101.8	0.0204	9.20
CH_4 (Overall)	29.05	102.2	0.0185	8.51
N_2 (Run1)	16.91	99.14	0.0025	2.01
N_2 (Run2)	18.64	90.45	0.0030	3.50
N_2 (Overall)	18.18	91.79	0.0038	3.46

Table 31. LRC Model Representation of Adsorption of Binary Mixtures

Mixture Molar Ratio	%AAD			RMSE (mmole/g coal)		
CH_4 / N_2 Mixture	CH_4	N_2	Total	CH_4	N_2	Total
20%/80%	5.59	16.12	6.82	0.00967	0.0286	0.0237
40%/60%	4.94	9.05	4.03	0.0173	0.0168	0.0152
60%/40%	3.67	7.50	3.39	0.0188	0.0109	0.0282
80%/20%	5.19	29.90	3.20	0.0369	0.0132	0.0294
Overall	4.85	15.64	4.36	0.0229	0.0187	0.0248
CH_4 / CO_2 Mixture	CH_4	CO_2	Total	CH_4	CO_2	Total
20%/80%	44.07	8.74	5.14	0.0347	0.0339	0.0459
40%/60%	43.79	5.12	7.76	0.0666	0.0289	0.0532
60%/40%	10.61	7.85	2.12	0.0348	0.0470	0.0138
80%/20%	8.80	2.99	3.62	0.0670	0.0256	0.0367
Overall	26.82	6.17	4.66	0.0532	0.0348	0.0403
N_2 / CO_2 Mixture	N_2	CO_2	Total	N_2	CO_2	Total
20%/80%	35.47	2.77	6.05	0.0202	0.0330	0.0525
40%/60%	19.26	2.68	2.11	0.0193	0.0252	0.0296
60%/40%	36.05	3.77	2.92	0.0269	0.0192	0.0157
80%/20%	17.57	12.67	4.09	0.0245	0.0281	0.0269
Overall	27.09	5.47	3.79	0.0227	0.0263	0.0312

Table 32. ZGR Equation of State Representation of Binary Mixtures

Mixture Molar Ratio	%AAD			RMSE (mmole/g coal)		
CH_4 / N_2 Mixture	CH_4	N_2	Total	CH_4	N_2	Total
20%/80%	17.58	11.05	2.89	0.0281	0.0229	0.0092
40%/60%	6.07	3.77	3.61	0.0174	0.0066	0.0140
60%/40%	3.37	10.34	4.98	0.0119	0.0093	0.0190
80%/20%	10.94	33.33	8.34	0.0505	0.0163	0.0380
Overall	9.48	14.63	4.95	0.0270	0.0138	0.0200
CH_4 / CO_2 Mixture	CH_4	CO_2	Total	CH_4	CO_2	Total
20%/80%	15.28	15.91	8.04	0.0112	0.0542	0.0607
40%/60%	12.64	7.26	5.24	0.0210	0.0549	0.0371
60%/40%	11.03	6.33	4.07	0.0297	0.0328	0.0421
80%/20%	5.46	5.83	6.17	0.0202	0.0419	0.0491
Overall	11.10	8.84	5.88	0.0206	0.0459	0.0472
N_2 / CO_2 Mixture	N_2	CO_2	Total	N_2	CO_2	Total
20%/80%	31.80	3.94	4.54	0.0100	0.0320	0.0411
40%/60%	15.24	2.96	2.97	0.0097	0.0188	0.0249
60%/40%	9.15	4.70	4.91	0.0098	0.0177	0.0213
80%/20%	3.46	4.75	3.65	0.0070	0.0157	0.0211
Overall	14.92	4.09	4.02	0.0092	0.0211	0.0271

Table 33. Database Used in BWR EOS Parameter Regressions

Fluid	Range of Data			NPTS	Reference
	Temperature (K)	Pressure (psia)	Mole Fraction (comp. 1)		
CH_4	300.0 - 350.0	3.0 - 2180.0	1.0000	27	*[21]*
N_2	300.0 - 350.0	1.5 - 2900.7	1.0000	68	[22]
CO_2	300.0 - 350.0	1.5 - 2175.6	1.0000	55	[20]
CH_4 - N_2	320.0 - 323.2	4.0 - 2900.7	0.0000 - 1.0000	44	[21,22,24]
CH_4 - CO_2	344.3 - 423.2	306.3 - 2010.8	0.0989 - 0.9017	39	[25]
N_2 – CO_2	344.3 - 410.9	3.0 - 2900.7	0.0000 - 1.0000	158	[20,22,26]

Table 34. BWR EOS Parameters for Binary Mixtures

Component	$B_0 \times 10^2$	A_0	$C_0 \times 10^{-5}$	$b \times 10^3$	a	a ´ 10^5	$c \times 10^{-4}$	g ´ 10^3
Methane/Nitrogen with k_{ij} =0.0415								
CH_4	4.6380	1.8857	0.2612	3.8637	0.0713	46.6259	0.2692	20.1885
N_2	4.1316	1.0468	0.0621	1.6206	0.0189	65.3417	0.1203	0.00001
Methane/carbon dioxide with k_{ij} =0.0427								
CH_4	4.2258	1.8295	0.2101	4.2206	0.0784	23.3796	0.2574	8.6201
CO_2	3.0974	1.8288	1.8040	5.7442	0.2364	6.2277	2.1642	5.6924
Nitrogen/carbon dioxide with k_{ij} =-0.0480								
N_2	4.0534	0.9972	0.0650	2.0455	0.0271	11.4010	0.0812	5.5679
CO_2	3.2012	1.8314	1.7649	6.1757	0.2401	4.9506	1.9054	4.3071

Figure 1. Schematic Diagram of Experimental Apparatus

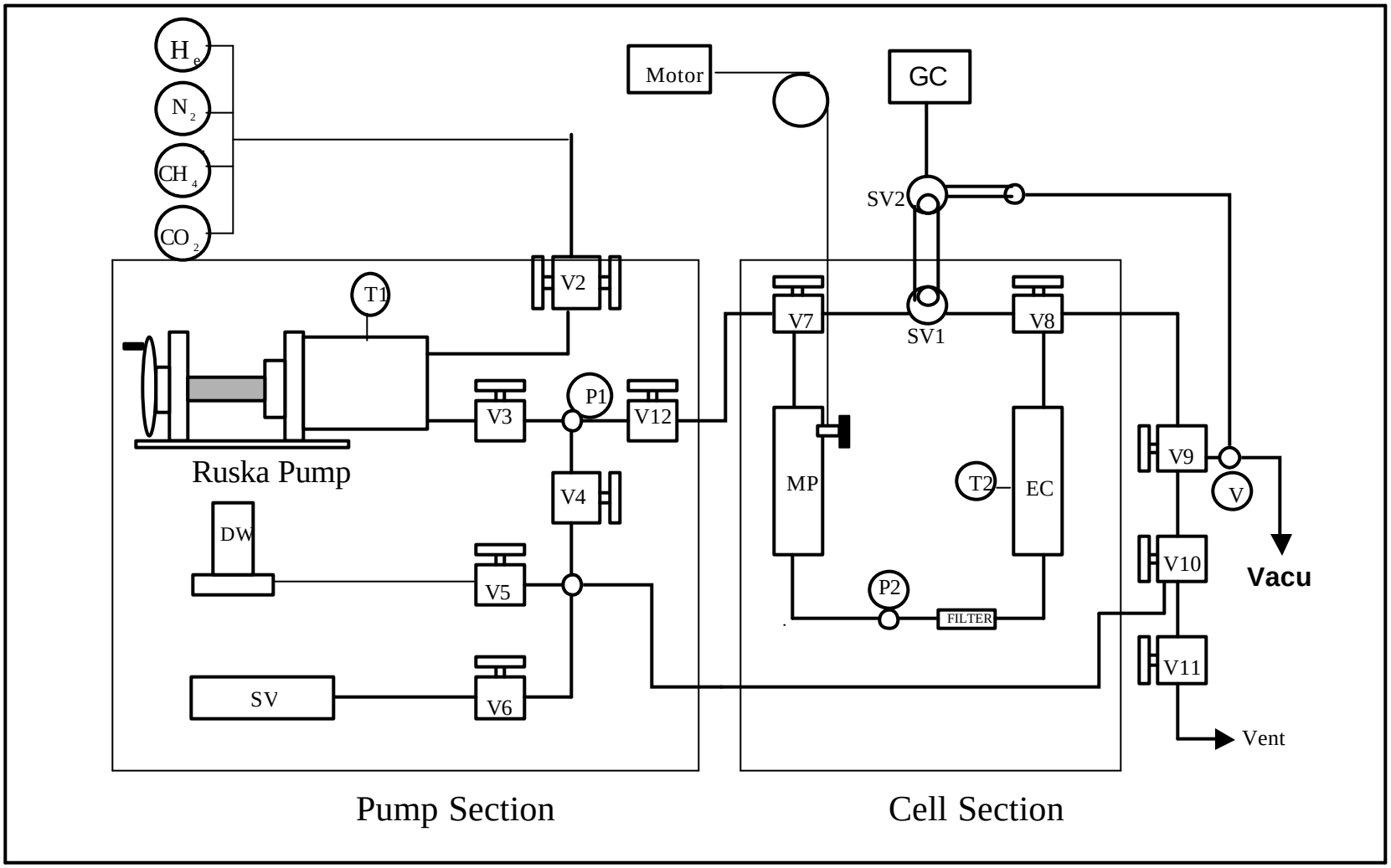

Figure 2. Comparison of Gibbs Adsorption of Nitrogen on Fruitland Coal at 115°F on Mineral-Matter Free Basis

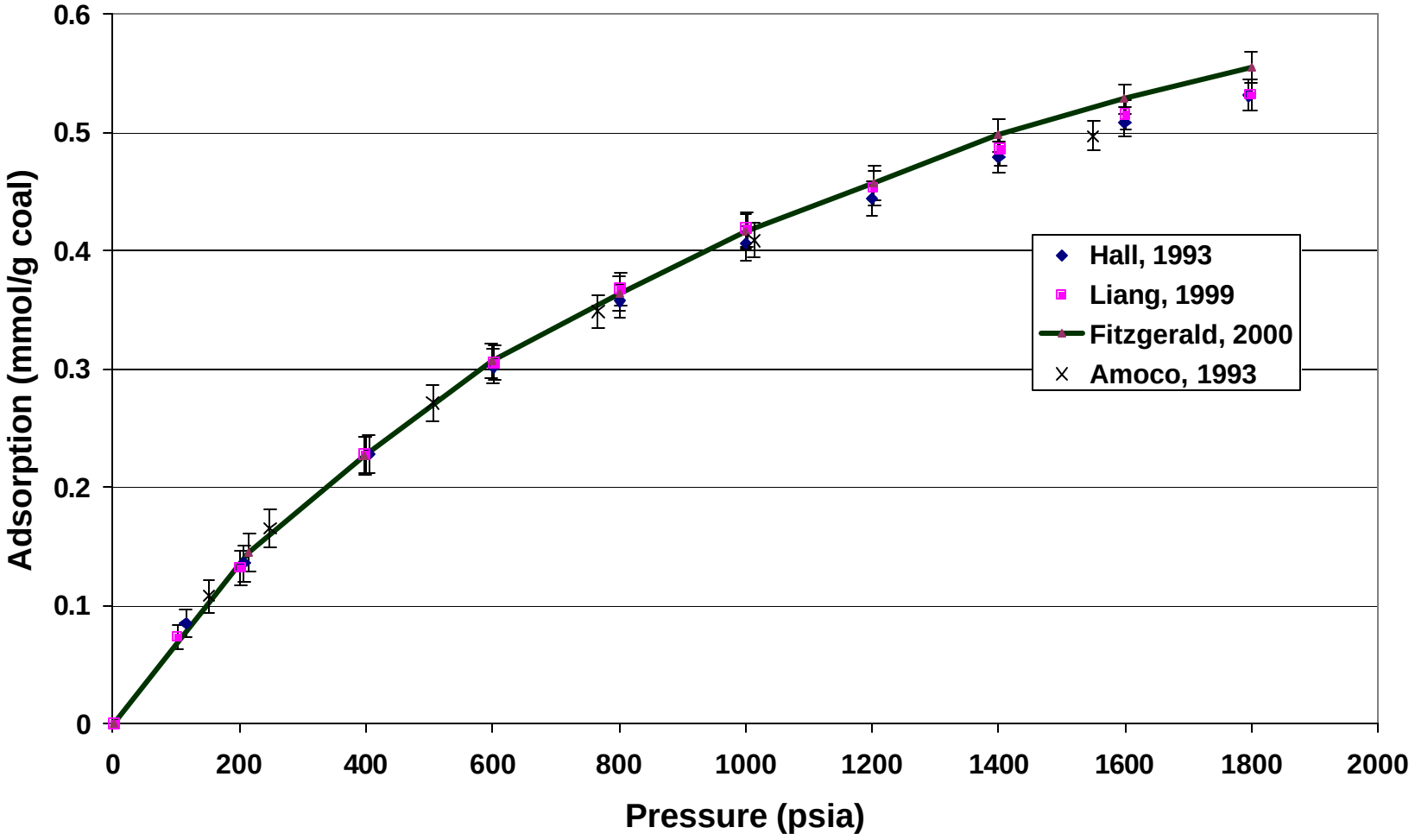

Figure 3. Comparison of Gibbs Adsorption of CO_2 on Fruitland Coal at 115°F on Mineral-Matter Free Basis

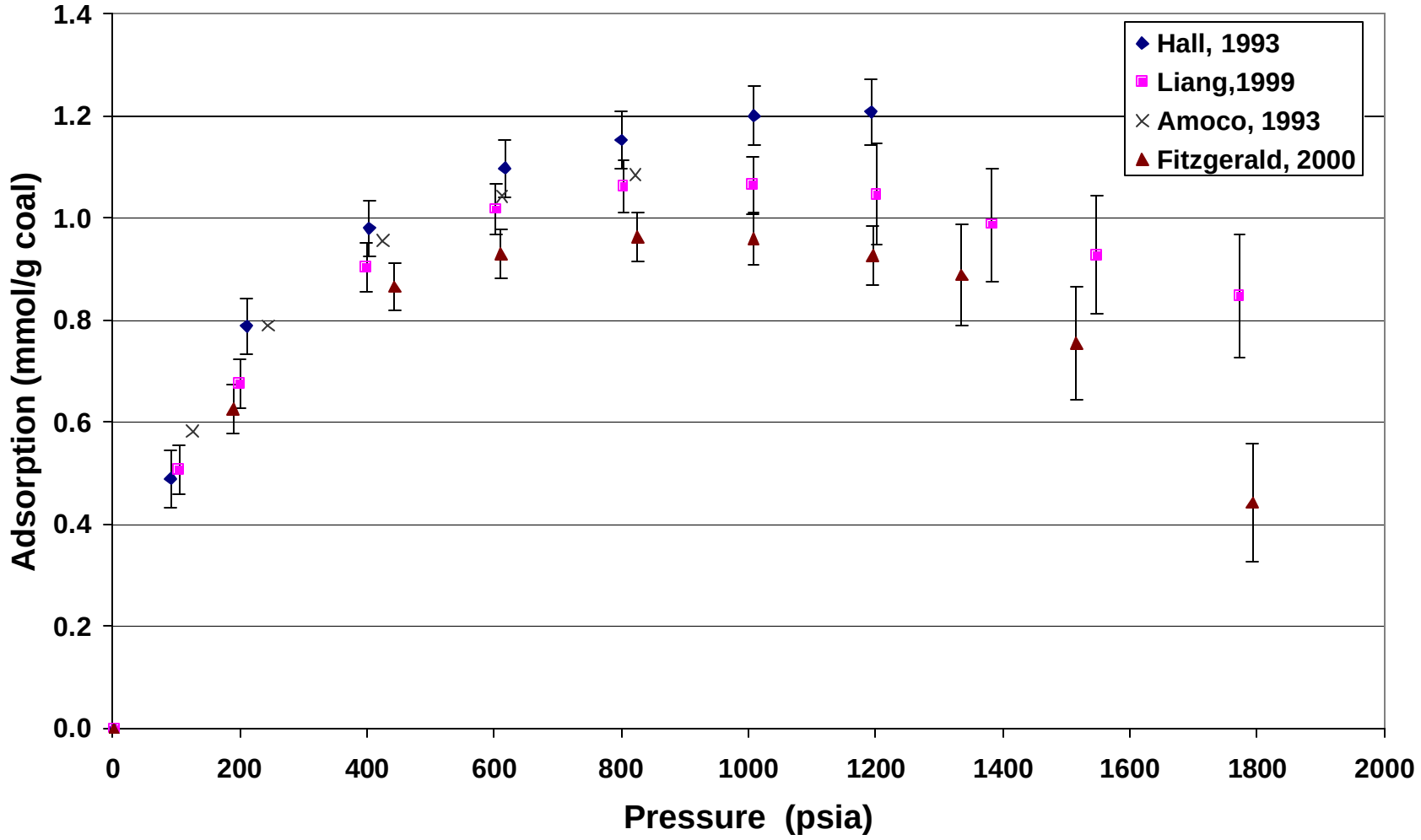

Figure 4. Gibbs Adsorption of CO_2 on Activated Carbon at 113°F

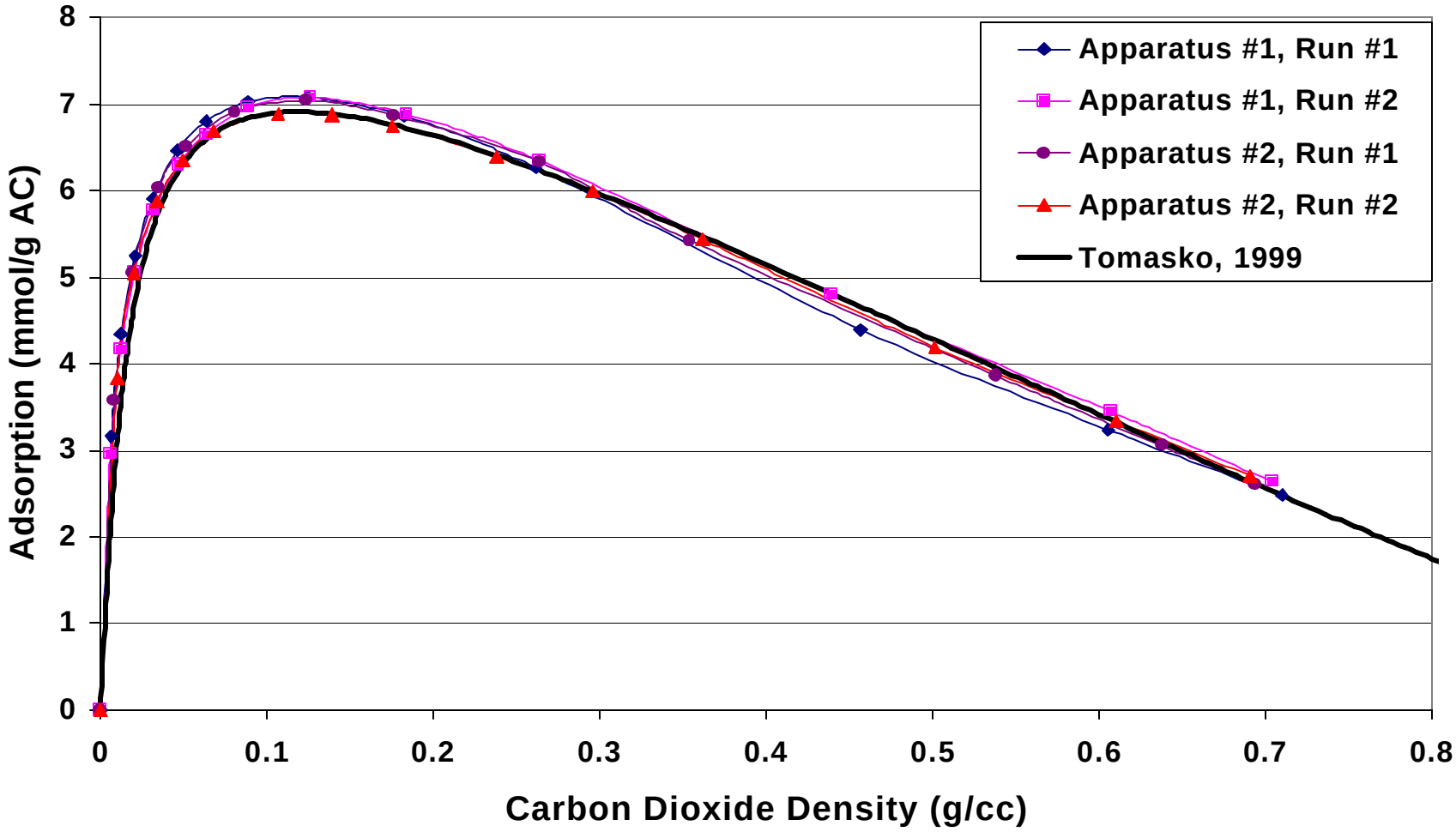

Figure 5. Gibbs Adsorption of CO_2 on Activated Carbon at 113 °F

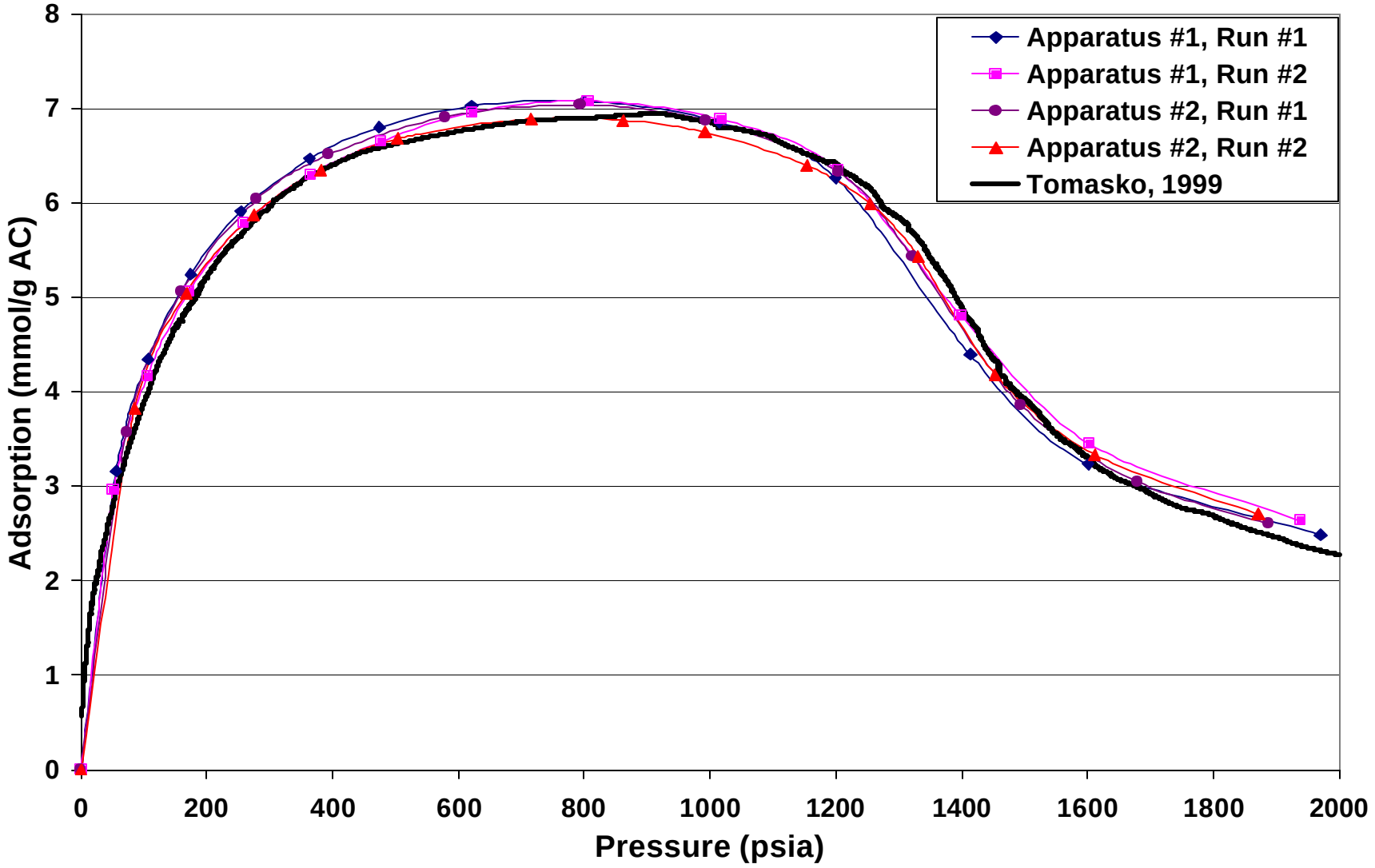

Figure 6. Gibbs Adsorption on Activated Carbon at 113°F

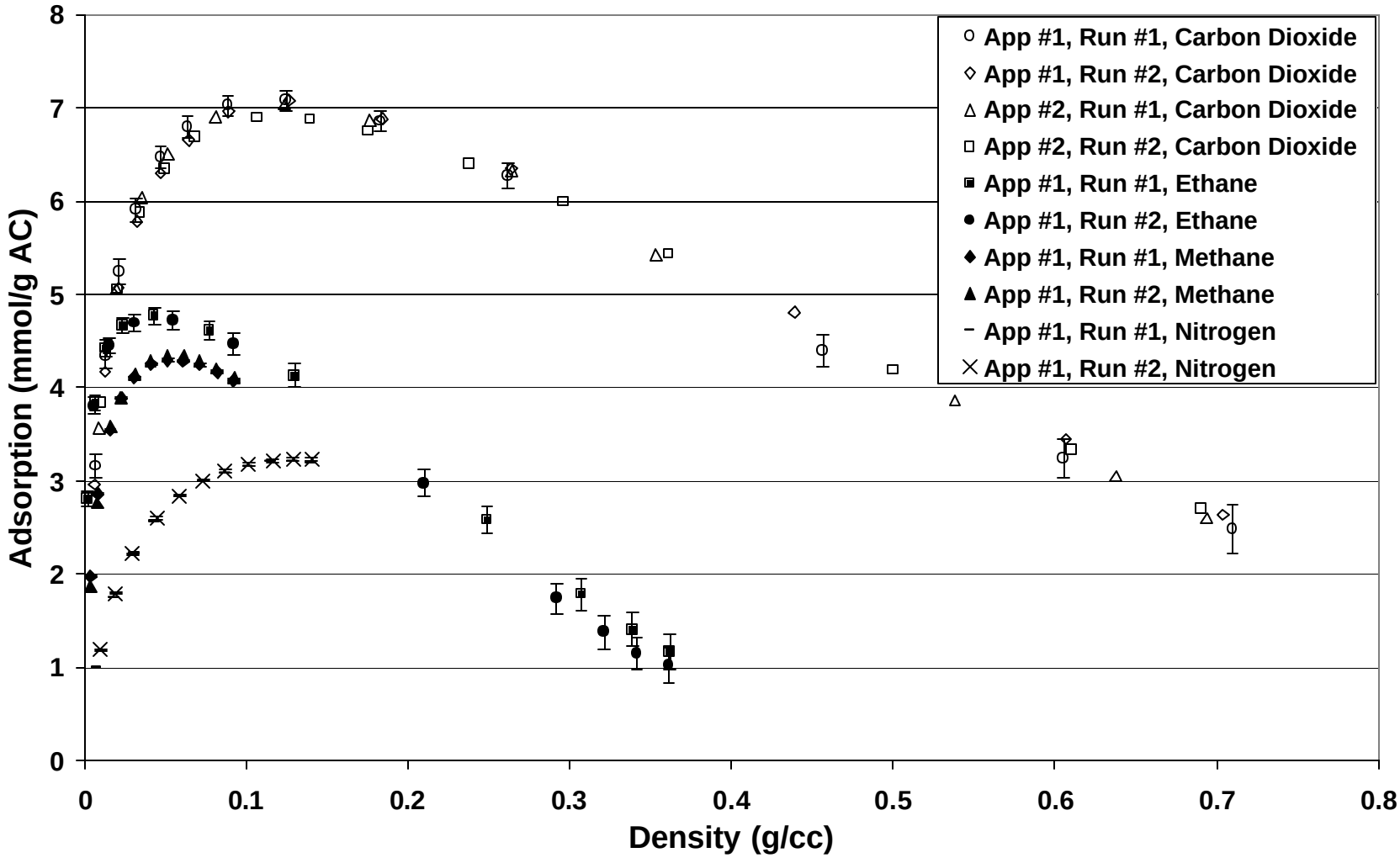

Figure 7. Absolute Adsorption on Activated Carbon at 113°F

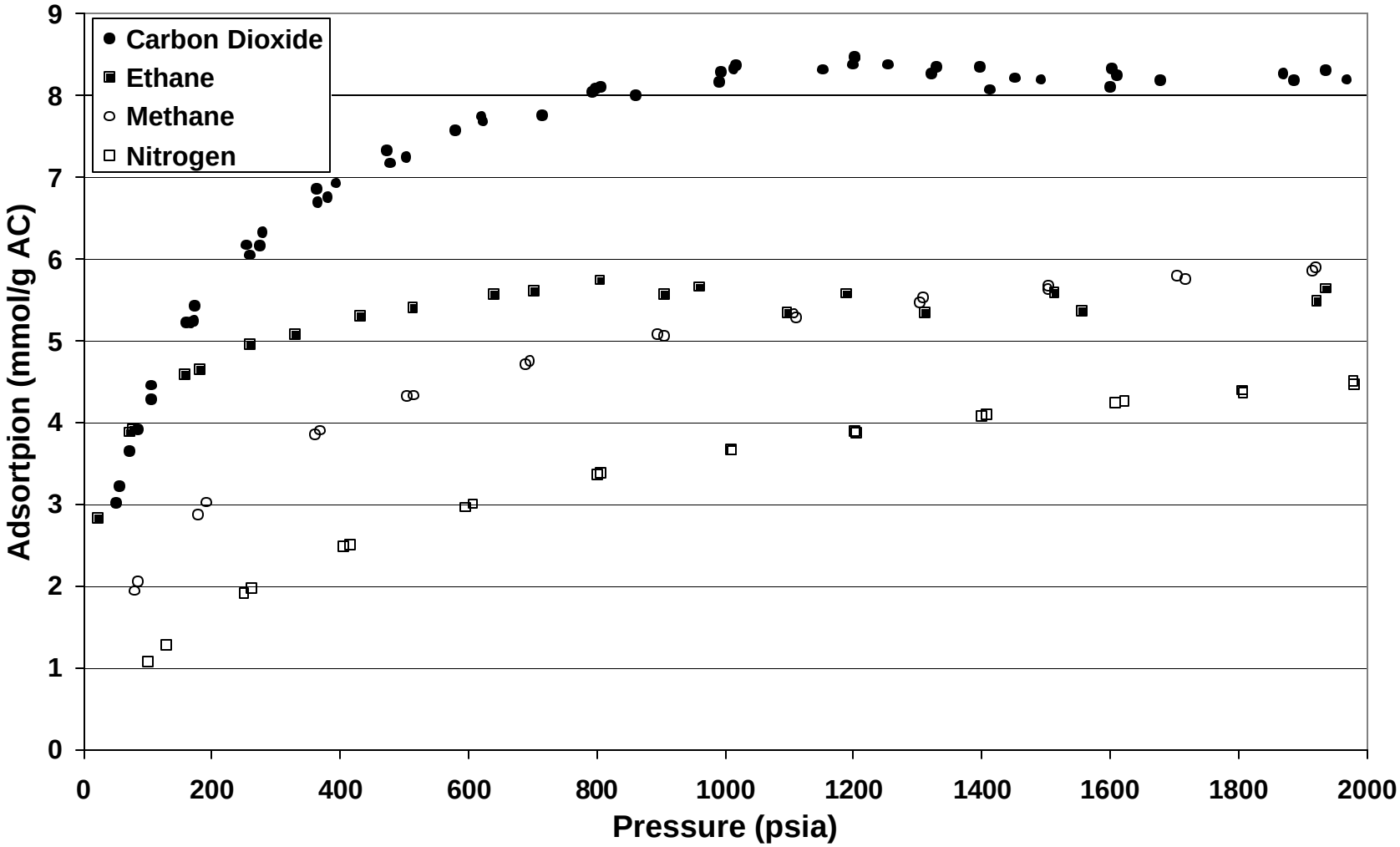

Figure 8. Gas Adsorption on Wet Illinois-6 Coal at 115 °F

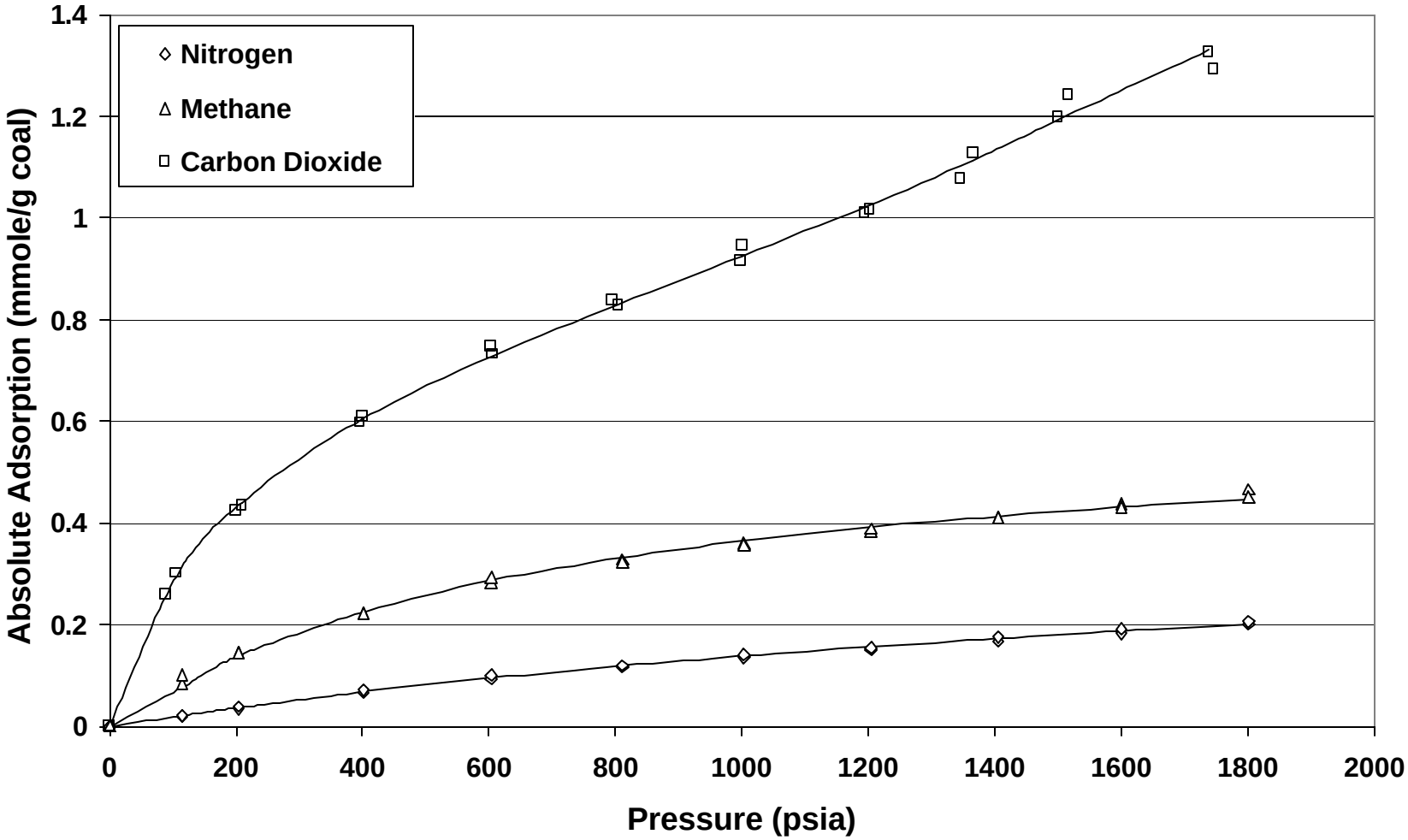

Figure 9. Methane/Carbon Dioxide Binary Mixture Adsorption on Wet Fruitland Coal at 115 °F: Methane

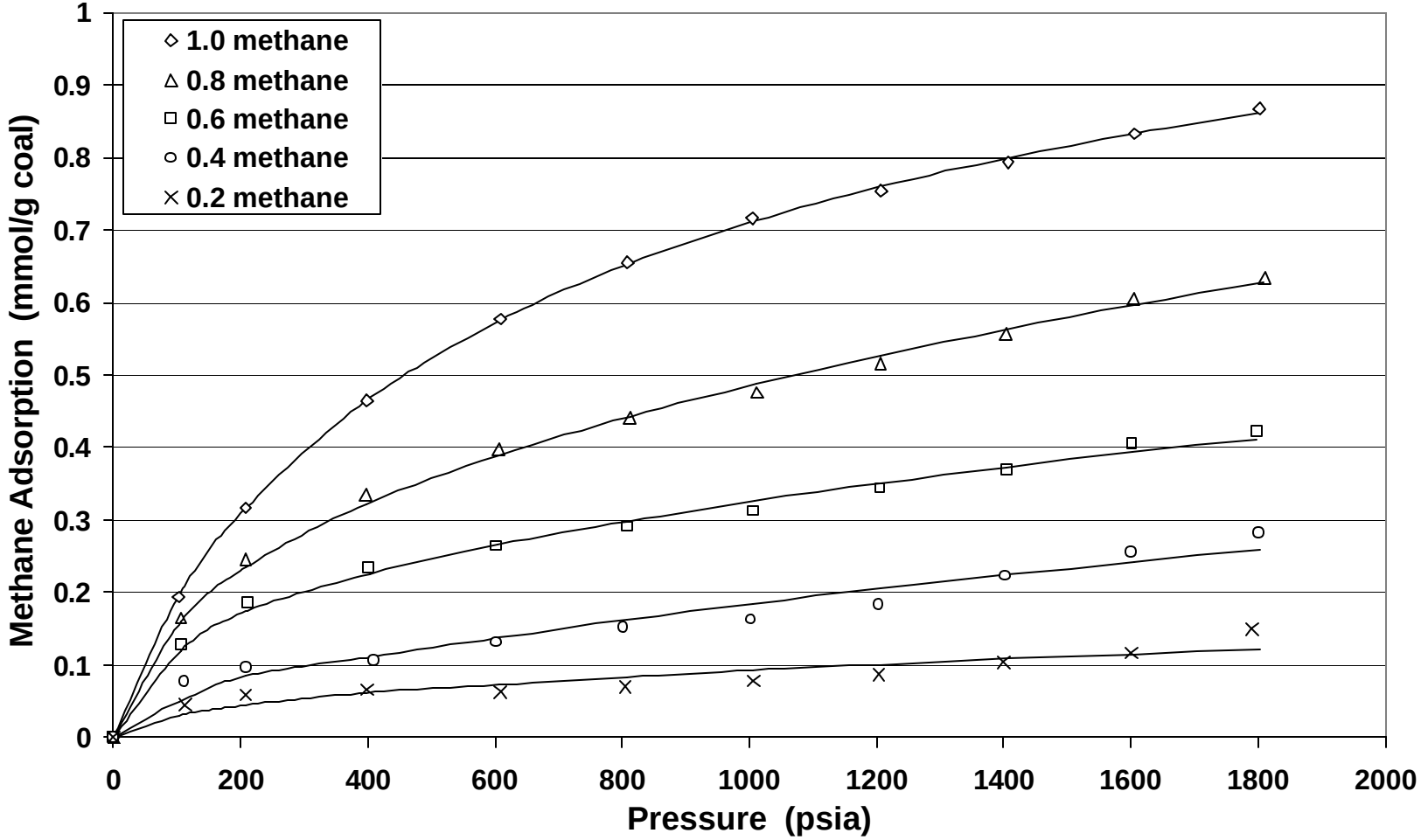

Figure 10. Methane/Carbon Dioxide Binary Mixture Adsorption on Wet Fruitland Coal at 115 °F: Carbon Dioxide

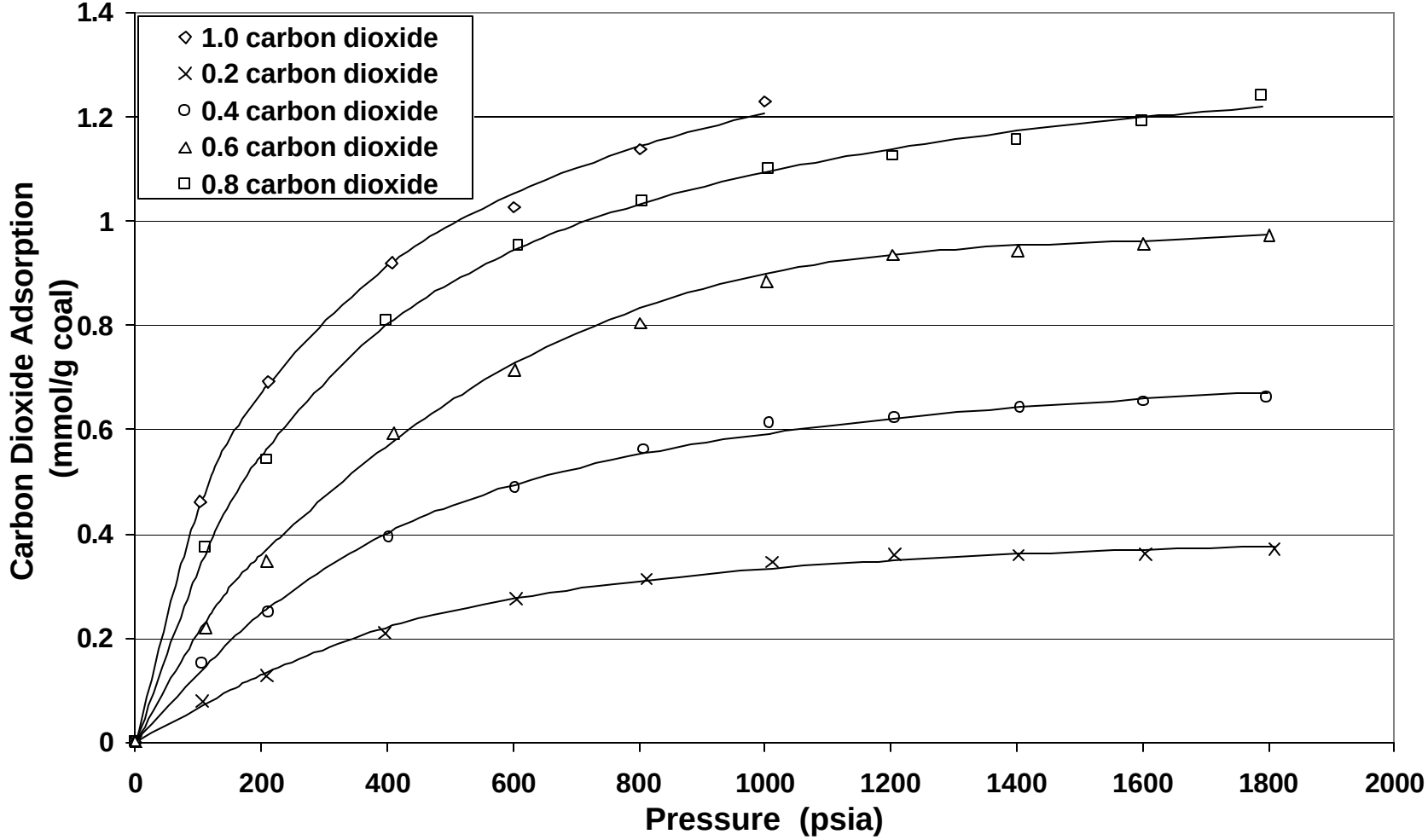

Figure 11. Methane/Carbon Dioxide Binary Mixture Adsorption on Wet Fruitland Coal at 115 ^{o}F: Total

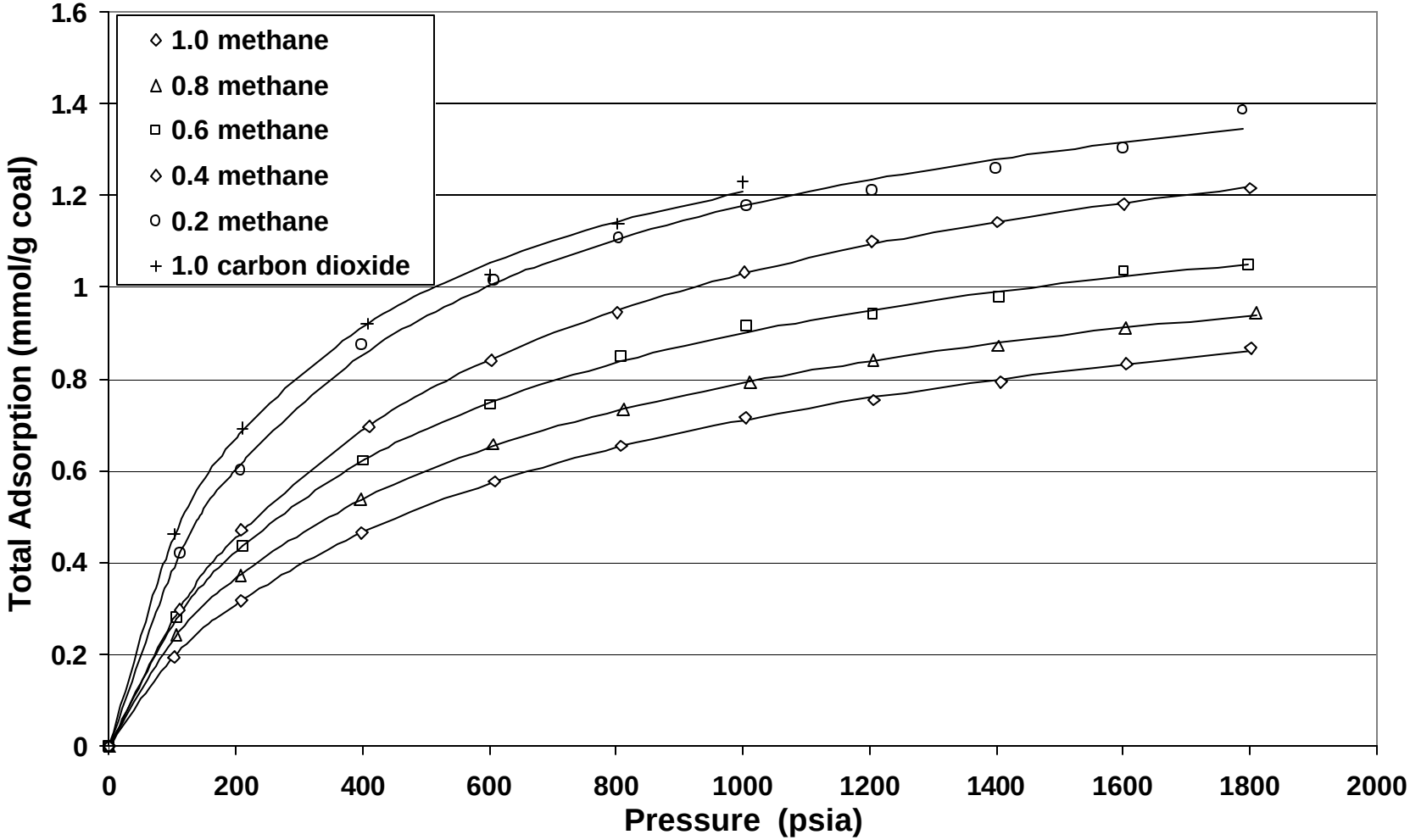

Figure 12. Methane/Nitrogen Binary Mixture Adsorption on Wet Fruitland Coal at 115 °F: Methane

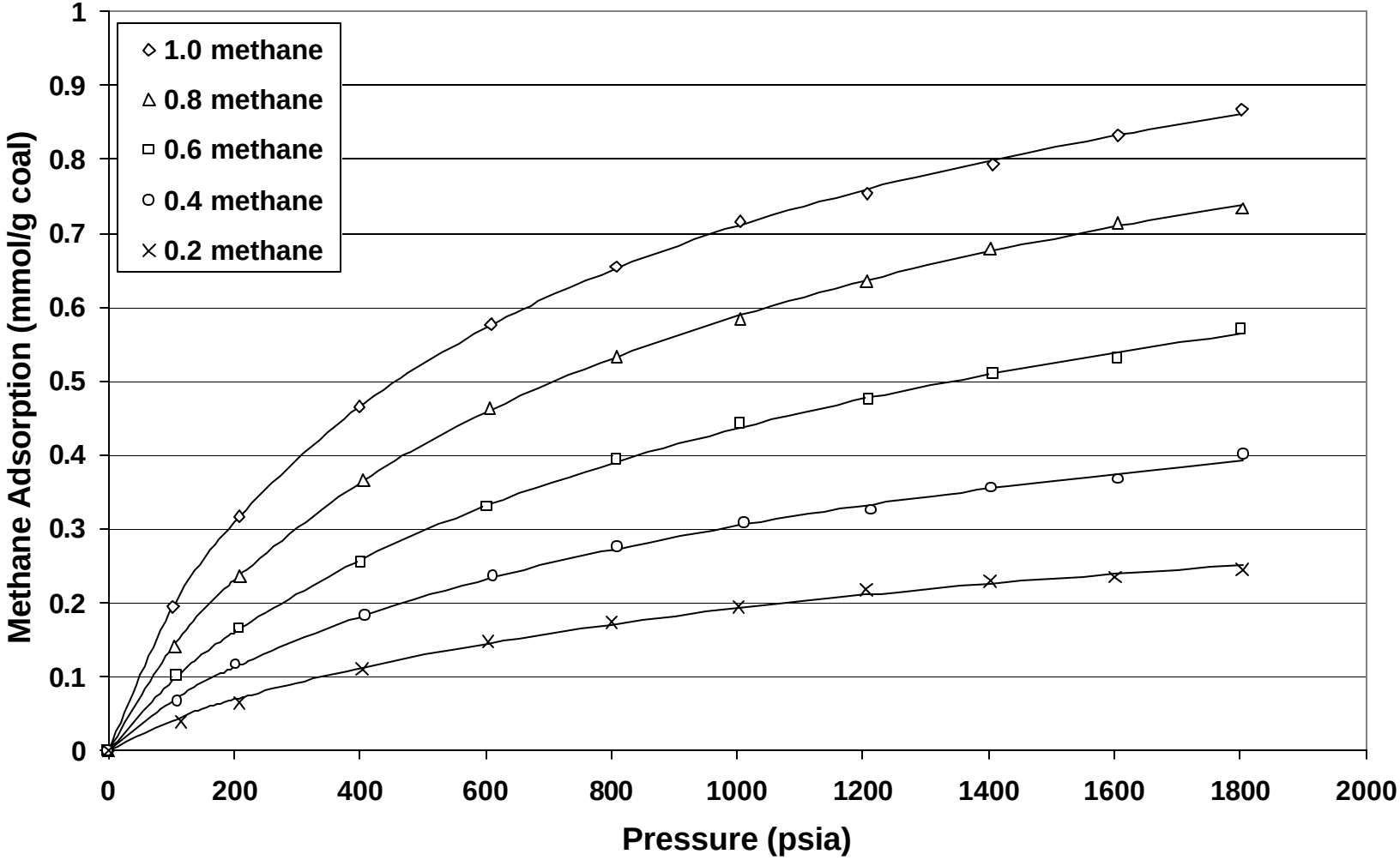

Figure 13. Methane/Nitrogen Binary Mixture Adsorption on Wet Fruitland Coal at 115 °F: Nitrogen

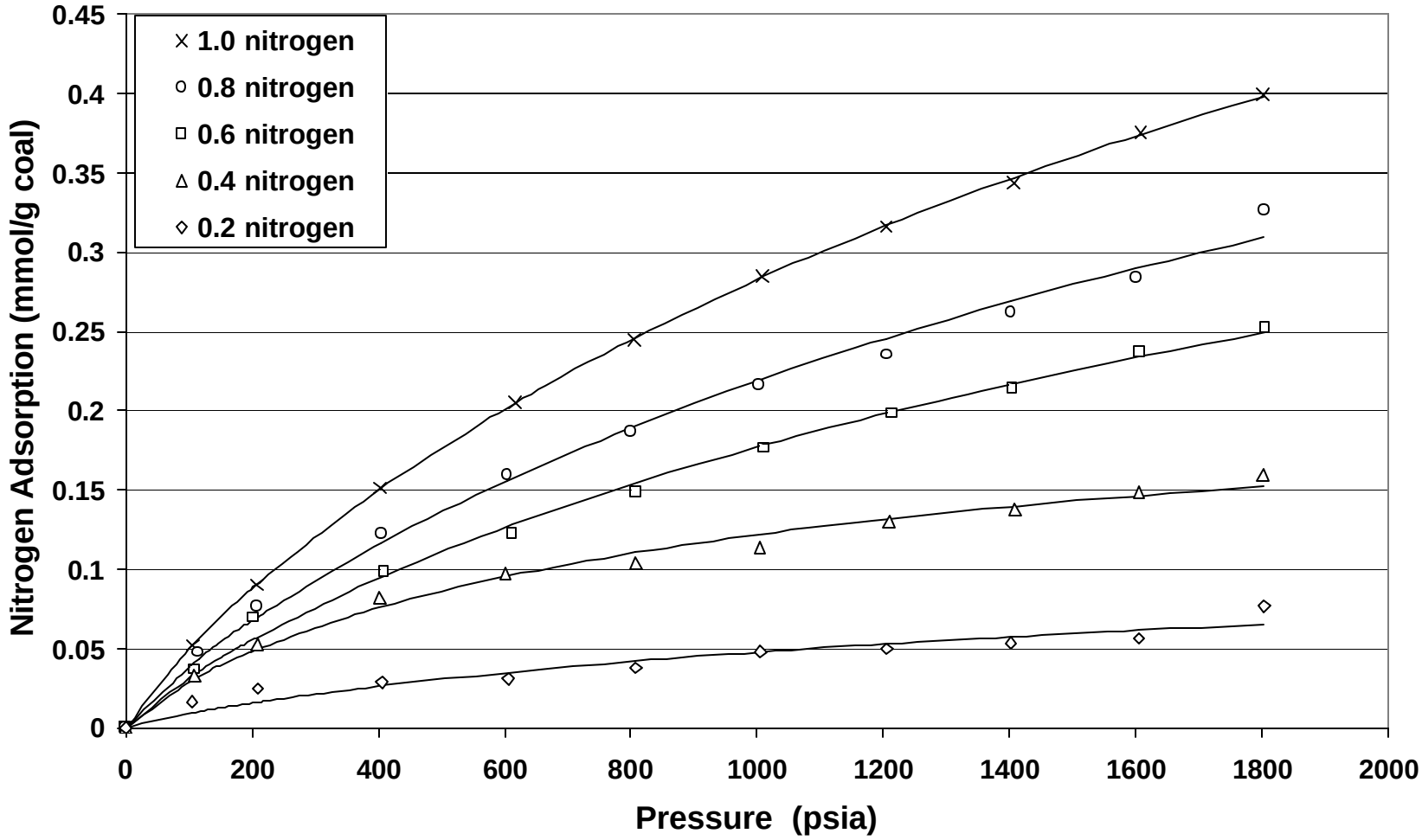

Figure 14. Methane/Nitrogen Binary Mixture Adsorption on Wet Fruitland Coal at 115 °F: Total

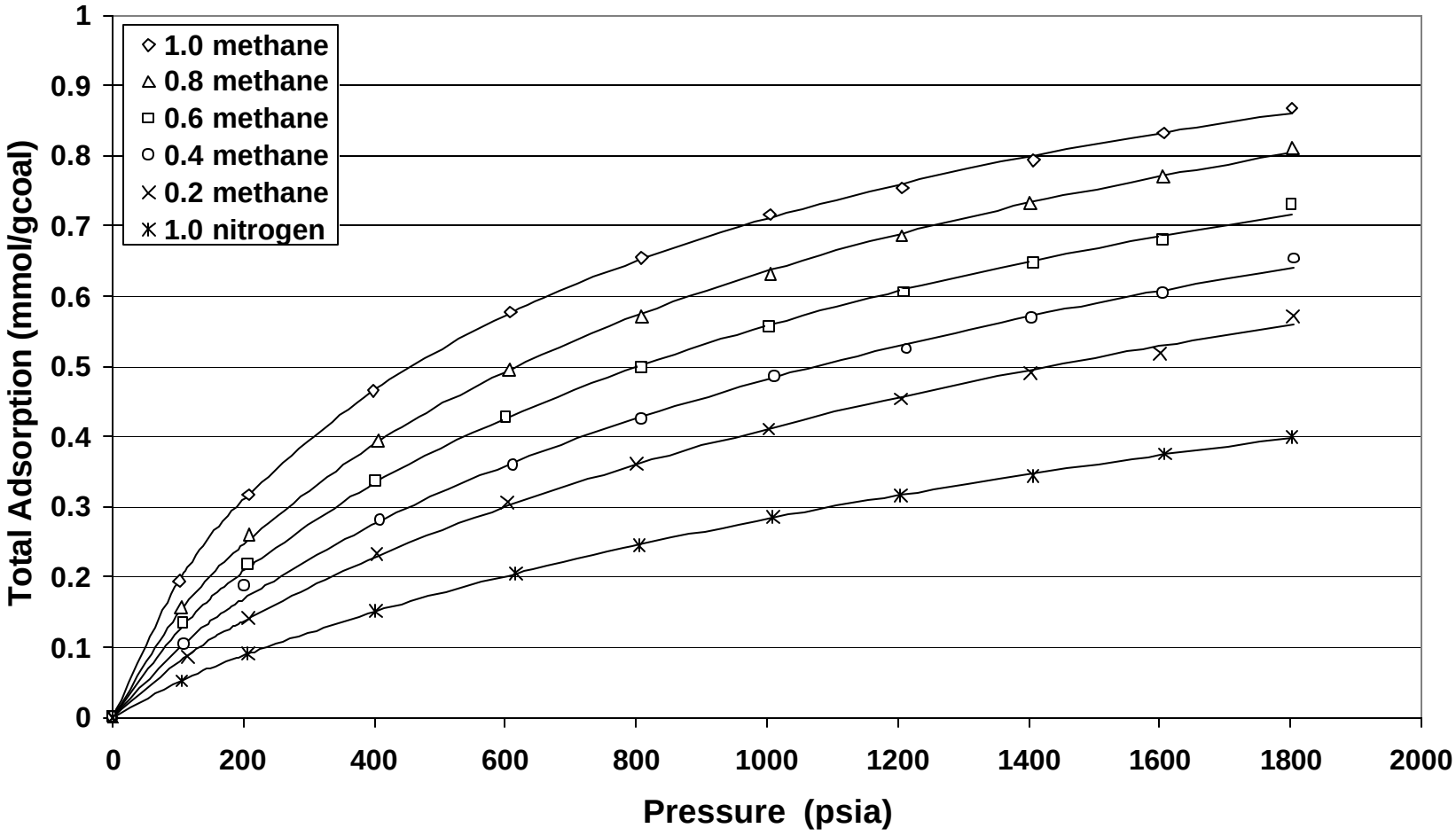

Figure 15. Nitrogen/Carbon Dioxide Binary Mixture Adsorption on Wet Fruitland Coal at 115 °F: Nitrogen

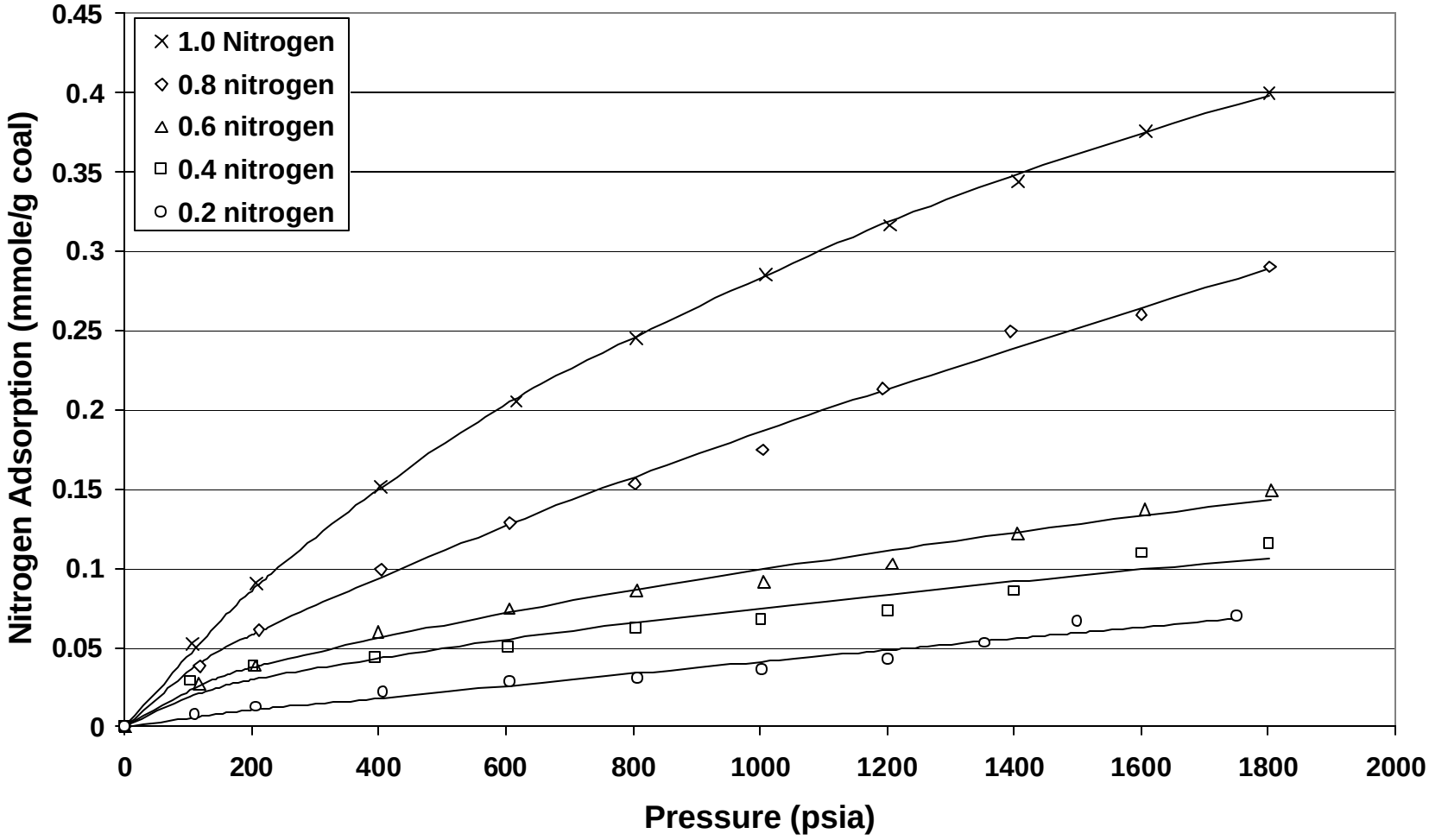

Figure 16. Nitrogen/Carbon Dioxide Binary Mixture Adsorption on Wet Fruitland Coal at 115 °F: Carbon Dioxide

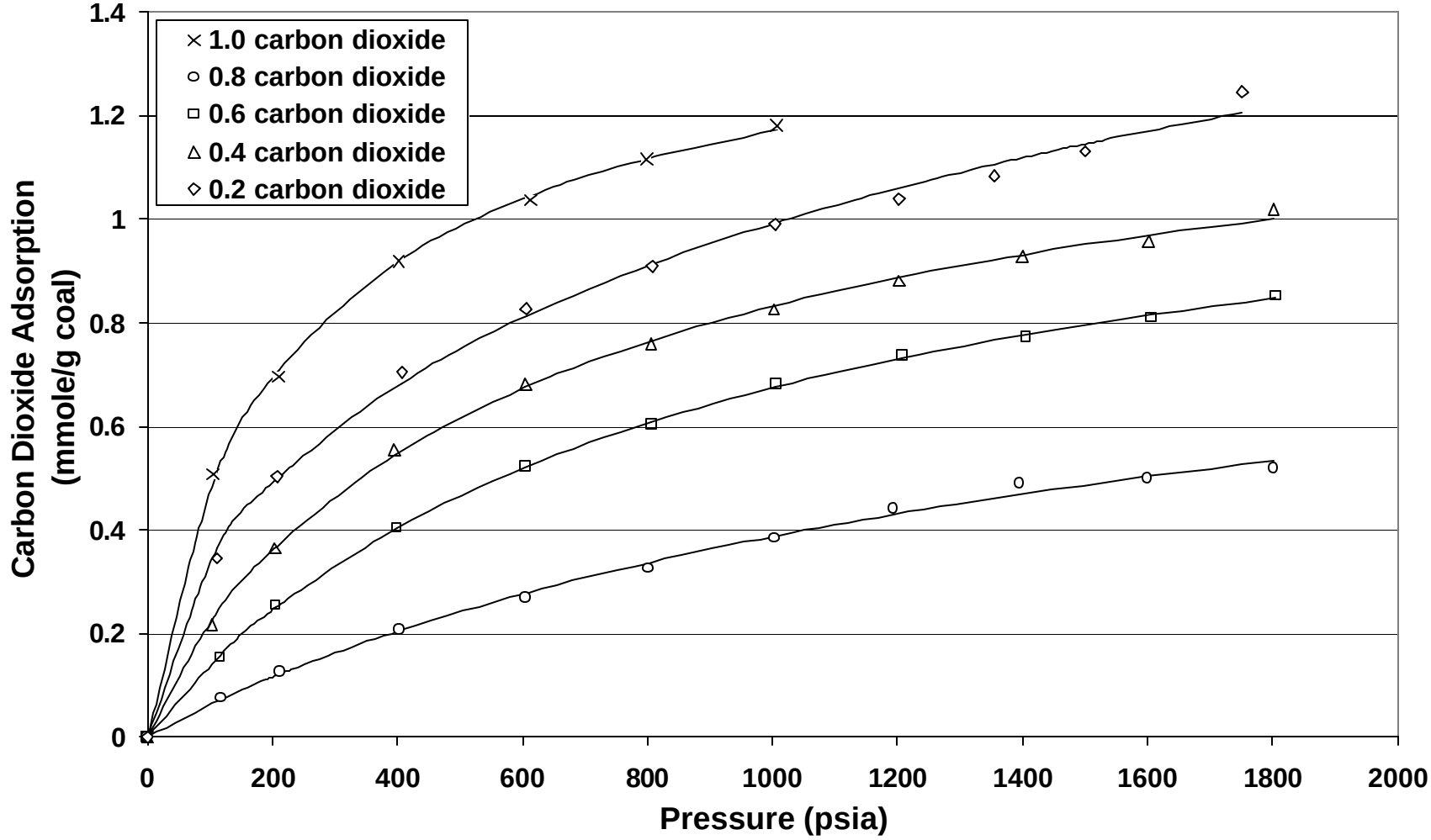

Figure 17. Nitrogen/Carbon Dioxide Binary Mixture Adsorption on Wet Fruitland Coal at 115 °F: Total

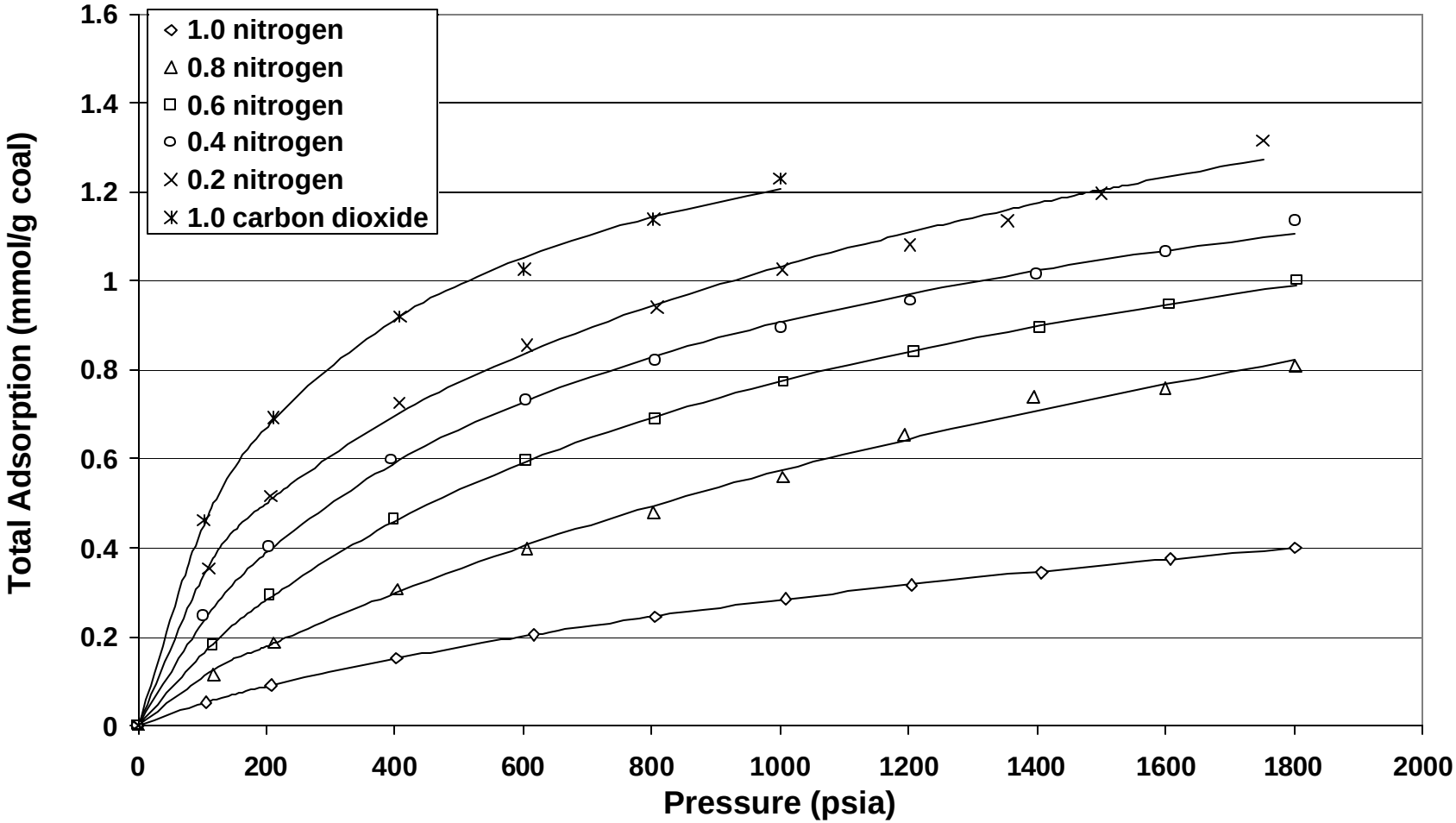

Figure. 18. Pure Carbon Dioxide Adsorption on Wet Frutiland Coal at 115 ^{o}F

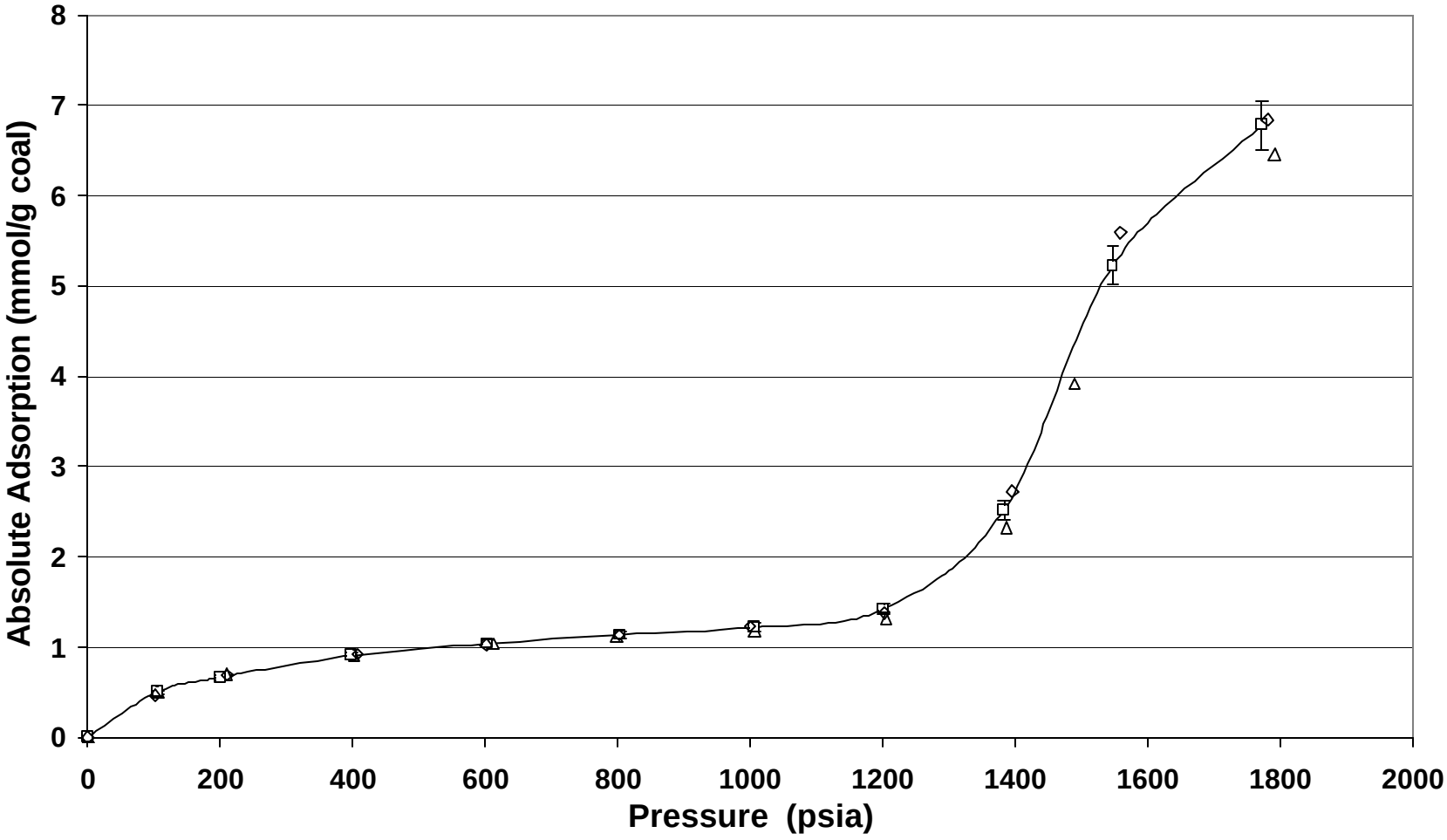

Figure 19. Absolute Adsorption of CO_2 on Fruitland Coal at 115°F

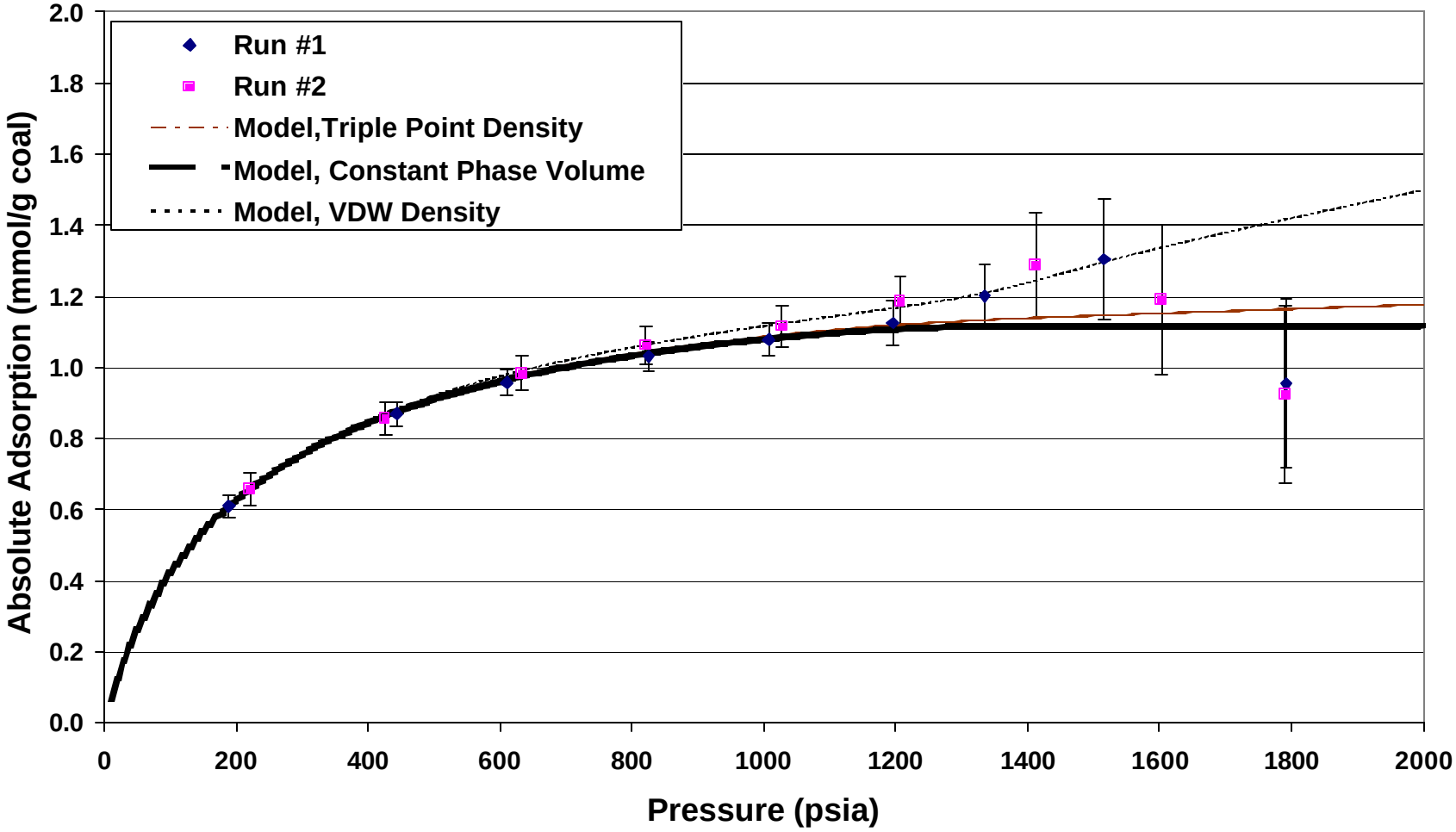

Figure 20. Gibbs Adsorption of CO_2 on Fruitland Coal at 115°F

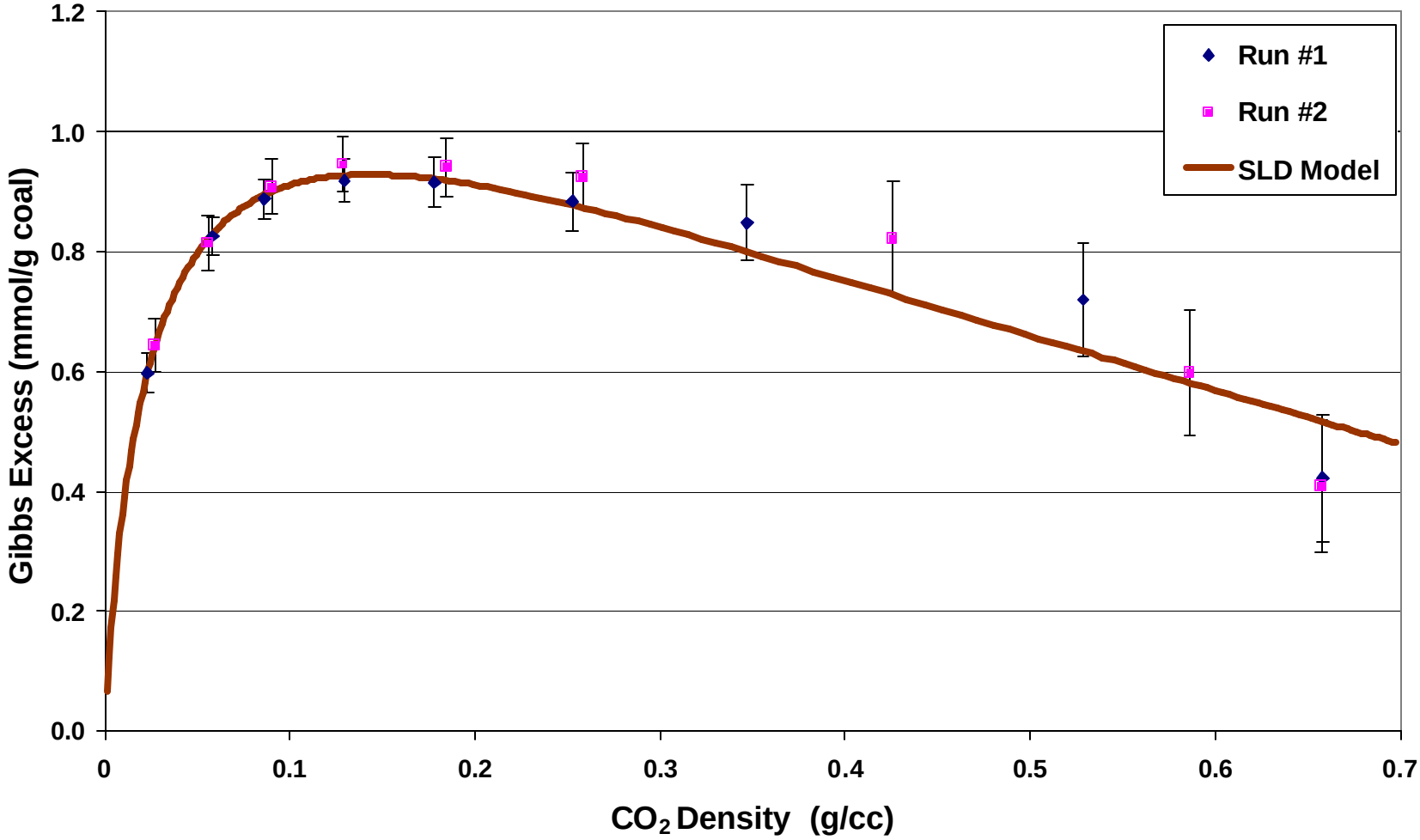

Figure 21. Prediction of Pure Gas Adsorption on Wet Fruitland Coal at 115F Using LRC and PGR EOS Models

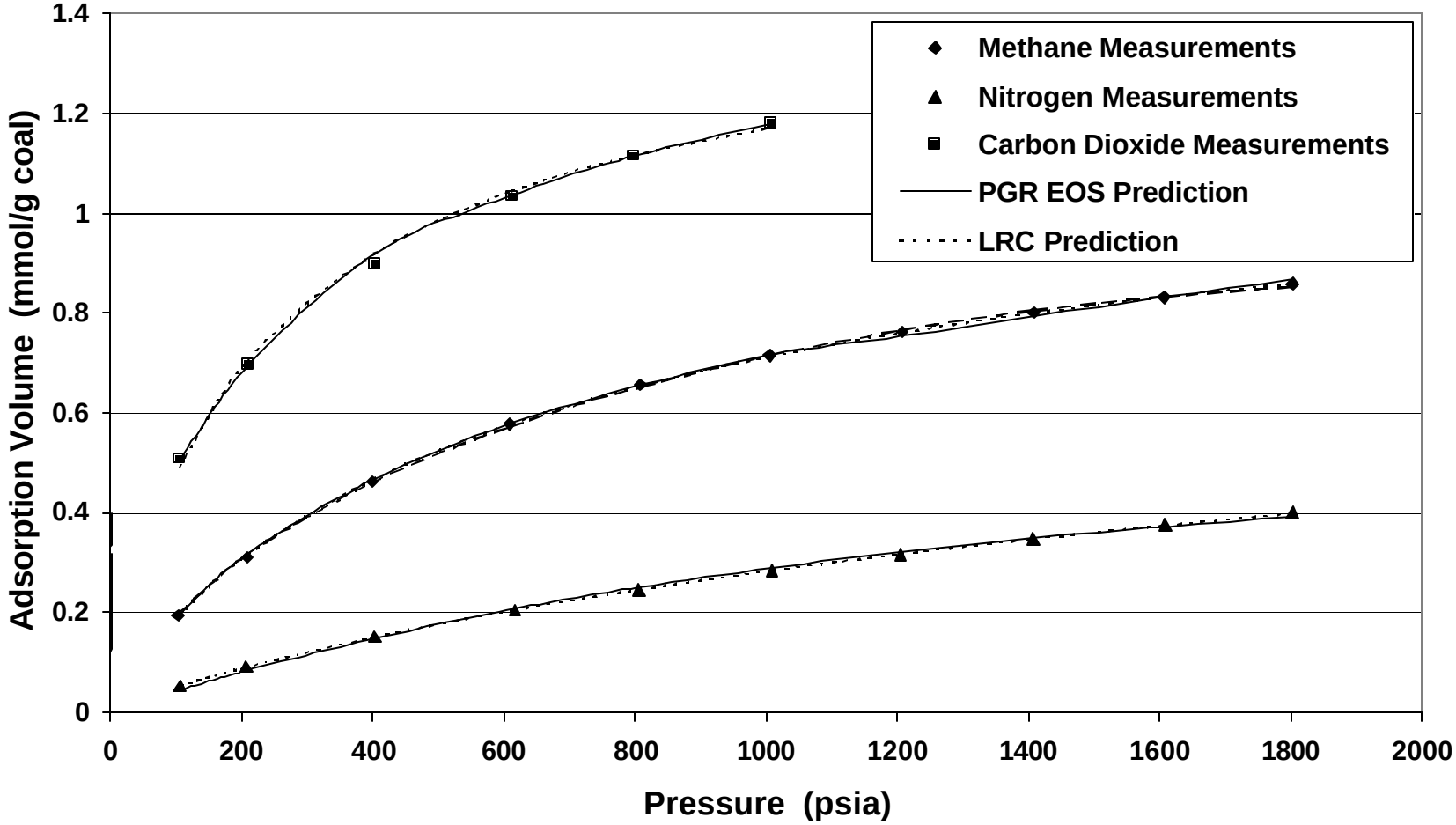

Figure 22. SLD Model of Gibbs Adsorption of Pure Gases on Activated Carbon at 113°F

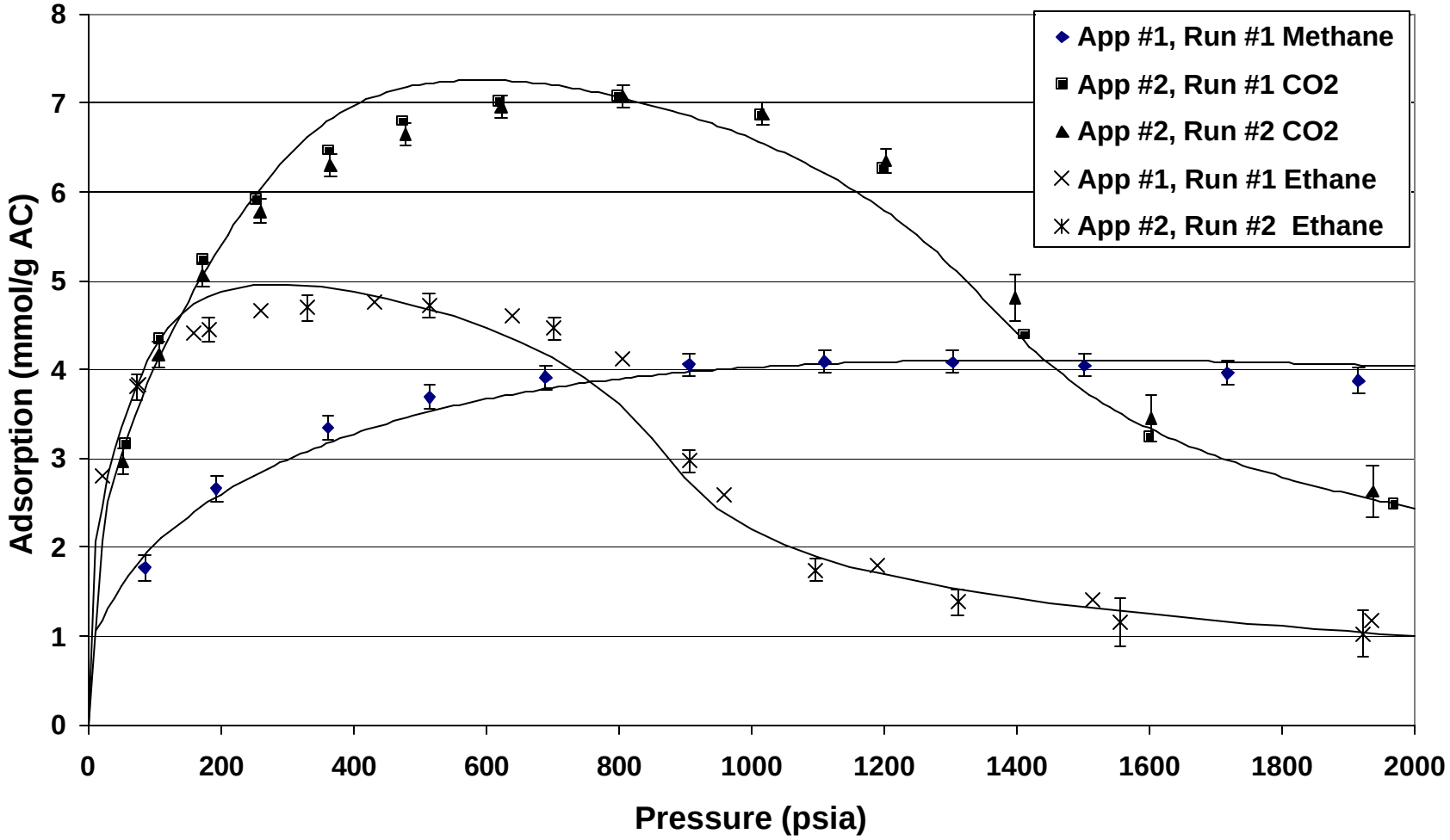

Figure 23. SLD Model for the Gibbs Adsorption of Pure Gases on Fruitland Coal at 115°F

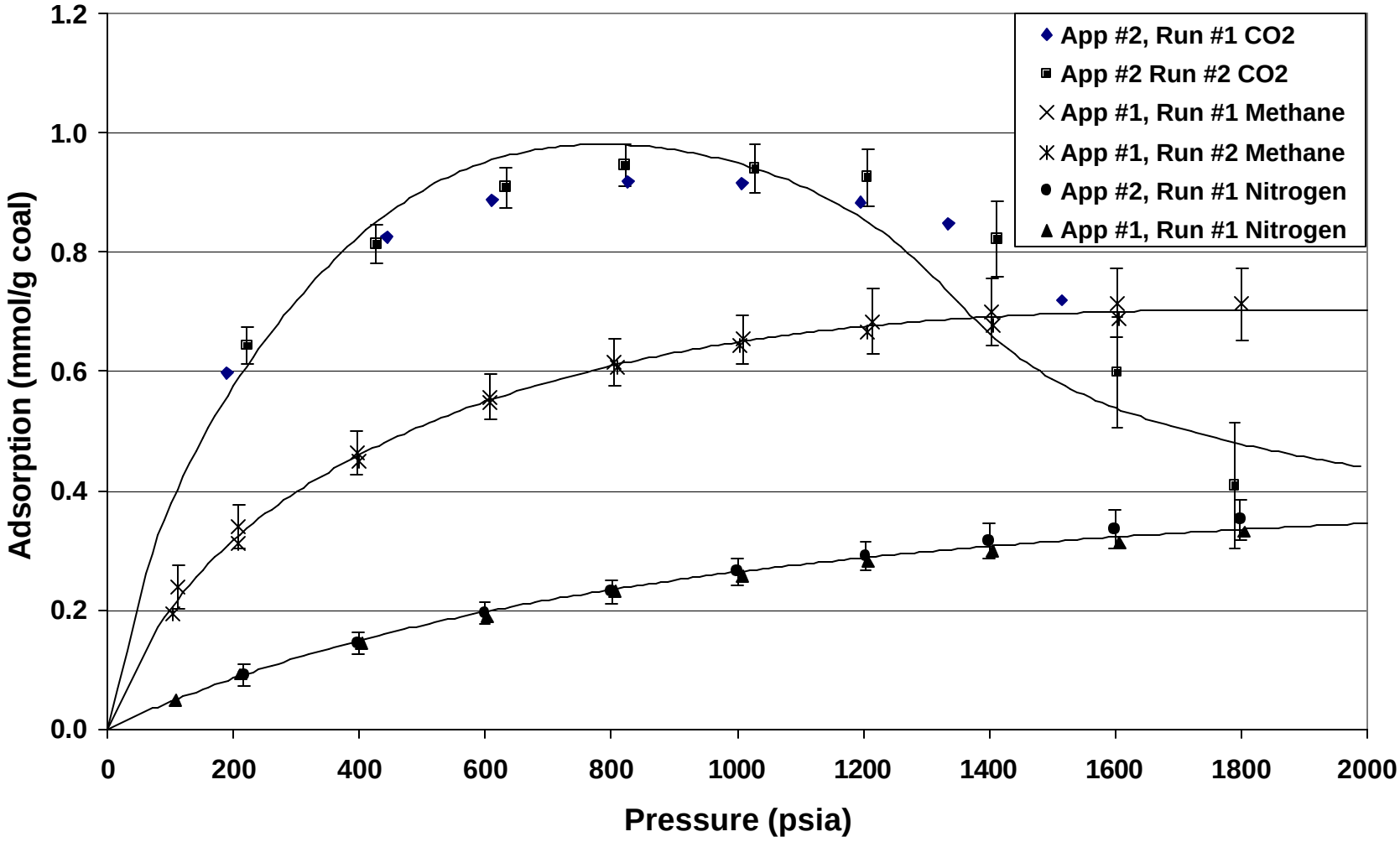

Figure 24. SLD Model of Gibbs Adsorption of Pure Gases on Wet Illinois-6 Coal at 115°F

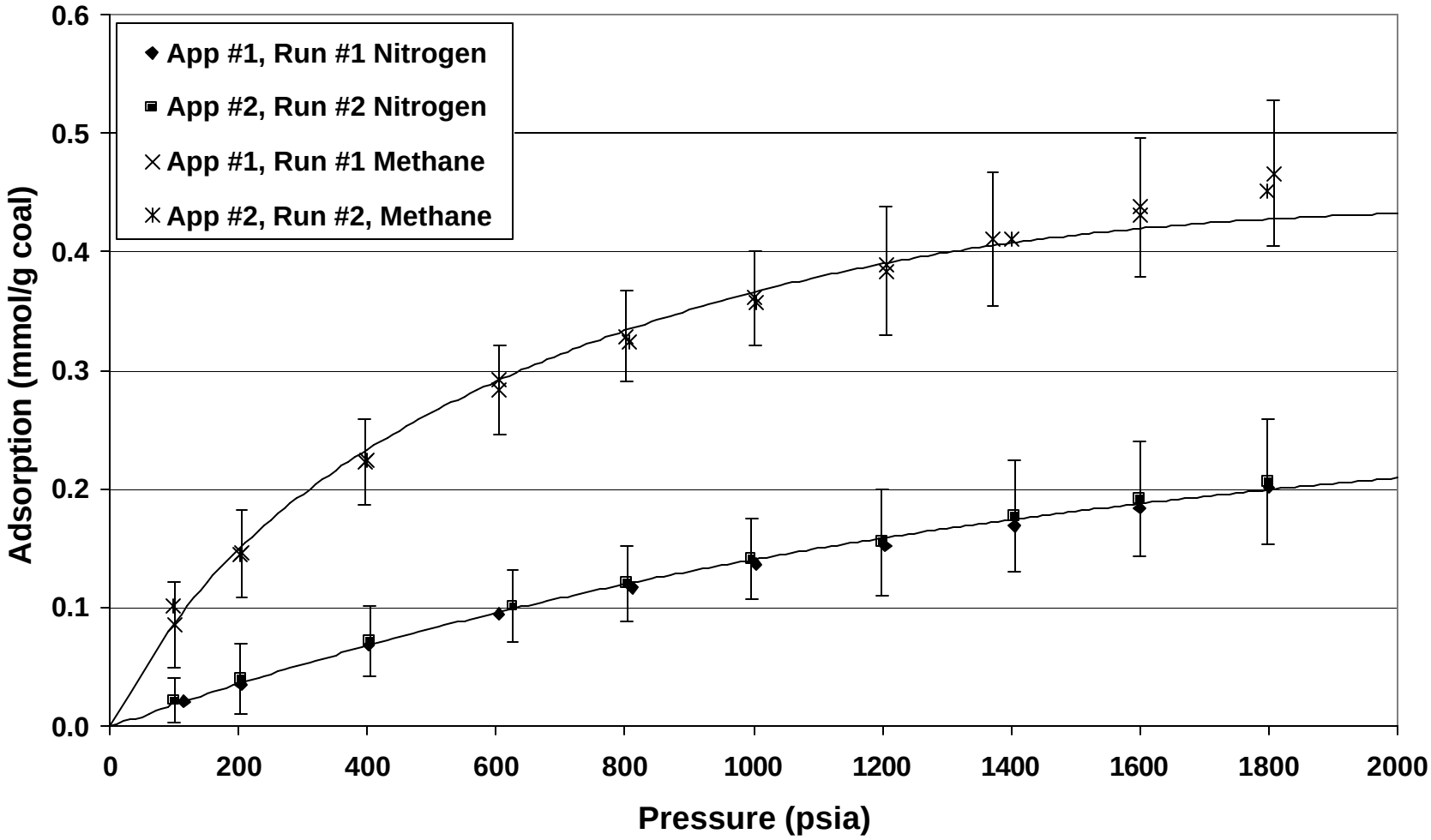

Figure 25. LRC Representation of Methane/Carbon Dioxide Binary Mixture Adsorption on Wet Fruitland Coal at 115 °F: Carbon Dioxide

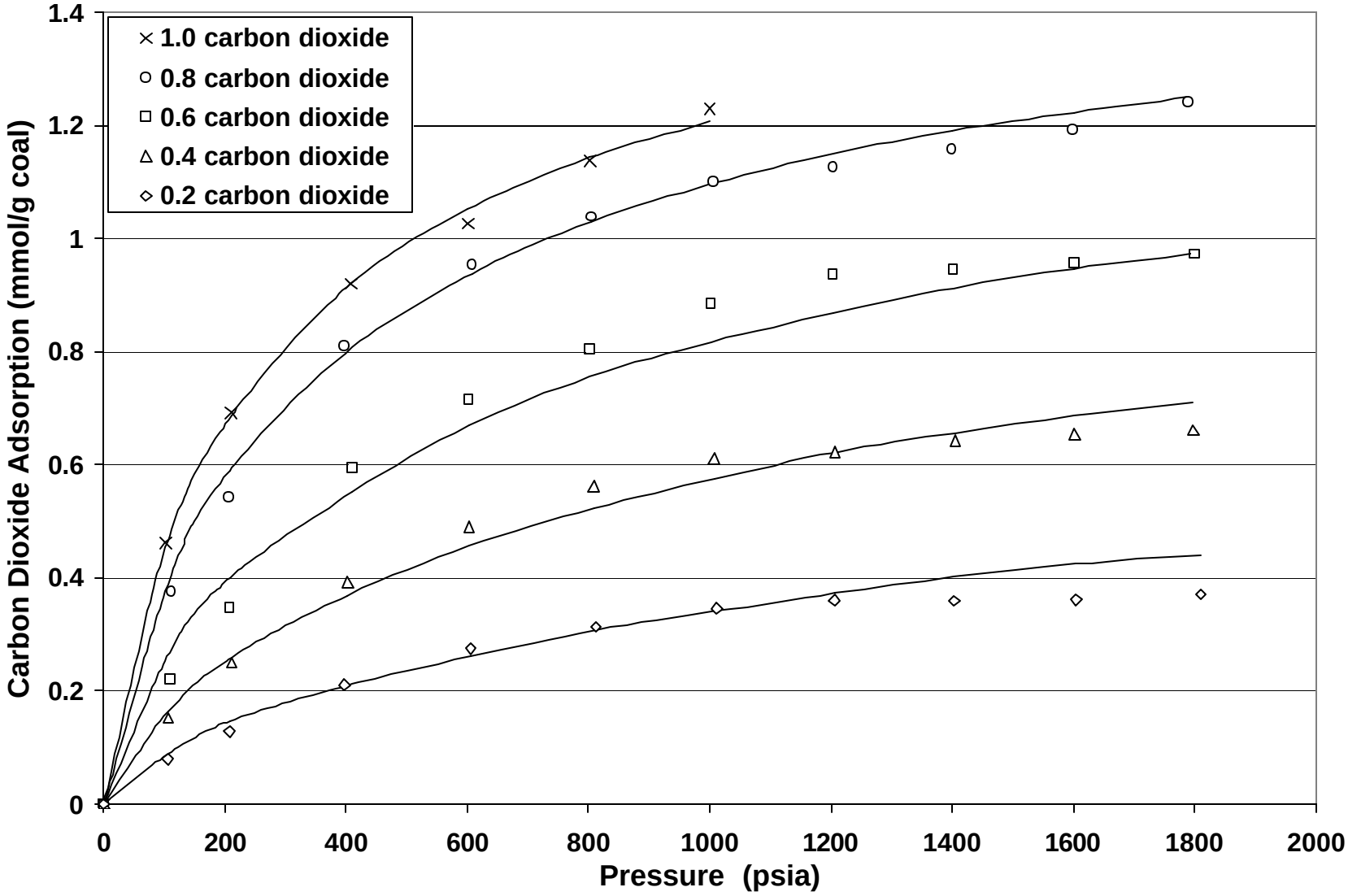

Figure 26. BWR Z Factor Deviations: Methane/Nitrogen

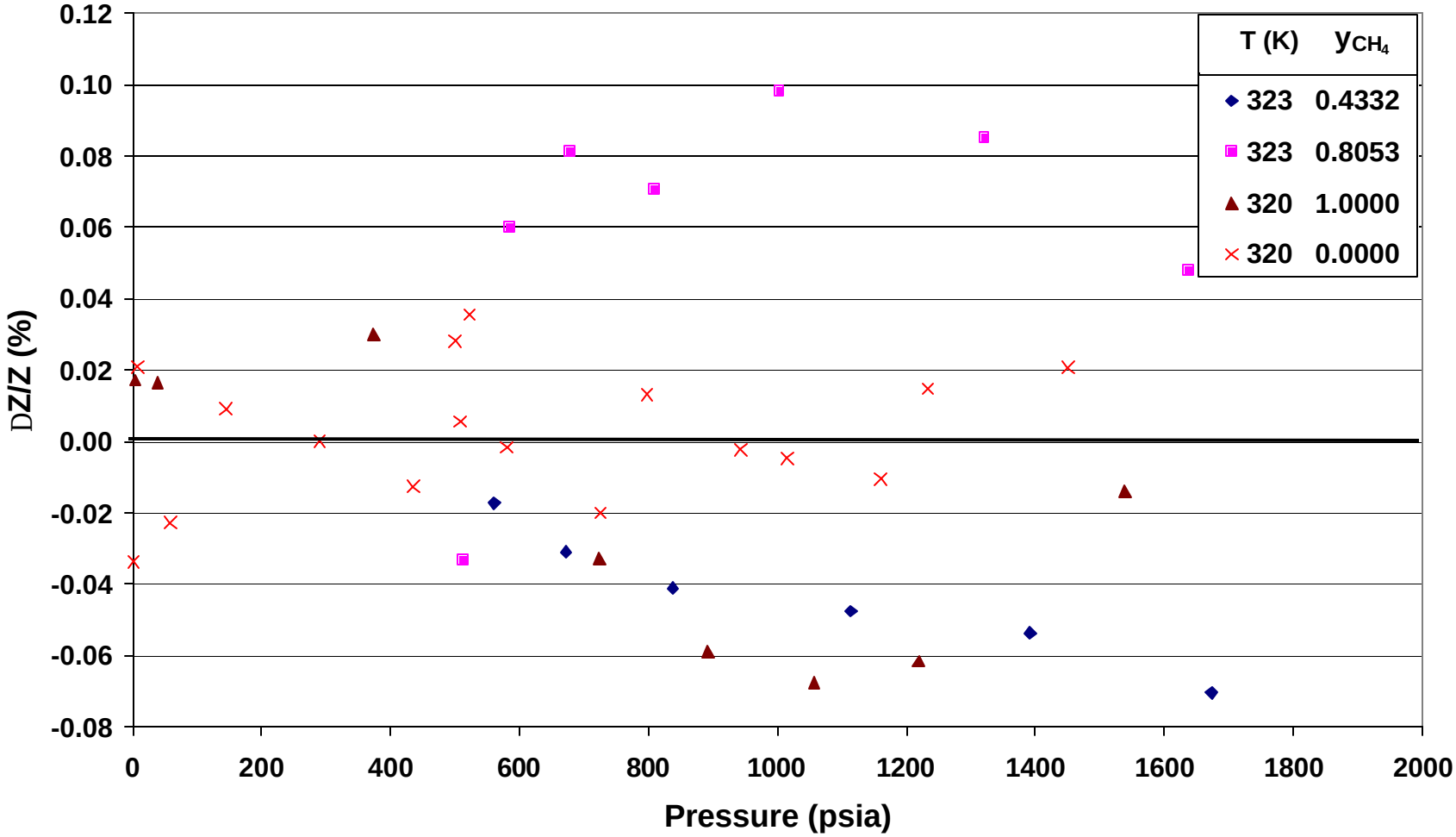

Figure 27. BWR Z Factor Deviations: Methane/Carbon Dioxide

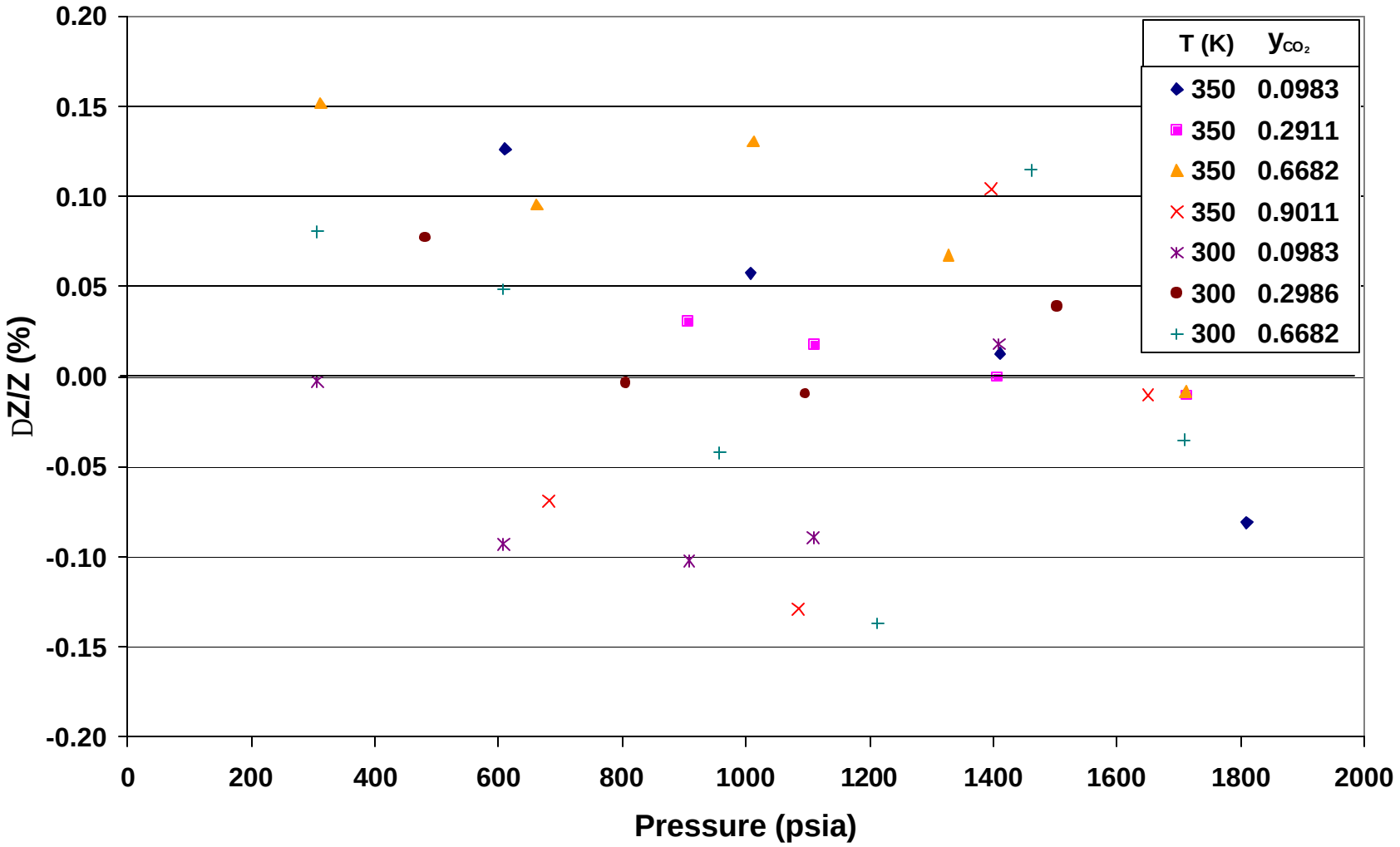

Figure 28. BWR Z Factor Deviations: Nitrogen/Carbon Dioxide

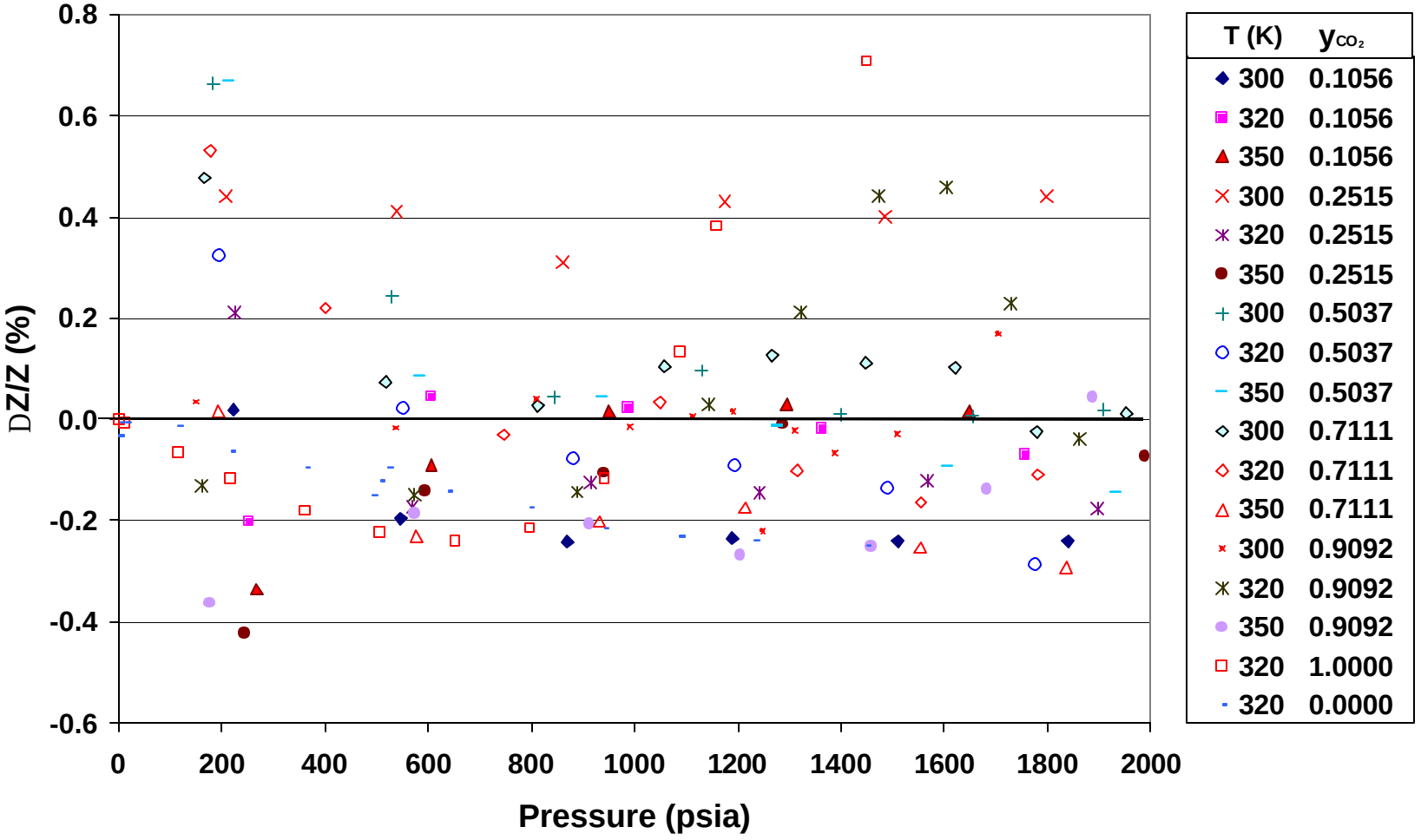

Sequestering Carbon Dioxide in Coalbeds

Penn State Portion of

Technical Progress Report

Reporting Period
from September 28, 1999 to October 28, 2000

L. R. Radovic

Pennsylvania State University
Department of Energy and
Geo-Environmental Engineering
University Park, PA 16802

PREPARED FOR THE UNITED STATES
DEPARTMENT OF ENERGY
DE-FC26-98FT40426

UPTAKES AND DIFFERENTIAL ADSORPTION HEATS OF CO_2 vs. CH_4

Introduction

Not long ago, when supplies of natural gas were thought to be very limited, there was considerable interest in injecting gases such as nitrogen and carbon dioxide into coal mines to recover the coalbed methane before extracting the coal (and venting the methane). Interestingly, at that time it was concluded that such a proposition would not be practical because it had been reported (Reznik et al., 1984) that an "excessive" amount of CO_2 would be required to displace the adsorbed methane. Today, with the greenhouse effect on our minds, this "excessive" amount is viewed as an attractive feature of CO_2 sequestration in coal mines. The fundamental questions remain the same, however. How many moles of CO_2 are needed to displace one mole of adsorbed CH_4? How does this ratio vary with the nature of the coal and with sequestration conditions? The experiments described below are a contribution toward the answers to these questions. We report CO_2 and methane adsorption properties for coals of different rank. The results, when combined with the studies of our OSU colleagues, are expected to reveal which coalbeds are best suited for sequestering CO_2 in them and for simultaneously releasing the largest quantity of methane.

Experimental

Samples. The coals used in this study are from the Argonne Premium sample bank, covering the rank range from lignite to low-volatile bituminous. The following abbreviation code is used:

Beulah (lignite)	BE
Smith Roland (subbituminous)	SM
Illinois #6 (high-volatile bituminous)	IL
Pittsburgh #8 (high-volatile bituminous)	PI
Stockton-Lewiston (medium-volatile bituminous)	ST
Pocahontas (low-volatile bituminous)	PO

Table 1 summarizes their properties. Preliminary results of their surface area measurements are reported in Table 2. Nitrogen adsorption at 77 K was carried out after pretreatment of Smith Roland and Illinois #6 coals at 110 ^{o}C under vacuum for 24 h. Beulah lignite was dried at 80-90 °C (Gumkowski et al., 1988). The CO_2 adsorption data were analyzed using the Dubinin-Polanyi (or Dubinin-Radushkevich) equation for the Beulah lignite and the Smith Roland coal (Larsen et al., 1987) and the BET equation for the Illinois #6 coal (The Penn State Coal Sample Bank and Database).

Apparatus. The present study focuses on measurements of uptakes and differential adsorption heats. The equipment for these measurements consists of a Tian-Calvet type heat flow calorimeter, described in detail elsewhere (O'Niel et al., 1985). It uses a cylindrical glass cell sandwiched between two thermopiles, which in turn are located between heat sinks. The heat output is measured by integrating the voltage output from the thermopiles, which is proportional to the heat of adsorption. The output signal is amplified and collected using a Swan 386/25 PC

equipped with a Labmaster data acquisition card. The amount of gas adsorbed is determined by measuring the pressure change in the dosing chamber. Two Baratron pressure sensors monitor the pressure, one used for 0.0001–1 Torr measurements and one for 1–1000 Torr measurements. The pressure measurements are also recorded using a PC. The system is calibrated using a 491-ohm resistor and a constant-power supply (Research Instrument Shop, University Park, PA).

Measurement procedures. Measurements on six coals (Table 1) were performed in this reporting period. In previous tests (described in our 1st annual report) the adsorption behavior of an activated carbon was compared to that of the Illinois #6 coal. The coal samples used were all of the same particle size, less than 60 mesh. Experiments were carried out using two different pretreatment temperatures: 313 K and 383 K. The coal was heated for 4 hours under vacuum, then it was allowed to cool and was transferred into the sample cell without exposure to air. The calorimeter was kept at constant temperature of ca. 298 K overnight, maintaining a dynamic vacuum in the sample cell. The residual pressure after the sample outgassing was ca. 10^{-2} Torr.

The experimental protocol consisted of four experiments for each coal. The investigated pressure range was from 1 to ca. 600 Torr. Each measurement was taken when the equilibrium pressure was reached, and this was assumed to occur when the variation in pressure was less than 0.1 Torr in 10 min. Usually this condition was satisfied within 30 min for CH_4 adsorption and in more than 1 hour for CO_2 adsorption. However, the equilibration time for adsorption was dependent on the sample and the gas used. Therefore we also studied the kinetics of CO_2 and CH_4 uptake: the approach to equilibrium was monitored during each dosing sequence by following the changes in pressure with time.

Results

Adsorption Kinetics. The kinetics of adsorption were monitored by continuously measuring the pressure in the sample cell. In Figures 1 and 2 the pressure variations vs. time are reported. The parameter on the y axis is the unaccomplished pressure change and it is defined as follows (Walker, 1981):

$$(P_t - P_f) / (P_0 - P_f)$$

Here P_0 is the initial pressure, P_f is the final pressure and P_t is the pressure at time t. P_0 is the pressure in the dose volume recorded before the gas enters the sample cell. The initial decrease is due, therefore, to both expansion and adsorption. The pressure drop due to expansion is a constant contribution independent of the coal sample used. Thus the differences in pressure profiles are due only to differences in adsorption and diffusion properties of the samples.

In Figure 1 the kinetics of adsorption are reported for the Illinois #6 coal and Beulah lignite at low pressure, with P_0 being ca. 25 Torr. For both coals it is seen that CH_4 is adsorbed faster than CO_2. The CH_4 adsorption profile is very similar for both coals and the average ratio between the two profiles in the first 100 s is 0.99, while the same parameter for CO_2 adsorption is 0.6.

Figure 2 shows the kinetics of adsorption at higher pressure, starting from ca. 300 Torr. Also in this case the adsorption of methane is faster. Moreover, the adsorption at higher pressure is generally faster than at lower pressure.

Adsorption Equilibria. The adsorption isotherms of CO_2 and methane for three coals are shown in Figures 3-5. The temperatures shown in these figures (313 and 383 K) represent the conditions of outgassing prior to adsorption measurements. Each adsorption isotherm was always recorded at ambient temperature. In Figure 5 the CO_2 uptake shows a step at about 370 Torr. This behavior is attributed to an experimental error; in fact, previous measurements on the same coal did not show the same trend.

From these data we conclude that adsorption of both CO_2 and methane on these coals does not depend on the outgassing temperature. One exception may be CO_2 adsorption on Illinois #6 coal, which seems to exhibit some dependence on outgassing temperature; this difference, however, may be within the limits of experimental error. Therefore a comparison among the uptakes by different coals can be made taking into account only one outgassing temperature. The choice of 313 K is better because this is closer to the temperature at which CO_2 sequestration is expected to occur in a coal mine. Therefore subsequent runs using the other coals were performed at only one outgassing temperature, 313 K.

Figure 6 compares the uptakes of CO_2 by the six coals. The lignite adsorbs more CO_2 than the other coals, followed by the subbituminous coal. Bituminous coals sligtly increase their capacity of adsorbing CO_2 at incresing rank from the high-volatile to the low-volatile, even if this trend is not very evident. It is thus concluded that the CO_2 adsorption capacity is not very sensitive to variations in rank for higher-rank coals.

Figure 7 shows the adsorption isotherms of methane on the same six coals. In this case the gas uptake depends only slightly on rank. The Smith Roland coal adsorbs the greatest amount of methane among the coals investigated, followed by the lignite. The bituminous coals adsorb less methane than the lower-rank coals.

A comparison between Figures 6 and 7 shows that all the coals investigated have higher affinity for CO_2 than for CH_4 and the mean ratio between the CO_2 and CH_4 uptake is 6.3.
Table 3 summarizes all these results. The ratio between the amounts of CO_2 and CH_4 adsorbed is calculated at 600 Torr. It is important to note the differences among the six coals in the ratio of the amount of CO_2 adsorbed with respect to the amount of CH_4. These differences are mainly due to the different amounts of adsorbed CO_2. The ratio of uptakes does not exhibit a clear dependence on coal rank: it is the highest for the lignite, but in the case of higher-rank coals a clear trend does not exist for this data set.

Adsorption Heats. Figures 8-10 show the heats of adsorption vs coverage for the Beulah lignite, the Smith Roland and the Illinois #6 coal. The lignite shows a steep decrease in the adsorption heat for carbon dioxide at low coverage (up to 0.1 mmol/g), and then the heat of adsorption remains constant. It starts at ca. 50 kJ/mol in the first region and decreases to ca. 28 kJ/mol, values that are rather high for a physical adsorption process.

The adsorption heat for methane also shows a decrease at increasing coverage. This trend is not very evident, however, because in this case the measured absolute heats are quite small and almost of the same order as the experimental error. At low coverage the estimated heat is ca. 19 kJ/mol and it decreases to ca. 8 kJ/mol.

The Smith Roland coal behaves differently, as shown in Figure 9. The heat of adsorption for CO_2 exhibits a gradual decrease in the entire coverage range investigated, starting from 40 kJ/mol to about 20 kJ/mol. The adsorption heat for methane appears to increase slightly with coverage, although a clear trend is not evident, and its value is ca. 20 kJ/mol.

The Illinois #6 coal (Figure 10) shows higher heats of adsorption for CO_2 at lower coverage, starting from ca. 35 kJ/mol to 30 kJ/mol. Also in this case a clear trend for methane adsorption cannot be seen and the average value of the adsorption heat is ca. 24 kJ/mol.

From the results shown above, one sees that the outgassing temperature does not have any effect on the value of the adsorption heat, so that in the comparison of the results for coals of different rank only the experiments performed with an outgassing temperature of 313 K are shown.

Figure 11 presents the comparison of the CO_2 adsorption heats for the six coals. At lower coverage the adsorption heat on Beulah lignite appeares to be the highest. Above 0.12 mmol/g all the heats reach a value within the same range. In general, the heat of adsorption appears to decrease with coverage for all the coals investigated, as expected for a heterogeneous surface. The Pocahontas low-volatile bitouminous coal behaves differently, however, the adsorption heat for CO_2 appearing to increase somewhat at higher coverages.

The heats of CH_4 adsorption for the Smith Roland and Illinois #6 coals are very close in the entire coverage range investigated and these coals have the highest adsorption heat, whereas the lignite has the lowest heat (Figure 12).

These results are summarized in Table 4, where the adsorption heats of CO_2 and CH_4 and their ratio for the six coals are evaluated at 600 Torr.

Discussion

In all cases CO_2 uptake exceeds that of CH_4 by five-fold or more. This can be due to both adsorbate–adsorbate and adsorbate–adsorbent interactions. In an initial attempt to separate the two effects, the adsorption isotherms are reported on a normalized pressure scale. In Figure 13 isotherms for four coals are normalized using the vapor pressure of the adsorbate. For methane, which is at supercritical conditions, the extrapolated vapor pressure is used (Laxminarayana and Crosdale, 1999). It is seen that CH_4 uptakes by all coals fall on the same curve, while the uptakes of CO_2 are much higher than those of CH_4 and also differ from sample to sample. In particular, the lower-rank coals, as expected from knowledge of their surface chemistry, exhibit higher normalized uptakes. Similar results are obtained in Figure 14, where data normalization is performed using the critical pressure. It will be interesting to see how sensitive these conclusions are to the choice of the normalization parameter. In recent studies of Kaneko and coworkers (Kaneko and Murata, 1997), it has been proposed that a modified version of the Dubinin-

Radushkevich equation, involving the use of a quasi-saturated vapor pressure from a Langmuir plot, should be used for supercritical gases.

Another reason for the observed differences in uptake may be related to the size and shape of the two adsorbates. The CO_2 molecule is rod-like and its minimum dimension is 2.8 Å, whereas the CH_4 molecule is spherical with a slightly larger diameter. Therefore coal can behave as a molecular sieve and methane may be excluded from pores accessible to CO_2. The results presented in Figures 1 and 2 are evidence that this factor should be taken into account.

It is also important to analyze the effect of pretreatment of the coal. As discussed above, the adsorption behavior of both CO_2 and CH_4 was found to be independent of the degassing temperature *when fresh samples are used in each experiment*. Our previous tests (unpublished results; Weigle, 1999) using the same coals have shown different results. The effect of degassing temperature was much more significant: less gas was adsorbed after high-temperature outgassing than after low-temperature outgassing. Also the heat released was lower in the second run. In the present work each isotherm was recorded using always fresh samples.

In previous experiments (Weigle, 1999) we had used the same coal sample for both degassing temperatures and the observed behavior (described above) can be considered to be a combination of two different effects. It is well known that when coals are exposed to sorbates, they can swell to different extents. The geometry of the pores can change and even small differences in the porous structure may cause significant changes in uptakes and in interaction energies between gases and coal (Walker and Mahajan, 1993; Grillet and Starzewski, 1990). Also a hysteresis phenomenon can occur. Once the gas enters the pores, it may interact strongly with some sites on the coal surface and may not be removed totally after the second degassing. An enhancement of irreversible CO_2 adsorption may be evidence of "permanent" sequestration.

Among the six coals investigated no clear trend can be seen in the adsorption uptakes and heats with respect to coal rank. The lignite does seem to be the best candidate for CO_2 sequestration because, having the highest adsorption heat, it adsorbs the greatest amount of CO_2. Also a larger amount of CO_2 can be adsorbed by displacing a given volume of methane; in fact, in this case the ratio of uptakes is the highest and its value is 8.4. Also the CH_4 adsorption heats and isotherms for the lignite show that this coal is well suited for methane recovery. However, it should be kept in mind that the greatest amount of methane in a coal mine is typically generated by medium- and low-volatile bituminous coals (Ayers and Kelso, 1989).

At the other extreme, the highest-rank coal investigated, Pocahontas, had the lowest ratio of uptakes. Moreover, if we consider the entire range of bituminous coals, it is seen that the methane adsorption capacity decreases from the Illinois #6 to the Stockton coal and then it increases again at higher rank. This is in agreement with what was found by earlier investigators (Laxminarayana and Crosdale, 1999). It is intriguing to note that the coal surface area has a minimum in the same rank range (Gan et al., 1972). The Stockton coal has a high ratio of uptakes but the amounts of CO_2 and CH_4 adsorbed are the lowest when compared with the other coals, so this coal cannot be considered as best suited for CO_2 sequestration.

Summary

Significant differences in CO_2 sequestration ability have been observed for different coals. Furthermore, when these differences are compared to the relative affinities of coals for CO_2 vs. methane, it is concluded that they are mostly due to differences in CO_2 uptakes on different coals. Future studies will be focused, therefore, on rationalizing these differences. Results to date suggest that they are due primarily to the different surface chemistries of the coals. To what extent the coal's surface area, pore size distribution and molecular sieving ability also contribute to these differences remains an important fundamental question.

Bibliography

Ayers, W.B. and Kelso, B.S., *Oil and Gas J.*, Oct 23, 1989, p. 64.
Chaback J. J., Morgan W. D., Yee D., *Fluid Phase Equilibria*, 117 (1996).
Gan, H., Nandi, S.P., Walker P.L., Jr., *Fuel*, 51, 272 (1972).
Grillet, Y., Starzewski, P., in "Advanced Methodologies in Coal Characterization, Coal Science and Technologies" (H. Charcosset, Ed.), 83-101, Elsevier (1990).
Gumkowski, M., Liu, Q., Arnett, E. M., *Energy Fuels*, 2, (1988).
Kaneko, K., Murata, K., *Adsorption*, 3, 197 (1997).
Larsen, J. W., Wernett, P., *Preprints, Fuel Chemistry Div., Amer. Chem. Soc.*, 32, 232-236, 1987.
Laxminarayana C., Crosdale P. J., *International Journal of Coal Geology*, 40, 309 (1999).
O'Niel, M., Lovrien, R., Phillips, J., *Rev. Sci. Instrum.*, 56, (1985).
Reznik, A.A., Singh, P.K., Foley W.L., *Society of Petroleum Engineers Journal*, Oct. 1984.
Walker, P. L. Jr., *Phil. Trans. R. Soc. Lond. A* 300 (1981).
Walker P.L., Jr., Mahajan O.P. *Energy Fuels*, 7, 559 (1993).
Weigle J., Ph.D. Thesis, The Pennsylvania State University (1999).

Table 1

Proximate and Ultimate Analysis of the Coals

Coal	**BE**	**SM**	**IL**	**PI**	**ST**	**PO**
Proximate Analysis						
% Moisture, A.R.	33.38	28.42	7.97	2.40	2.64	1.01
% Ash, dry	9.56	13.83	15.48	10.25	20.30	4.60
% Volatile Matter, daf	62.01	52.49	47.39	40.13	39.61	19.19
% Fixed Carbon, daf	37.99	47.51	52.61	59.87	60.39	80.81
Ultimate Analysis						
% C, daf	73.14	74.43	77.67	83.32	83.25	89.87
% H, daf	4.46	5.23	5.00	5.69	5.65	40.90
% N, daf	1.00	1.00	1.37	1.37	1.38	1.14
% S, daf	0.82	0.85	5.72	1.25	0.92	0.78
% O, daf (by diff.)	20.59	18.49	10.24	8.37	8.81	3.31

Table 2

Surface Areas of the Coals

Coal	**BE**	**SM**	**IL**	**PI**	**ST**	**PO**
N_2 Surface Area, m^2/g	1.85	6.20	23.53	2.38	tbd	2.77
CO_2 Surface Area, m^2/g	206	229	132	tbd	tbd	tbd

tbd= to be determined

Table 3

Amounts of CO_2 and CH_4 Adsorbed at P_0 = 600 Torr

and Their Ratio for the Six Coals Investigated

Coal	Adsorbed CO_2 (mmol/g)	Adsorbed CH_4 (mmol/g)	CO_2/CH_4 ratio (mol/mol)
BE	0.646	0.077	8.4
SM	0.558	0.096	5.8
IL	0.348	0.068	5.1
PI	0.303	0.049	6.2
ST	0.245	0.034	7.2
PO	0.336	0.068	4.9

Table 4

Heats of CO_2 and CH_4 Adsorption at P_0 = 600 Torr

and Their Ratio for the Six Coals Investigated

Coal	CO_2 (kJ/mol)	Methane (kJ/mol)	Ratio (kJ/kJ)
BE	28	8	3.5
SM	26	24	1.1
IL	27	17	1.6
PI	25	18	1.4
ST	13	14	0.9
PO	29	23	1.3

Figure 1. Pressure drop vs. time at ca. 25 Torr for Beulah lignite and Illinois #6 coal.

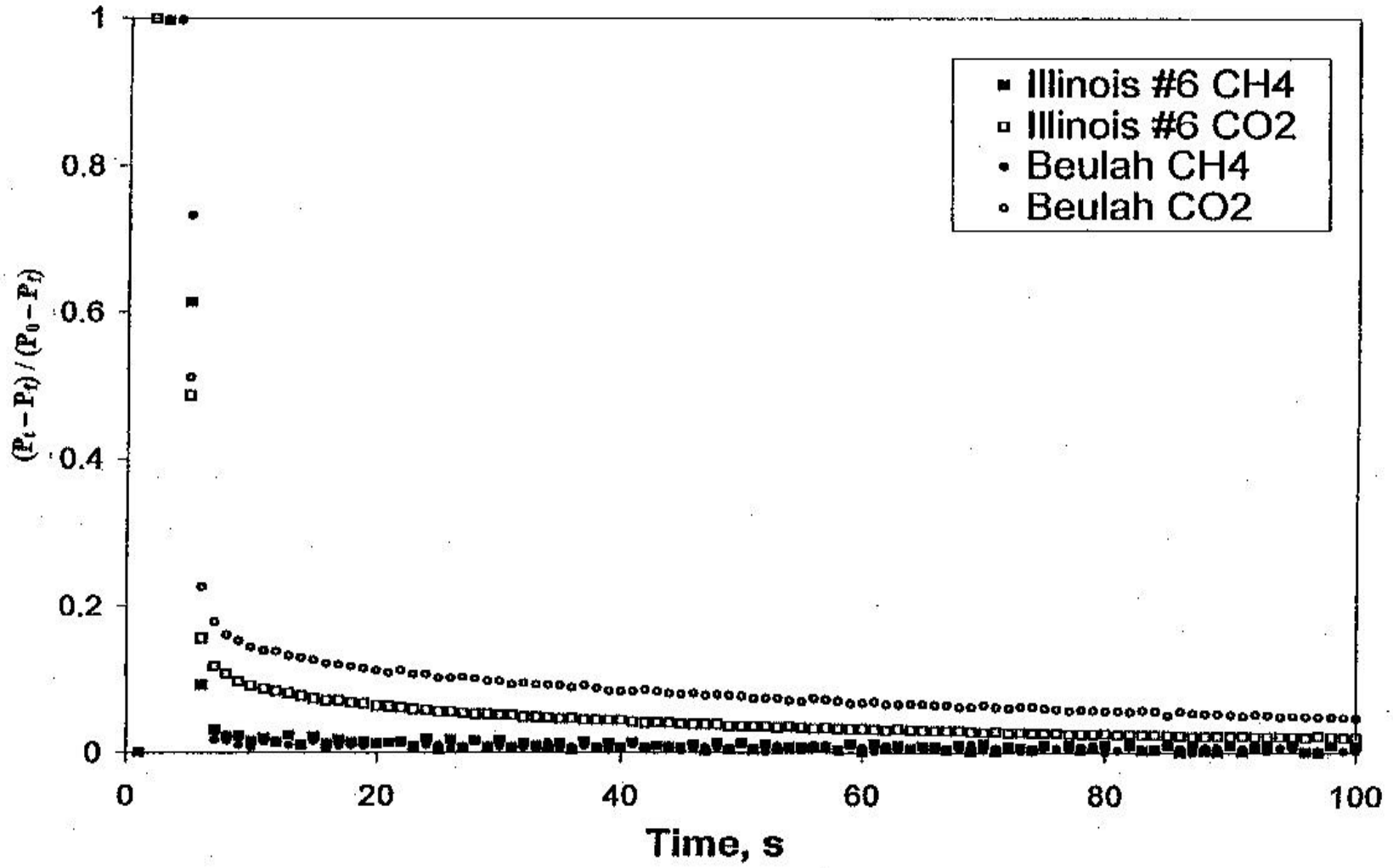

Figure 2. Pressure drop vs. time at ca. 300 Torr for Beulah lignite and Illinois #6 coal.

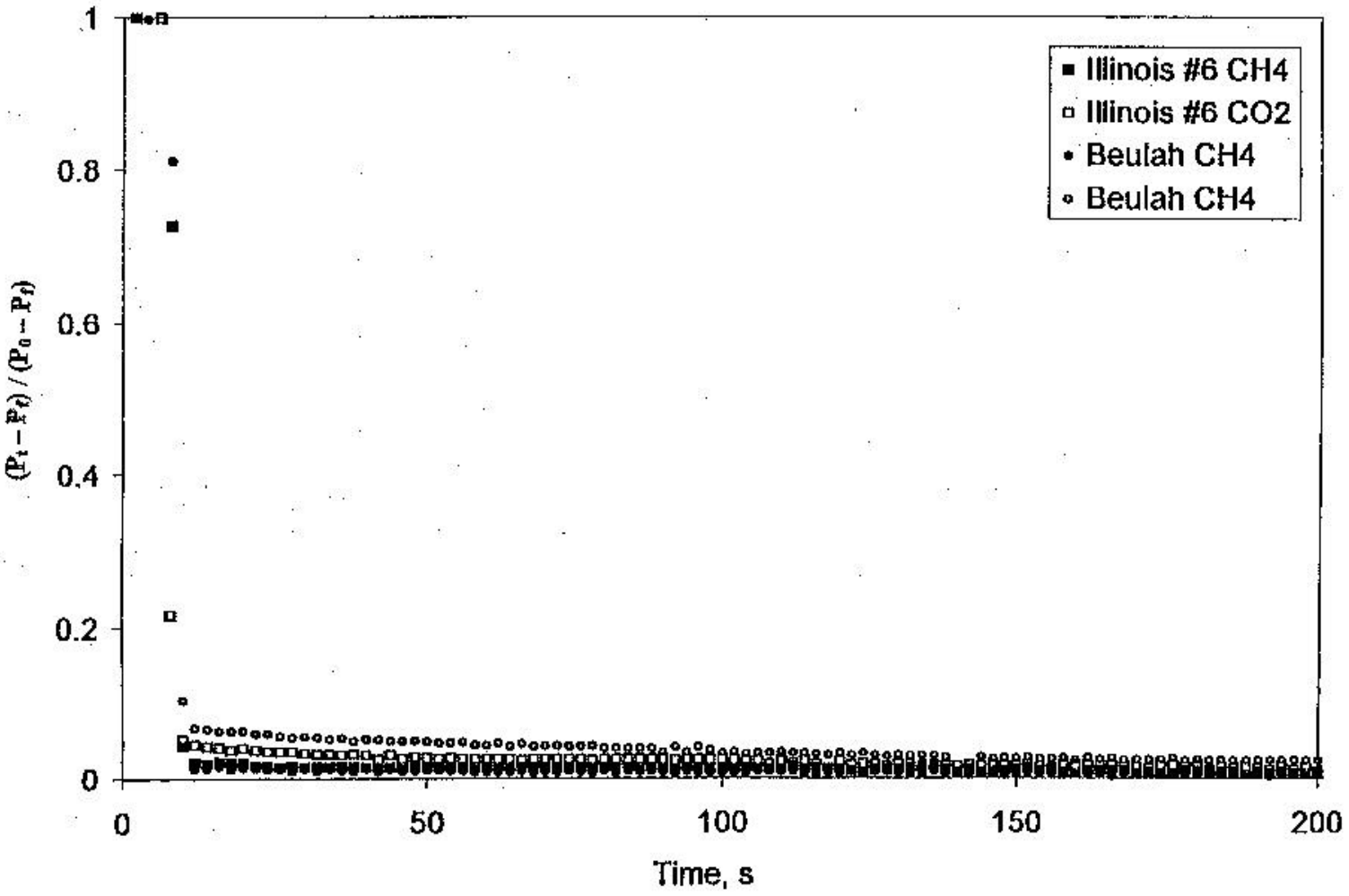

Figure 3. Adsorption isotherms of CO_2 and CH_4 on Beulah lignite.

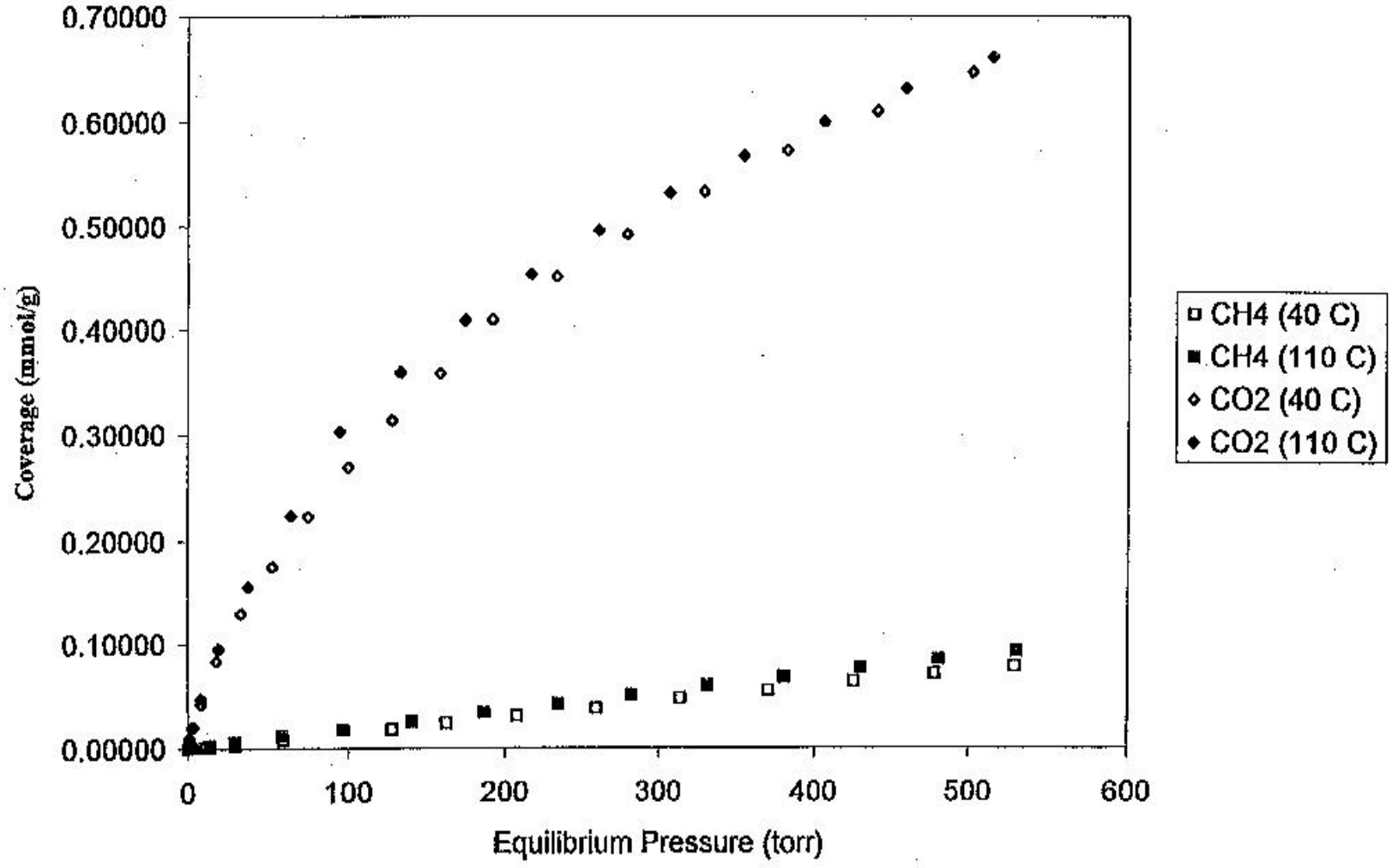

Figure 4. Adsorption isotherms of CO_2 and CH_4 on Smith Roland coal.

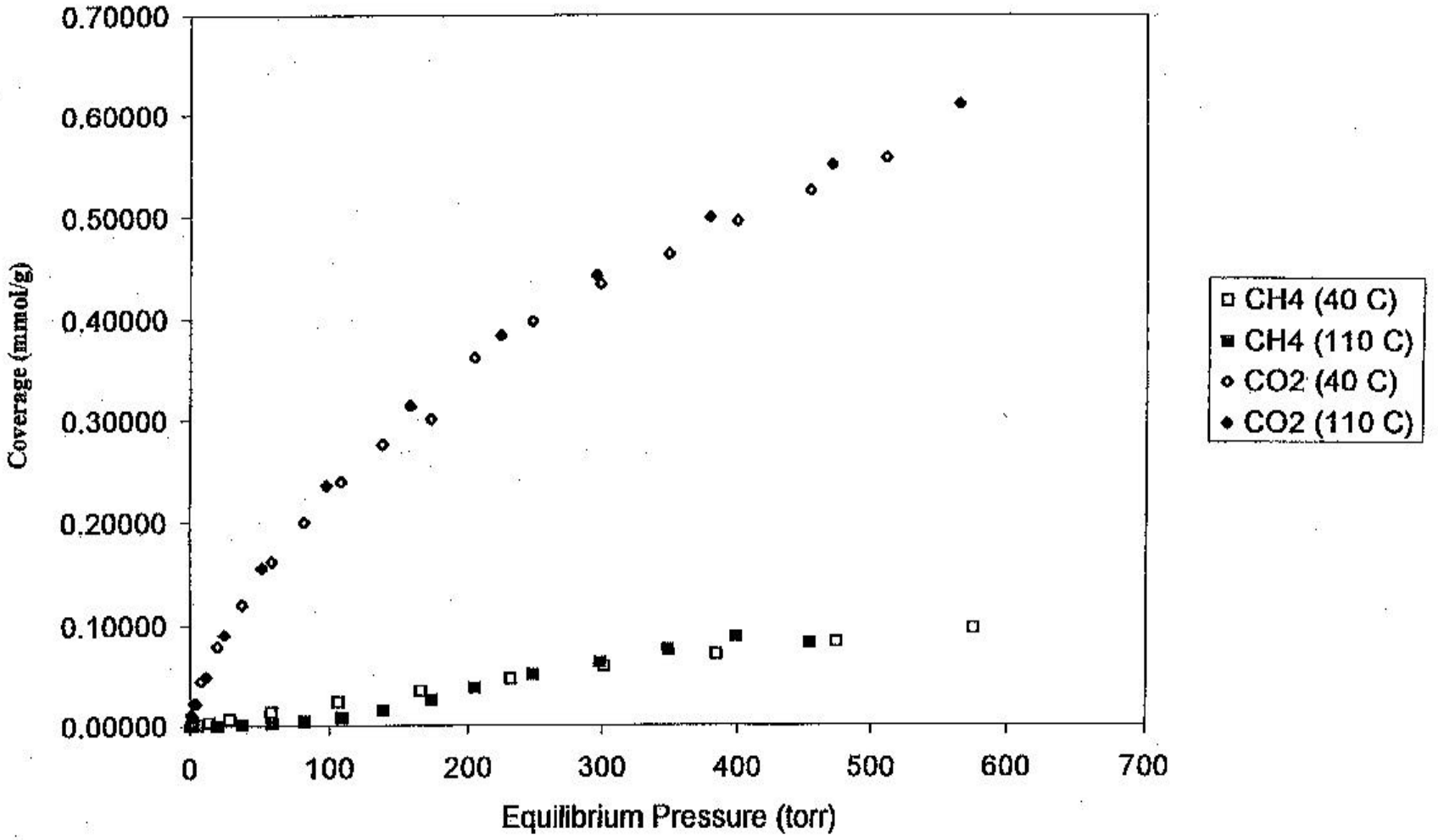

Figure 5. Adsorption isotherms of CO_2 and CH_4 on Illinois #6 coal.

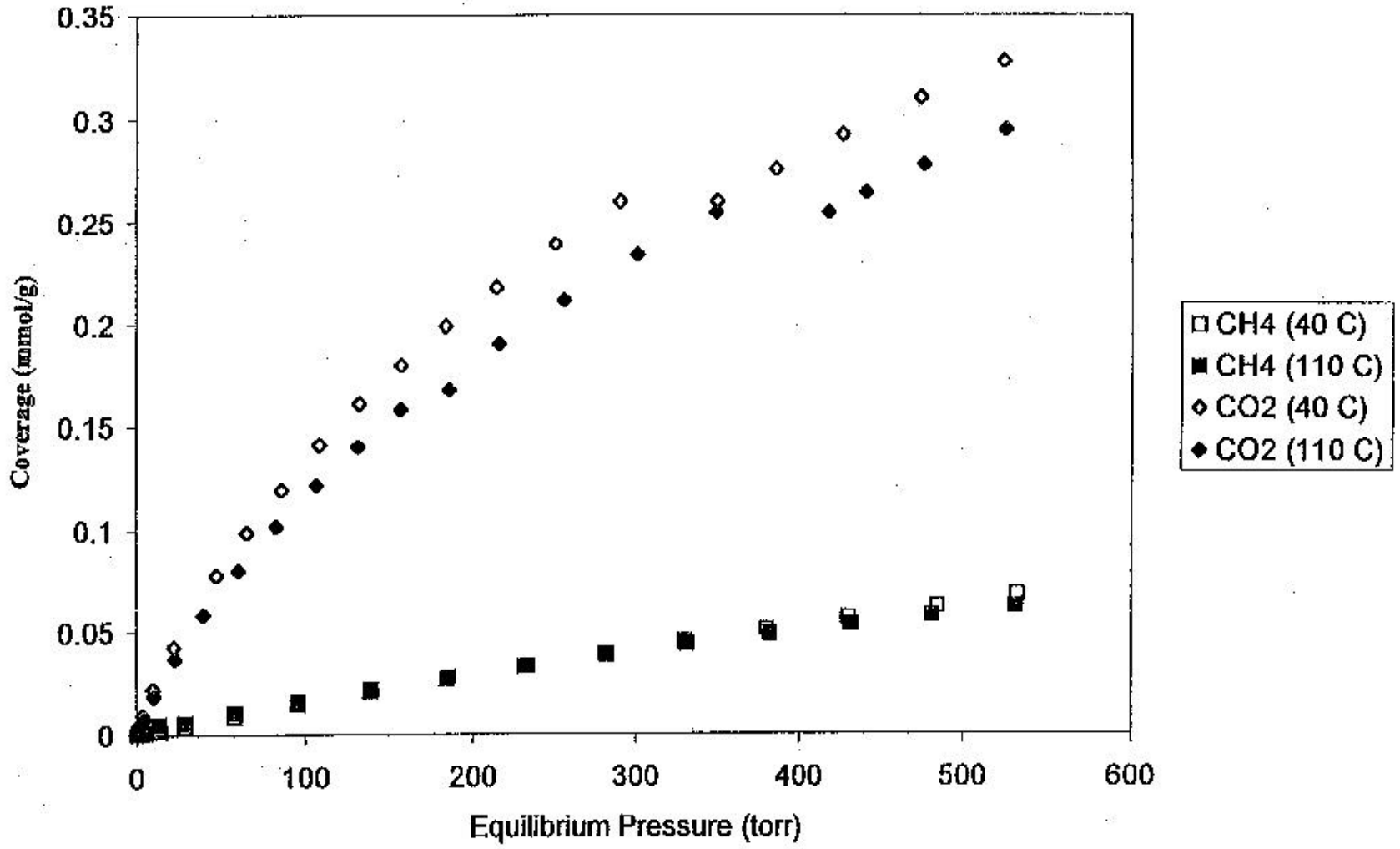

Figure 6. Comparison of uptakes of CO_2 for the six coals investigated.

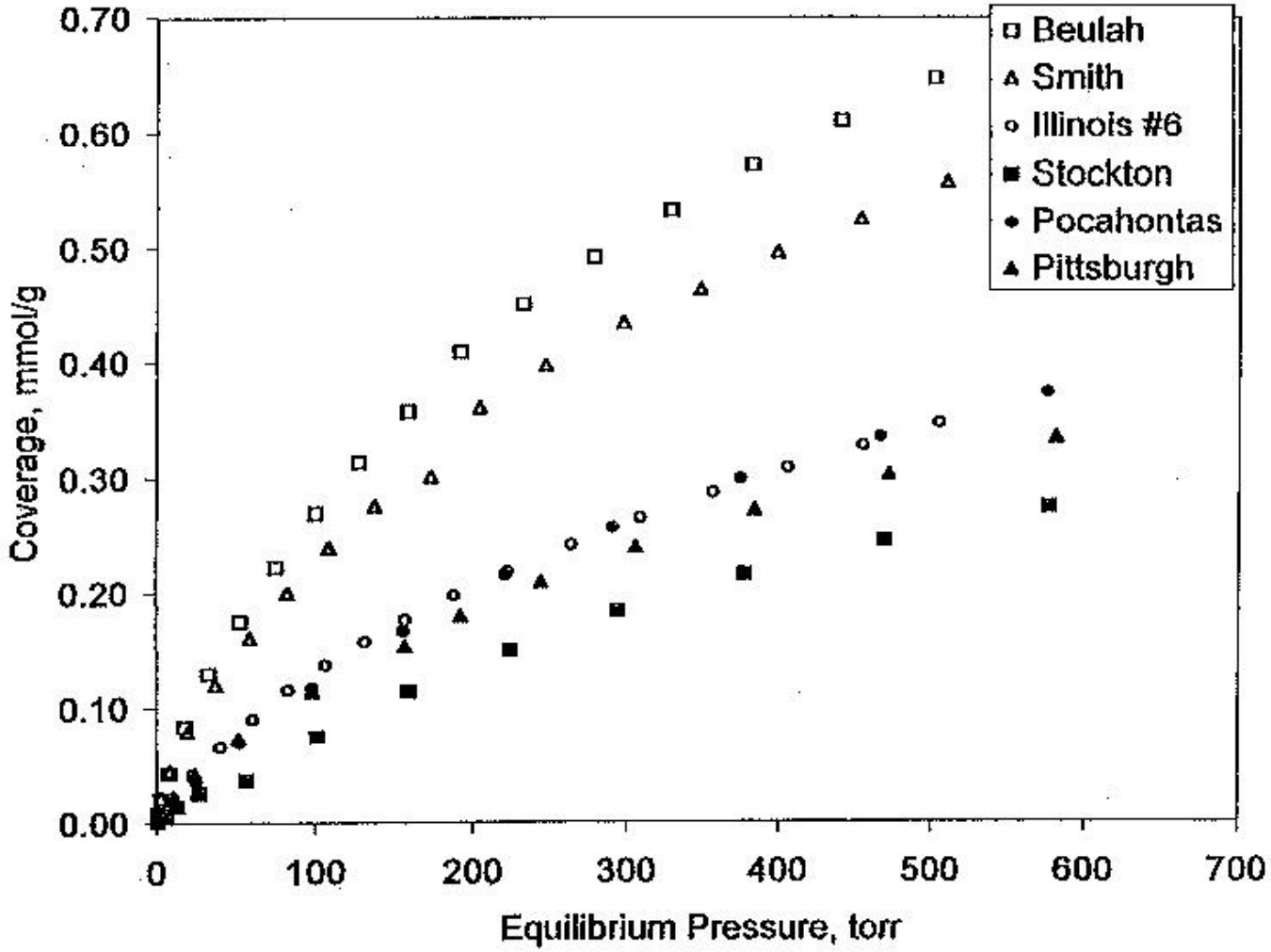

Figure 7. Comparison of uptakes of CH_4 for the six coals investigated.

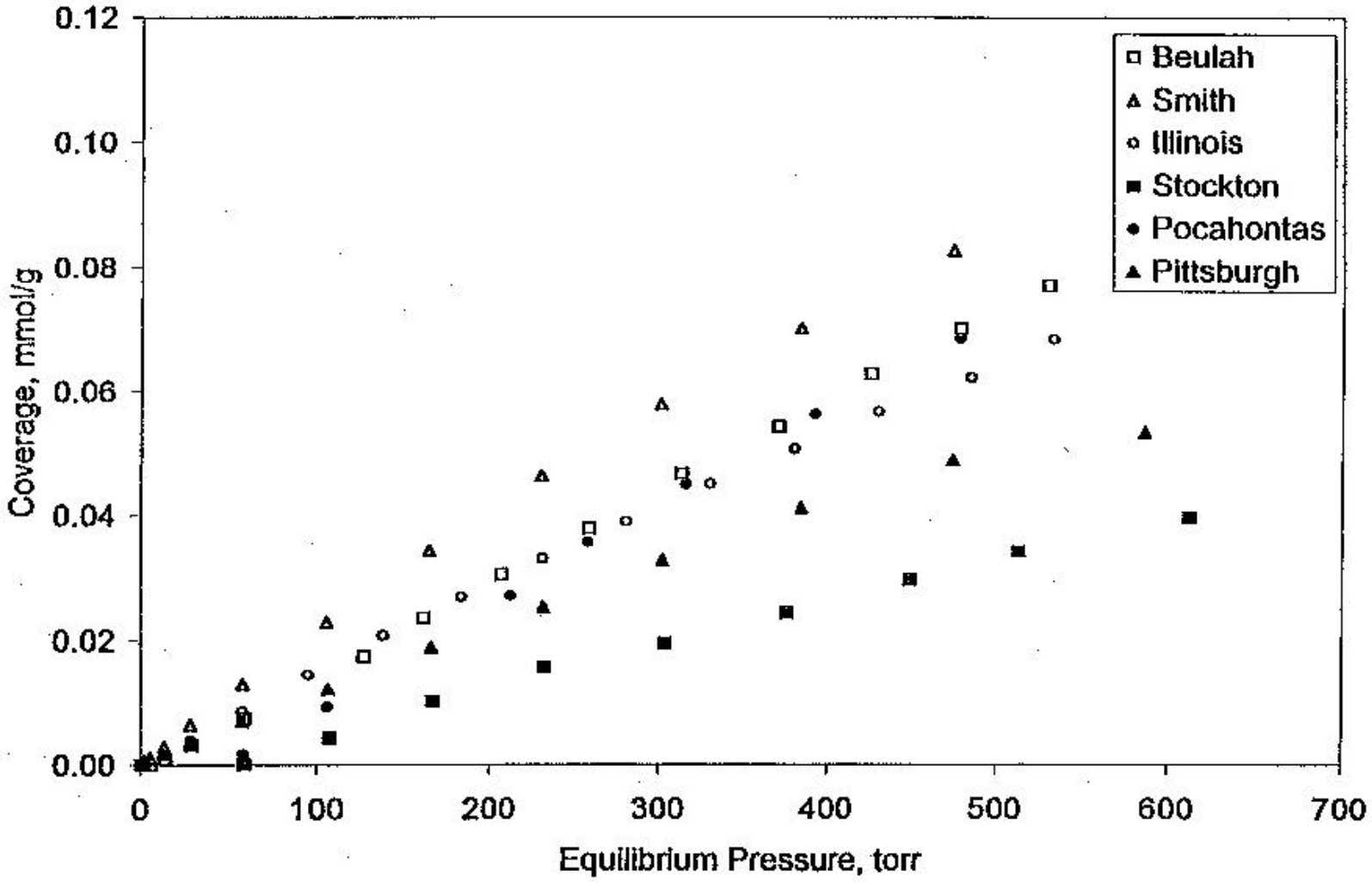

Figure 8. Adsorption heats vs. coverage for Beulah lignite.

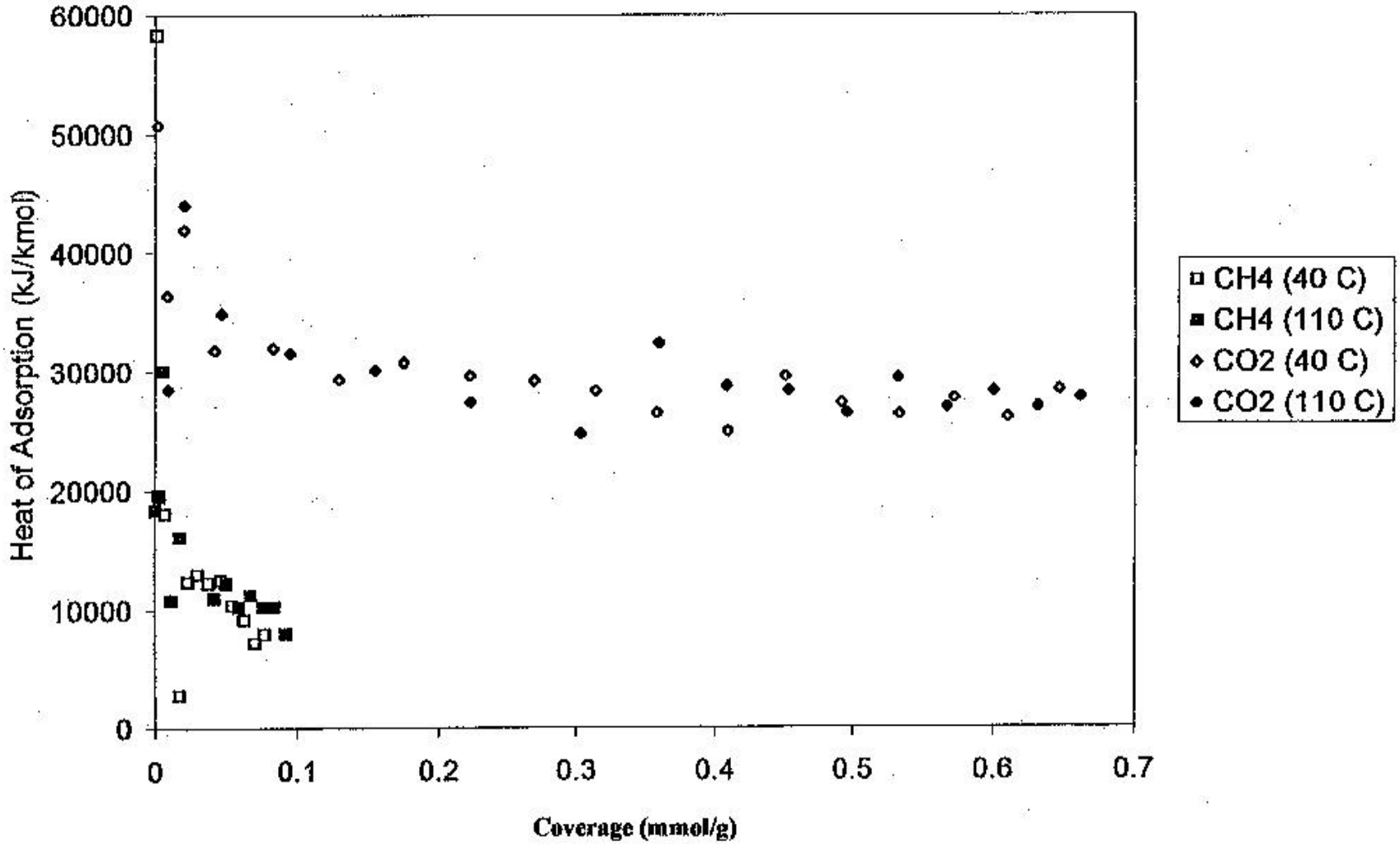

Figure 9. Adsorption heats vs. coverage for Smith Roland coal.

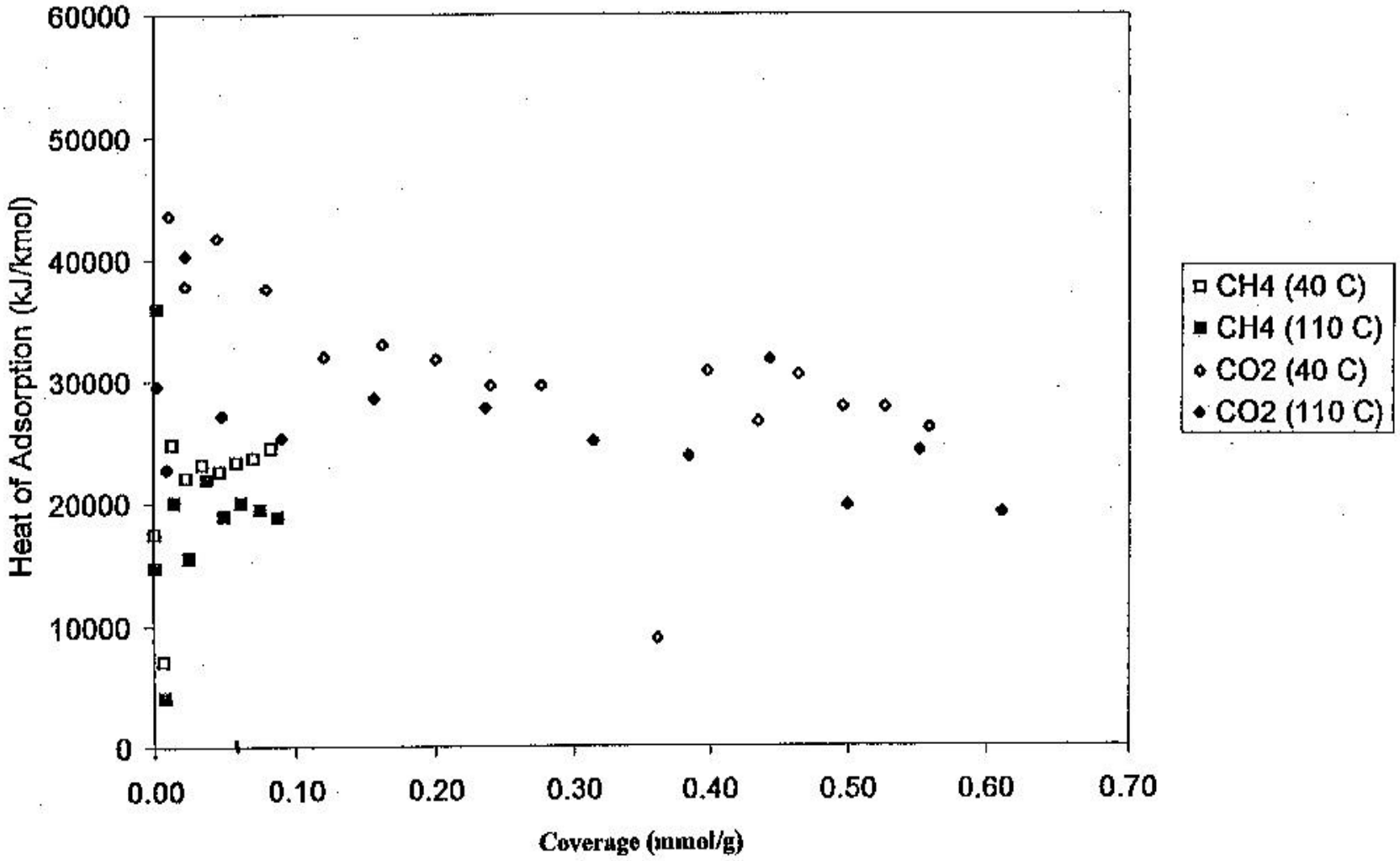

Figure 10. Adsorption heats vs. coverage for Illinois #6 coal

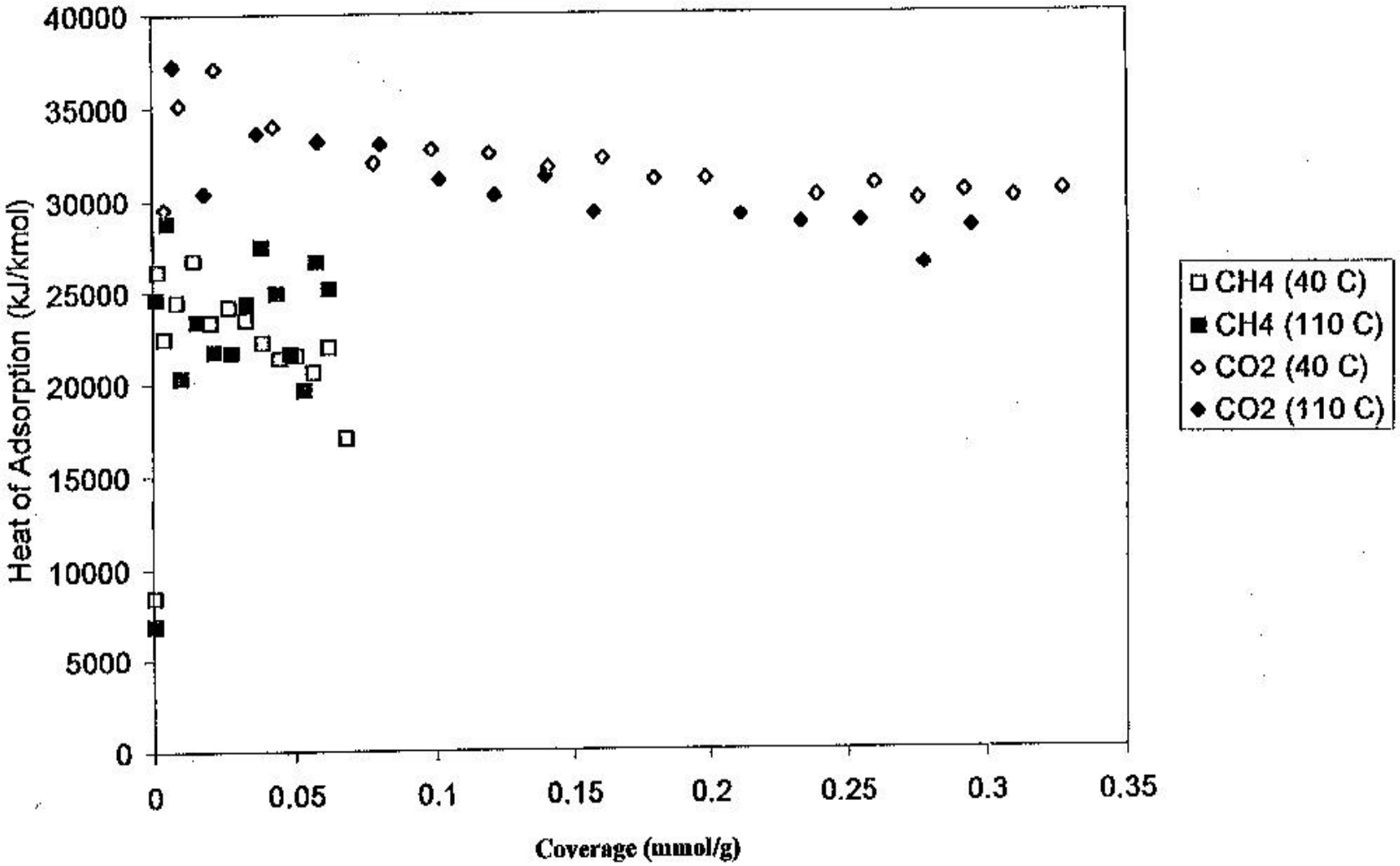

Figure 11. Comparison of CO_2 adsorption heats for the six coals investigated.

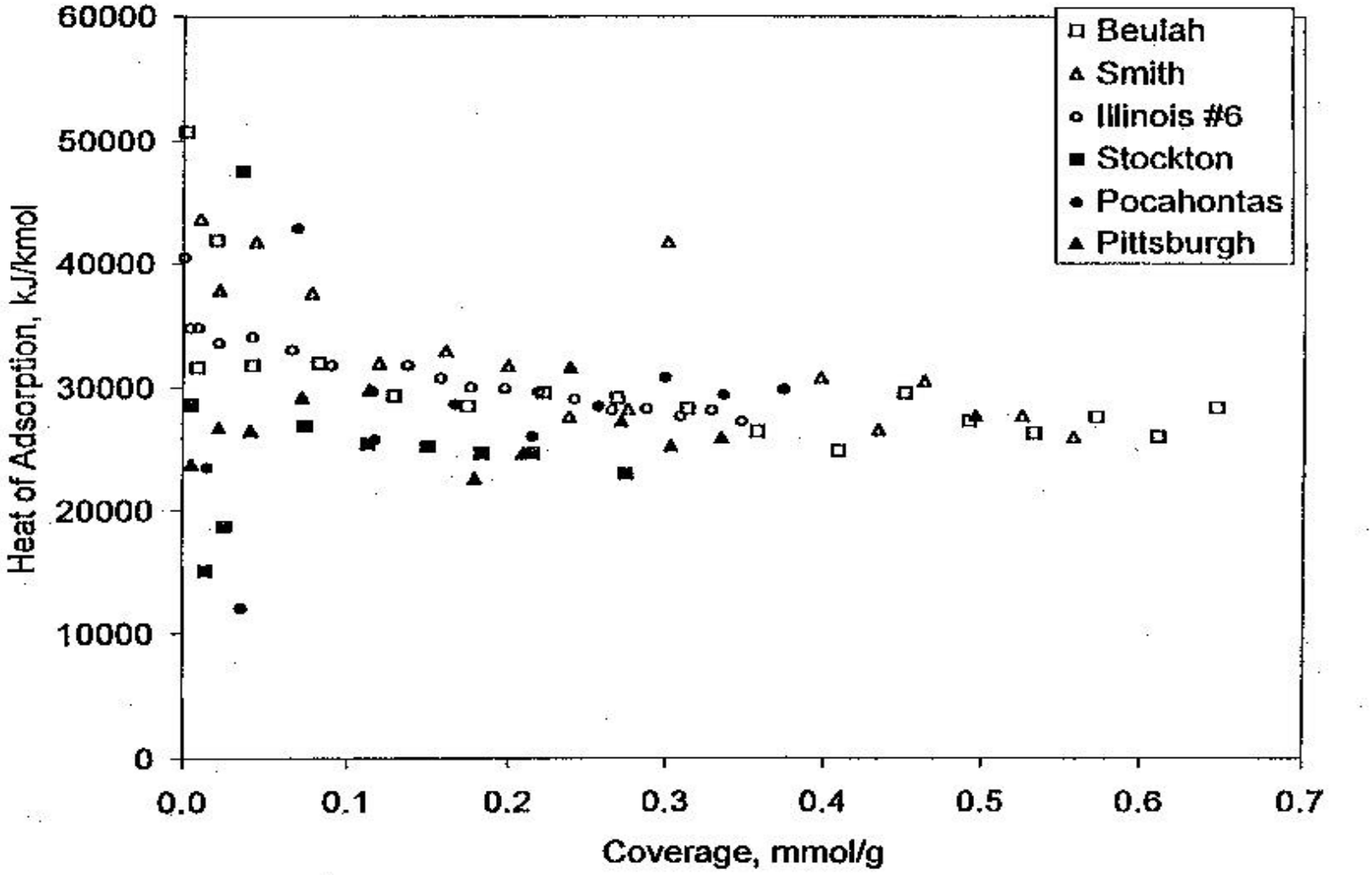

Figure 12. Comparison of CH_4 adsorption heats for the six coals investigated.

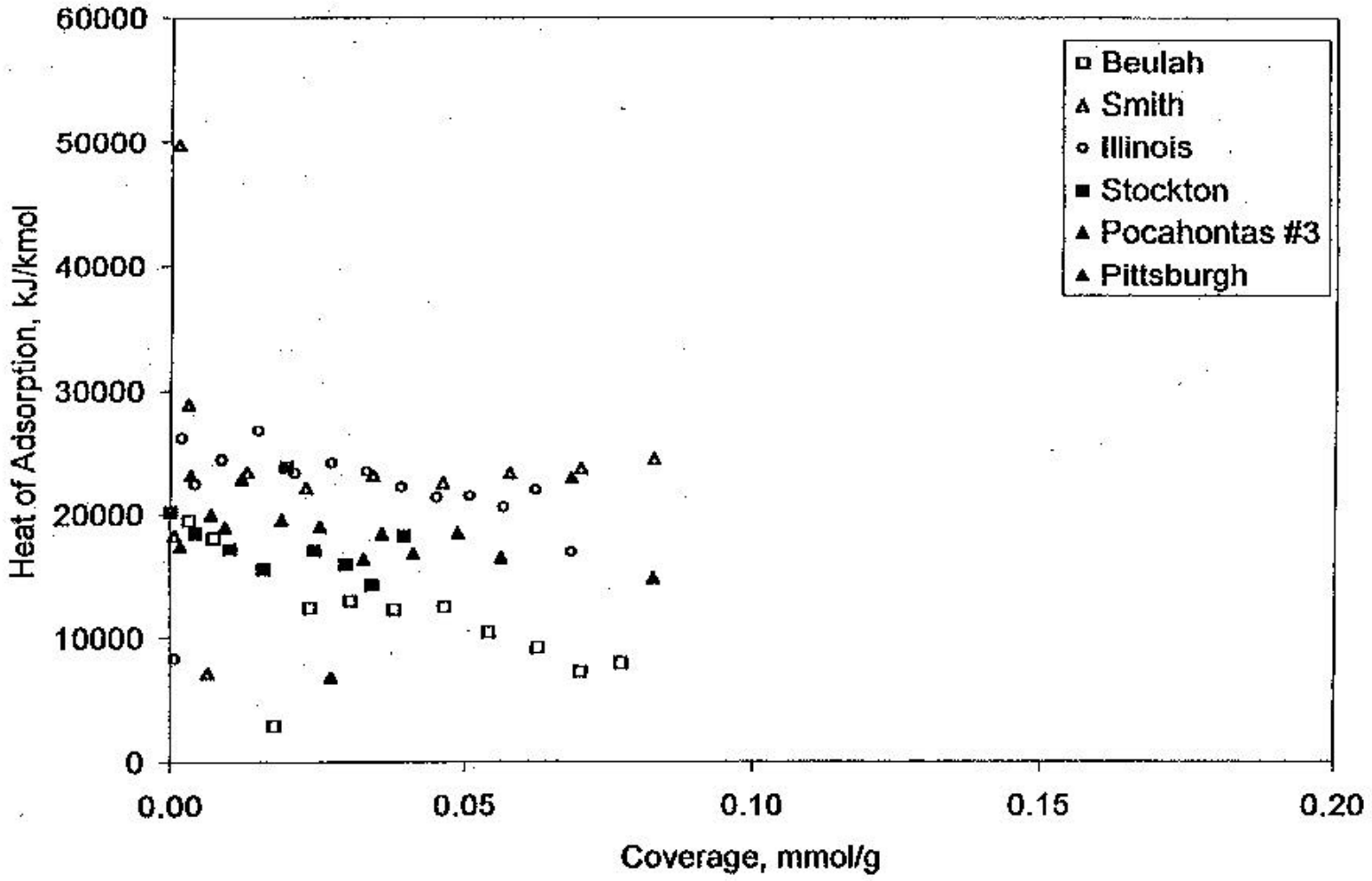

Figure 13. Normalized CO_2 and CH_4 adsorption isotherms using vapor pressures.

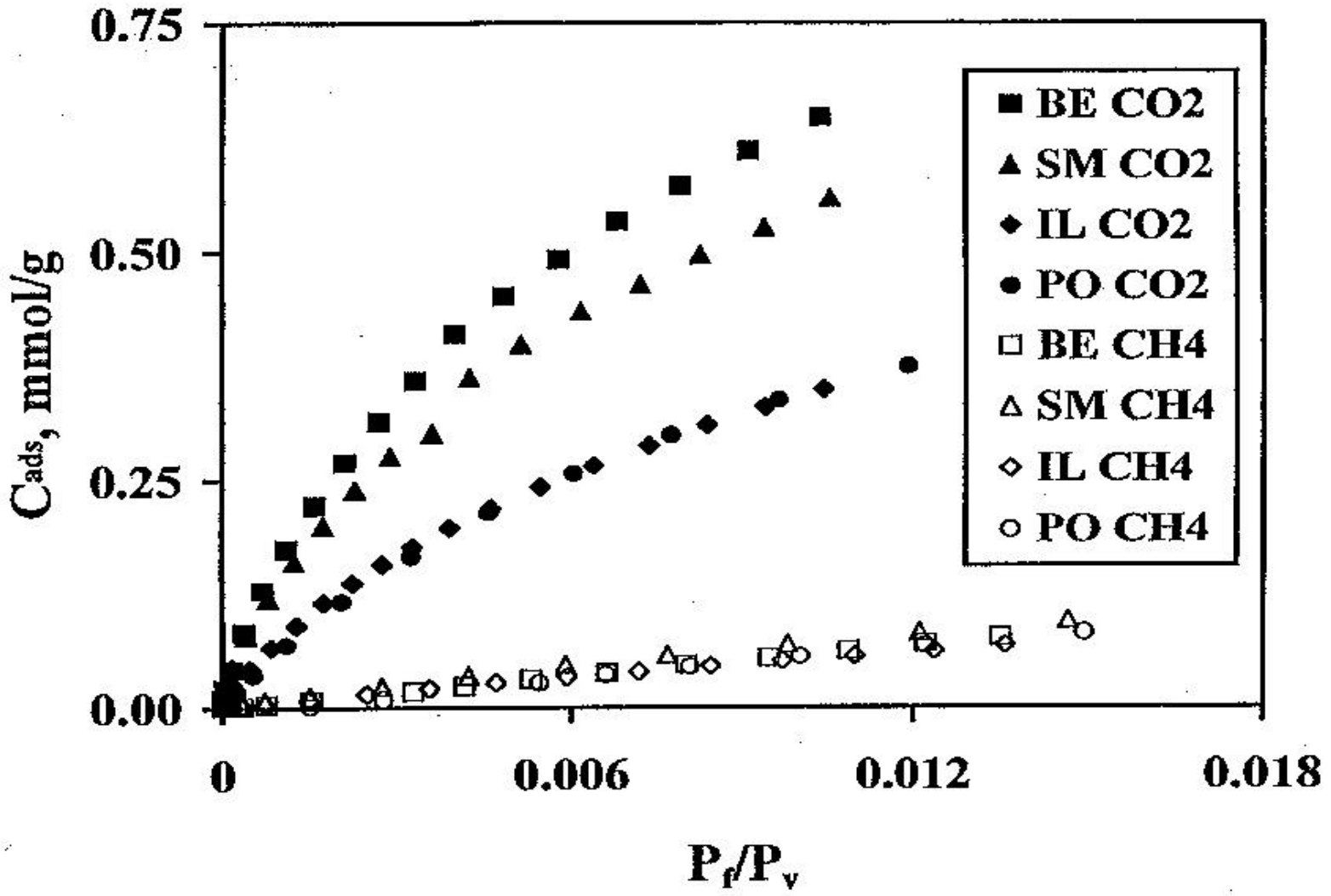

Figure 14. Normalized CO_2 and CH_4 adsorption isotherms using critical pressures.